Coherent Transport through Interacting Quantum Dots

UNIVERSITÄT DUISBURG ESSEN

Offen im Denken

von der Fakultät für Physik genehmigte

Dissertation

zur Erlangung des Grades Doktor des Naturwissenschaften

von

Bastian Hiltscher

Referent: Prof. Dr. J. König

Korreferent: Prof. Dr. V. Meden

Tag der mündlichen Prüfung: 05.10.2012

Deutsche Zusammenfassung

Die vorliegende Dissertation setzt sich aus vier unterschiedlichen Arbeiten zusammen. Jede beschäftigt sich mit kohärentem Transport durch wechselwirkende Quantenpunkte, die über Tunnelbarrieren an externe Zuleitungen gekoppelt sind. Es gibt zwei Hauptmotivationen, Quantenpunkte zu untersuchen. Erstens eignen sie sich hervorragend um den Einfluss starker Coulomb-Abstoßung zu studieren, und zweitens können ihre diskreten Energielevel leicht durch externe Gate-Elektroden kontrolliert werden, so dass verschiedene Transportregime entstehen. Der Begriff Kohärenz beinhaltet ein sehr breites Spektrum an physikalischen Korrelationen, wodurch die vier Arbeiten im Wesentlichen unabhängig voneinander sind. Bevor die einzelnen Arbeiten im Detail motiviert und vorgestellt werden, merken wir an, dass in allen Arbeiten eine diagrammatische Real-Zeit-Störungstheorie benutzt wird. Die fermionischen Freiheitsgrade der Zuleitungen werden ausgespurt und die Elemente der resultierenden reduzierten Dichtematrix können explizit mit Hilfe einer generalisierten Mastergleichung behandelt werden. Wie diese Gleichung gelöst wird, hängt von den Details des jeweiligen Problems ab.

In der ersten der vier Arbeiten wird adiabatisches Pumpen durch ein Aharonov-Bohm-Interferometer untersucht, in dessen zwei Arme jeweils ein Quantenpunkt eingebettet wird. Beim adiabatischen Pumpen wird Transport generiert, indem zwei Systemparameter periodisch in der Zeit variiert werden. Als diese Pumpparameter wählen wir die Energielevel der beiden Quantenpunkte. Da sie sich in unterschiedlichen Armen des Interferometers befinden, ist Pumpen dabei ein quantenmechanischer Effekt, der ausschließlich auf kohärenten Überlagerungen der Quantenpunkt-Zustände beruht. Es ist äußerst schwierig Quantenpumpen experimentell nachzuweisen, weil eine kapazitive Kopplung der Gate-Elektroden an die Zuleitungen eine ungewünschte AC Transportspannung hervorrufen kann, die durch eine zeitabhängige Leitfähigkeit gleichgerichtet wird. Daher werden Unterscheidungsmerkmale der beiden Transportmechanismen benötigt. Dabei, so stellt sich heraus, ist die Abhängigkeit vom Magnetfeld entscheidend. Während die gepumpte Ladung durch eine ungerade Funktion des magnetischen Flusses beschrieben wird, ist der gleichgerichtete Strom zumindest im linearen Leitwert gerade.

Die zweite Arbeit beschäftigt sich mit dem Anteil kohärenter Prozesse beim Transport durch Quantenpunkte. Zu diesem Zweck wird ein Quantenpunkt in einen der Arme eines Aharonov-Bohm-Interferometers eingebettet. In früheren theoretischen sowie experimentellen Arbeiten wurde beobachtet, dass Cotunnel-Prozesse, welche den Spin des Quantenpunkts umdrehen, eine wichtige Quelle für Dekohärenz sind. Um die Rolle des Spins im Detail zu beleuchten, betrachten wir eine ferromagnetische und eine normalleitende Zuleitung. Hauptsächlich interessieren uns in dieser Arbeit zwei Fragen: (1) Welcher Anteil am gesamten Strom durch einen Einzellevel-Quantenpunkt, der schwach an Elektroden gekoppelt wird, ist kohärent? (2) Wie und unter welchen Umständen lässt sich dieser Anteil von einer Strommessung in einem Aharonov-Bohm-Ring extratrahieren? Die messbare Größe in einem solchen Experiment ist der vom magnetischen Fluss abhängige Anteil des Gesamtstroms. Es stellt sich heraus, dass die Antworten auf die beiden Fragen stark von der Position des Energielevels vom

Quantenpunkt, von der Polarisierung des Ferromagneten sowie von der Transportrichtung abhängen. Insbesondere sind der flussabhängige und der kohärente Anteil nicht notwendigerweise identisch.

Die Hauptmotivation für die dritte Arbeit ist es, Signaturen für nichtlokale Andreev-Reflexion in Quantenpunkten zu finden. Bei einem solchen Prozess teilt sich ein Cooper-Paar in zwei Einzelelektronen auf, welche in einem kohärenten Prozess in unterschiedliche Quantenpunkte transportiert werden. Wir betrachten einen Aufbau, bei dem zwei Quantenpunkte an denselben Supraleiter und jeder Quantenpunkt zusätzlich an einen Normalleiter gekoppelt werden. In vorherigen Arbeiten wurde eine Transportspannung zwischen dem Supraleiter und den Normalleitern angelegt. Drei verschiedene Prozesse sind dann am Transport beteiligt. Neben den nichtlokalen Andreev-Reflexionen treten auch lokale Andreev-Reflexion, wo beide Elektronen eines Cooper-Paars auf den gleichen Quantenpunkt tunneln, und Einzelelektronen-Tunneln auf. Dies verkompliziert die Identifikation nichtlokaler Andreev-Reflexionen. Daher schlagen wir adiabatisches Pumpen als Transportmechanismus vor. Die beiden Pumpparameter sind die Energielevel der beiden Quantenpunkte. Da diese räumlich voneinander getrennt sind und ein endliches Pumpsignal zwei Pumpparameter erfordert, beruht ein Netto-Transport auf Nichtlokalität. Somit tragen lokale Andreev-Reflexionen nicht zum gepumpten Strom bei. Um letztlich nichtlokale Andreev-Reflexionen ausfindig zu machen, müssen sie vom Einzelelektronen-Tunneln unterschieden werden, welches durch Überlagerungen von Zuständen der beiden Quantenpunkte entsteht. Wir finden heraus, dass durch die Abhängigkeit des Stroms zum einen vom mittleren Energielevel und zum anderen von der Symmetrie der Kopplungsstärken zwischen den Quantenpunkten und den Normalleitern die beiden Prozesse eindeutig voneinander unterschieden werden können. Dies ist ein wichtiger Vorteil des Pumpens, beispielsweise im Vergleich zur linearen Leitfähigkeit.

Schließlich untersuchen wir den AC-Josephson-Transport durch stark wechselwirkende Quantenpunkte. Zu diesem Zweck erweitern wir eine diagrammatische Theorie für den DC-Transport auf den zeitabhängigen Fall, wobei die Coulomb-Wechselwirkung nicht-störungstheoretisch behandelt wird. Dieser allgemeine Formalismus wird für die Beschreibung eines Systems benutzt, bei dem ein Quantenpunkt an einen Normalleiter und zwei Supraleiter mit unendlicher Energielücke gekoppelt wird. Da der AC-Josephson-Effekt zwei Supraleiter erfordert, beruht in der niedrigsten Ordnung der Störungsentwicklung ein endliches AC-Signal zwischen dem Quantenpunkt und dem Supraleiter $S1$ auf der Induzierung supraleitender Korrelationen auf den Quantenpunkt ausschließlich durch Supraleiter $S2$. Der größte Vorteil den Normalleiter einzusetzen besteht darin, dass die mittlere Quantenpunkt-Besetzung leicht durch das chemische Potential des Normalleiters geregelt werden kann. Somit lässt sich im betrachteten System im Gegensatz zu konventionellen Josephson-Kontakten nicht nur die Frequenz, sondern auch die Amplitude des AC-Signals mit einer DC-Transportspannung kontrollieren, die zwischen dem Normalleiter und den Supraleitern angelegt wird.

English Abstract

The present thesis is composed of four different works. All deal with coherent transport through interacting quantum dots, which are tunnel-coupled to external leads. There a two main motivations for the use of quantum dots. First, they are an ideal device to study the influence of strong Coulomb repulsion, and second, their discrete energy levels can easily be tuned by external gate electrodes to create different transport regimes. The expression of coherence includes a very wide range of physical correlations and, therefore, the four works are basically independent of each other. Before motivating and introducing the different works in more detail, we remark that in all works a diagrammatic real-time perturbation theory is used. The fermionic degrees of freedom of the leads are traced out and the elements of the resulting reduced density matrix can be treated explicitly by means of a generalized master equation. How this equation is solved, depends on the details of the problem under consideration.

In the first of the four works adiabatic pumping through an Aharonov-Bohm interferometer with a quantum dot embedded in each of the two arms is studied. In adiabatic pumping transport is generated by varying two system parameters periodically in time. We consider the two dot levels to be these two pumping parameters. Since they are located in different arms of the interferometer, pumping is a quantum mechanical effect purely relying on coherent superpositions of the dot states. It is very challenging to identify a quantum pumping mechanism in experiments, because a capacitive coupling of the gate electrodes to the leads may yield an undesired AC bias voltage, which is rectified by a time dependent conductance. Therefore, distinguishing features of these two transport mechanisms are required. We find that the dependence on the magnetic field is the key feature. While the pumped charge is an odd function of the magnetic flux, the rectified current is even, at least in the linear-conductance regime.

The second work deals with the ratio of coherent processes in transport through quantum dots. To this end, a quantum dot is embedded in one of the arms of an Aharonov-Bohm interferometer. In former theoretical as well as experimental works it has been observed that an important source of decoherence are cotunneling processes that flip the dot's spin. In order to elucidate the role of spin in more detail, we assume one of the leads to be ferromagnetic and the other one to be normal. The main motivations of our work are the two questions: (1) What fraction of the total current through a single-level quantum dot weakly coupled to the electrodes is coherent? (2) How and under which circumstances can this fraction be extracted from a current measurement in an Aharonov-Bohm setup? The measurable quantity in such an experiment is the magnetic-flux dependent ratio of the total current. It turns out that the answers of the two questions strongly depend on the dot level position, the polarization of the ferromagnet, and the transport direction. Especially the flux-dependent and the coherent ratios are not necessarily the same.

The main motivation of the third work is to identify crossed Andreev reflection in quantum dots, that is, a Cooper pair splits into two single electrons, which are transferred into different quantum dots in one coherent process. We consider a setup, where two quantum dots are tunnel coupled to the same superconductor and each dot is

additionally coupled to a normal conductor. In previous works a bias voltage has been applied between the superconductor and the normal conductors. Then, three processes sustain transport. Beside crossed Andreev reflection also local Andreev reflection, where both electrons of the Cooper pair tunnel into the same dot, and single-particle tunneling occur. This complicates the identification of crossed Andreev reflection. Therefore, we propose the transport mechanism of adiabatic pumping in the absence of any bias voltage. The two pumping parameters are the energy levels of the two dots. Since they are spatially separated and a finite pumping signal requires two pumping parameters, a net transport relies on nonlocality. As a consequence local Andreev reflection does not contribute to the pumping current. In order to clearly identify crossed Andreev reflection it has to be distinguished from single-particle tunneling arising due to superpositions of the states of the two dots. We find that the dependence of the current on the average dot level position as well as the symmetry of the coupling strengths between dots and normal conductors clearly distinguishes the two processes from each other. This is an important advantage of the pumping current, for example, in comparison to the linear conductance.

Finally, we focus on the AC Josephson transport through a strongly interacting quantum dot. To this end, we extent a diagrammatic theory on the DC Josephson transport to the time dependent case taking into account the Coulomb repulsion non-perturbatively. This general formalism is applied to a three-terminal device, where a quantum dot is tunnel coupled to a normal conductor and two superconductors with an infinite superconducting gap. Since the AC Josephson effect requires the presence of two superconductors, in lowest order of the perturbation expansion a finite AC signal between dot and superconductor $S1$ relies on the induction of superconducting correlations on the dot exclusively by superconductor $S2$. The main advantage of employing a normal conductor is that the average dot occupation can easily be tuned by the chemical potential of the normal conductor. Therefore, in the considered three-terminal device, in contrast to conventional Josephson junctions, not only the frequency but also the amplitude of the AC signal can be controlled by a DC bias voltage applied between the normal conductor and the two superconductors.

Contents

1 Introduction **1**

2 Physical Background **5**
2.1 Quantum Dots . . . 5
2.1.1 Transport Properties . . . 5
2.1.2 Quantum Coherence . . . 8
2.1.3 Model of a Single-Level Quantum Dot . . . 12
2.2 Electron Pumping . . . 13
2.2.1 Experimental Realization . . . 14
2.2.2 Theory of Pumping . . . 15
2.2.3 Limit of Weak Adiabatic Pumping . . . 17
2.3 Superconducting Heterostructures . . . 18
2.3.1 Andreev Reflection . . . 19
2.3.2 Josephson Effect . . . 21
2.3.3 BCS Hamiltonian . . . 22

3 Real-Time Transport Theory **25**
3.1 Reduced Density Matrix . . . 25
3.2 Generalized Master Equation . . . 26
3.3 Current Formula . . . 28

4 Adiabatic Pumping through a Double-Dot ABI **29**
4.1 Model . . . 29
4.2 Real-Time Approach to Adiabatic Pumping . . . 30
4.3 Results . . . 32
4.3.1 Weak Adiabatic Pumping . . . 32
4.3.2 Comparison with Rectification . . . 35
4.4 Conclusions . . . 35

5 Spin-Dependent Transport through Quantum-Dot ABIs **37**
5.1 Model . . . 38
5.2 Method . . . 39
5.3 Results . . . 41
5.3.1 Charge Current . . . 41
5.3.2 Fraction of Coherent Transport . . . 45
5.3.3 Visibility . . . 46
5.3.4 Visibility versus Coherence . . . 47
5.4 Conclusions . . . 48

6 Adiabatic Pumping in a Double-Dot Cooper-Pair Beam Splitter 49
6.1 Model . . . 50
6.1.1 Double-Dot Device . . . 51
6.1.2 Single-Dot Device . . . 52
6.1.3 Large-Δ Limit . . . 52
6.2 Method . . . 52
6.3 Results . . . 54
6.3.1 Local Andreev Reflection . . . 54
6.3.2 Crossed Andreev Reflection . . . 57
6.3.3 Single-Particle Transport . . . 59
6.4 Conclusions . . . 60

7 AC Josephson Transport through Interacting Quantum Dots 63
7.1 Model . . . 64
7.2 Method . . . 65
7.3 Results . . . 67
7.4 Conclusions . . . 71

A Diagrammatic Rules 73

B Sequential Tunneling vs. Cotunneling 77

C Calculation of a Cotunneling Rate 78

D Rates for the AC Josephson Transport 79

Bibliography 81

1 Introduction

In 1924 the French physicist Louis de Broglie made a fascinating theoretical prediction in his PhD thesis: Particles of matter, like electrons, also have wave like properties. Three years later this was confirmed by two independent electron diffraction experiments performed by Clinton Davisson, Lester Germer, and George Paget Thomson. The discovery and description of the wave-particle dualism of electrons changed the conception of matter in a very wide range and, therefore, resulted in Nobel prizes for de Broglie (1929) as well as Davisson and Thomson (1937). As a consequence of their wave properties, coherence becomes an important issue for transport of electrons. In its most general sense coherence simplify means the property that the electrons' wave functions correlate. The kind of correlations in the experiment mentioned above are interference effects, which strongly influence electronic transport. But also completely different phenomena can be explained by means of correlating wave functions. A very prominent example is the formation of a Cooper pair by two electrons in a superconductor. Of course, the extent of phenomena related to coherence strongly depends on the other specific ingredients of electronic transport. Especially, Coulomb interaction may have a substantial effect. Very convenient devices to study the interplay between coherence and interaction effects are quantum dots. A quantum dot is a region in condensed matter (e.g. semiconductor) which is strongly confined in all three spatial dimensions. Due to this confinement, electrons occupying the dot experience a strong Coulomb repulsion. Another important consequence is the formation of discrete dot energy levels. Since the position of the levels can easily be tuned be external gate electrodes, very different transport regimes can be investigated by means of the same quantum dot. A common theoretical description of quantum dots is the single-level model considering only one spin-degenerate orbital. This is an appropriate assumption even if a quantum dot accommodates many levels as long the distance between the levels is large enough so that only one level participates in transport. In order to study transport properties, quantum dots are attached to external electrodes in a variety of different geometries.

In this thesis we study transport of diverge systems, where the interplay of coherence and Coulomb interactions affects transport in completely different ways. First, we consider properties of *adiabatic pumping* through quantum dots. This is a transport mechanism in the absence of any bias voltage. A net transport is mediated by the explicit time dependence of at least two system parameters. The classification of pumping is related to coherence. While in classical pumping the mechanism has strong similarities, for example, to processes in the gastrointestinal tract, quantum pumping has no classical analog and relies purely on coherent superpositions. For the investigation of superpositions Aharonov-Bohm interferometers (ABIs) are convenient setups. Quantum dots can be embedded in either one or in both of the two arms.

Not only quantum pumping but interference effects in general can be studied in these kind of devices. To this end, the dependence of the current through an ABI on the magnetic flux penetrating the ABI plays an important role. Since this dependence relies on interference, coherence is an essential requirement. The detection of the path an electron has taken through the interferometer destroys coherence. One possibility of this which-path detection is a spin-flip cotunneling process through a quantum dot in one of the interferometer arms. The transferred electron leaves a trace in the environment in form of changing the spin state of the quantum dot. However, coherence itself cannot be measured. The flux dependent part of the total current is somehow related to coherence but not exactly equivalent. One main focus of this thesis is to quantify this relation.

But also coherence in the sense that Cooper pairs are formed by correlated electrons is going to be addressed in this thesis. In heterostructures containing superconductors different transport processes arise. In normal conductor-superconductor junctions Cooper pairs can be transferred into or out of the superconductor by *Andreev reflection*. In such a process an electron in the normal conductor that impinges on the interface is retroreflected as a hole while a Cooper pair is transferred into the superconductor. In junctions with more than one normal conductor also *crossed Andreev reflections* may occur, i.e. the two electrons forming the Cooper pair stem from different normal conductors (or tunnel into different normal contacts in the opposite transport process). Andreev reflection and even crossed Andreev reflection also occur in superconductors contacted to quantum dots. However, the distinction between these two processes is challenging. Up to now the influence of the conductance through one dot on the conductance through another dot has been the key feature. We propose the transport mechanism of adiabatic pumping to identify crossed Andreev reflection. A convenient choice of the pumping parameters excludes transport mediated by local Andreev reflection.

Another fascinating transport process arises in *Josephson junctions*, where two different superconductors are linked, for example, by an insulator. The macroscopic phase, which is a specific property of each superconductor, plays an important role in this context. Whenever the macroscopic phases of the two superconductors differs a supercurrent, mediated by Cooper pairs, builds up, even in the absence of any bias voltage. Furthermore, by applying a DC bias voltage an AC signal is generated, whose frequency is proportional to the voltage. These properties of Josephson junctions have become famous as the *DC* and the *AC Josephson effect*. Their discovery has been awarded with the Nobel prize in 1973. There are some possibilities for the device placed between the two superconductors in a Josephson junction. One of them is a quantum dot. As in the setups mentioned above the motivation for the use of quantum dots is their easy tuneability and that strong Coulomb repulsion can be included.

The variety of useful applications of quantum dots is obviously very large and the systems mentioned so far are only an incomplete sketch, picked due to their relevance for this thesis. Also a lot of theoretical methods for the calculation of transport through quantum dots exist. In this thesis we use a diagrammatic real-time perturbation expansion in tunnel coupling. The fermionic degrees of freedom of the leads are traced out and the resulting reduced density matrix is treated explicitly by means of a Keldysh

technique. Then, the reduced density matrix can be obtained by solving a generalized master equation.

The thesis is structured as follows. First, we give an overview of the most relevant physical principles, see Chapter 2. This includes the properties of quantum dots especially concerning coherence in transport, an introduction to pumping with a special focus on the adiabatic limit, and the different transport processes through superconducting heterostructures. In Chapter 3 we give a brief introduction to the used diagrammatic technique and derive the generalized master equation. The specific details of their solution are not given in this chapter but in the corresponding result chapters. The main part of this thesis are the four result chapters 4, 5, 6, and 7. Except their common context of coherent transport through interacting quantum dots, the four works are independent of each other.

The first of the four works is about adiabatic pumping through an ABI, where a quantum dot is embedded in each of the two arms, see Chapter 4. We choose the energy levels of the two dots as pumping parameters. Basically there are two different motivations for this work. At first, the two pumping parameters are located in two spatially separated arms of the interferometer. Due to this nonlocality pumping has to rely on coherent superpositions. Therefore, it is a convenient setup to investigate the properties of quantum pumping and especially the influence of strong Coulomb repulsion on this transport mechanism. The second motivation is to find features exclusively appearing in this mechanism. In former experiments quantum pumping has been obscured by rectification effects, which arose due to a capacitive coupling of the gate voltage to the leads. We compare the features of pumping and rectification, in order that both can be distinguished from each other in experiments.

In Chapter 5 we investigate the measurability of coherence of transport through a quantum dot. To this end, a quantum dot is embedded in one arm of an ABI. Although transport through quantum dots is at least partially coherent spin-flip processes lead to dephasing. In order to quantify the role played by the spin we attach the ABI to a ferromagnet and a normal conductor. Interesting phenomena as for example spin accumulation on the dot arise and influence the coherence in a nontrivial way. We focus mainly on two questions (1) What fraction of the total current through a single-level quantum dot weakly coupled to the electrodes is coherent? (2) How and under which circumstances can this fraction be extracted from a current measurement in an Aharonov-Bohm setup?

The transport mechanism in Chapter 6 is again adiabatic pumping. However, the context and motivation for the use of this transport mechanism is completely different to Chapter 4. We aim for an identification of crossed Andreev reflection processes. To this end, we consider a setup where a superconductor is tunnel coupled to two quantum dots and each quantum dot is additionally coupled to a normal conductor. This is an ideal setup to identify crossed Andreev reflection. The two dot levels are chosen as pumping parameter. Since a finite pumping signal always requires two pumping parameters, only nonlocal processes contribute to transport. As a consequence the undesired processes of local Andreev reflections are excluded from transport. Besides crossed Andreev reflection, single-electron pumping is the only mechanism leading to a finite signal. Therefore, we investigate features clearly distinguishing both from each

other. It turns out that the key distinguishing feature is not present in the linear conductance but exclusively arises in pumping.

The last of our four works is about the AC Josephson transport through an interacting quantum dot, see Chapter 7. Since Josephson currents are carried by Cooper pairs consisting of two electrons the Coulomb repulsion between electrons is crucial for transport. Placing a quantum dot between two superconductors enables the investigation of the interesting interplay of a strong Coulomb repulsion with superconducting properties in AC transport. For this purpose, we extend a real-time perturbation theory on interacting quantum dots tunnel coupled to superconducting leads to account for a time-dependent current. This general theory is applied in the limit of an infinite superconducting gap, where we include an additional normal conductor that guarantees a certain dot occupation. We focus on the lowest order contribution of the perturbation expansion. Then, a nonvanishing Josephson current requires superconducting correlations induced on the quantum dot by the proximity of the superconducting leads. Finally, we study the influence of the stationary chemical potential of the normal conductor on the amplitude of the AC signal.

2 Physical Background

2.1 Quantum Dots

A quantum dot (QD) is a region in condensed matter (e.g. semiconductor) which is strongly confined in all three spatial dimensions. This confinement has two important consequences. On the one hand the spectrum of the QD is discrete and on the other hand the capacitance is small. To achieve a discretization the size of a QD has to be in the range of the electron's Fermi wave length, i.e., typically a few nanometers up to several hundred nanometers. Due to its similarities to atoms QDs are also referred to as artificial atoms. QDs are of great relevance because its optical as well as electronic properties can be controlled by external gate voltages. They can, e.g., be realized in two dimensional electron gases,[1–3] in nanowires,[4–6] or in carbon nanotubes.[7–9] A typical setup is schematically shown in Fig. 2.1 where a QD is tunnel coupled to two reservoirs.

Some formulations of Sec. 2.1.2 and Sec. 2.1.3 have already been published in Ref. 10.

2.1.1 Transport Properties

Coulomb Blockade

We focus on the setup schematically shown in Fig. 2.1 where a QD is weakly tunnel coupled to two reservoirs and an external gate voltage V_G is applied. The external electrodes can be described by the three capacitances C_L, C_R (for the left and right reservoir, respectively), and C_G (for the contact to the external gate electrode). The total capacitance of the dot is the sum of all single capacitances $C = C_L + C_R + C_G$.

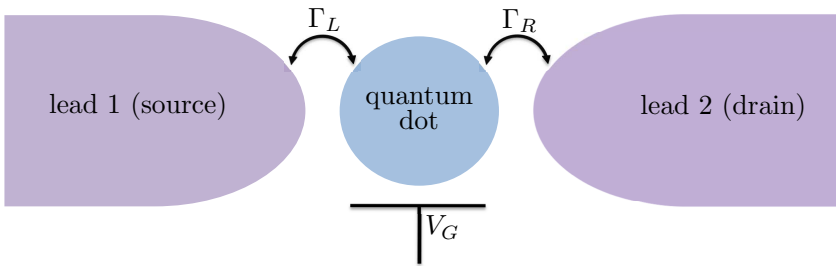

Figure 2.1: Scheme of a quantum dot tunnel coupled to two reservoirs. The dot's spectrum can be varied by an external gate voltage. The tunnel coupling strengths between dot and the left and right leads are denoted by Γ_L and Γ_R, respectively.

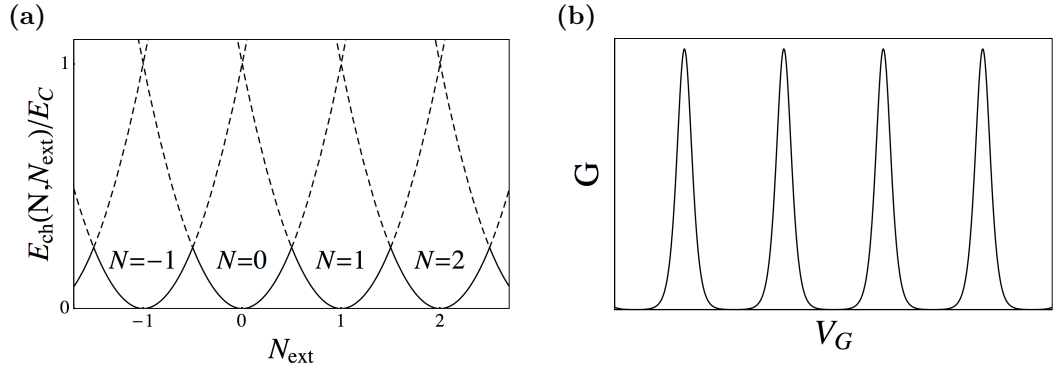

Figure 2.2: (a) Charging energy as a function of the external charge eN_{ext}. (b) Coulomb oscillations of the conductance as a function of the gate voltage V_G. The peaks and dips correspond to N_{ext} being half-integer and integer, respectively.

In equilibrium the energetically most favorable number of electrons occupying the dot corresponds to the external charge $eN_{\text{ext}} = C_L V_L + C_R V_R + C_G V_G$, where $eV_L = \mu_L$ and $eV_R = \mu_R$ are the chemical potentials of the left and right reservoirs, respectively. The charging energy of the dot is

$$E_{\text{ch}}(N, N_{\text{ext}}) = E_C(N - N_{\text{ext}})^2 \tag{2.1}$$

with $E_C = \frac{e^2}{2C}$ being the charging scale. The charging energy is a parabolic function of N_{ext}. Hence the number of electrons occupying the dot N is tunable by the gate voltage V_G, see Fig. 2.2(a). Obviously, the ground state is degenerate for N_{ext} being half-integer while the excitation energy is maximal for integer values of N_{ext}. In the limit of a large charging energy of one electron $E_C \gg k_B T, \mu_L, \mu_R$ the dot can only be excited close to the degeneration points. Since transport always requires a change of occupation it is suppressed whenever the external charge eN_{ext} is far away from the degeneration points. This effect is called *Coulomb blockade*. As a consequence of the Coulomb blockade the conductance through the QD strongly depends on the gate voltage V_G. A continuous enhancement of the gate voltage yields oscillations of the conductance, the so called *Coulomb oscillations*, see Fig. 2.2(b). The peaks and valleys correspond to N_{ext} being half-integer and integer, respectively. The width of the peaks is governed by temperature and the tunnel-coupling strengths Γ_L to the left lead and Γ_R to the right lead.

So far we did not consider the discretization of the dot's spectrum. However, in QDs the distances between the discrete energy levels ε_l are usually too large to be neglected. Therefore, the total dot energy is given by

$$E_N = E_{\text{ch}}(N, N_{\text{ext}}) + \sum_{l=0}^{N} \varepsilon_l \,. \tag{2.2}$$

In order to change the occupation of the dot from N to $N+1$ the excitation energy $E_{N+1} - E_N$ is required. Transport is enhanced whenever this excitation energy (mea-

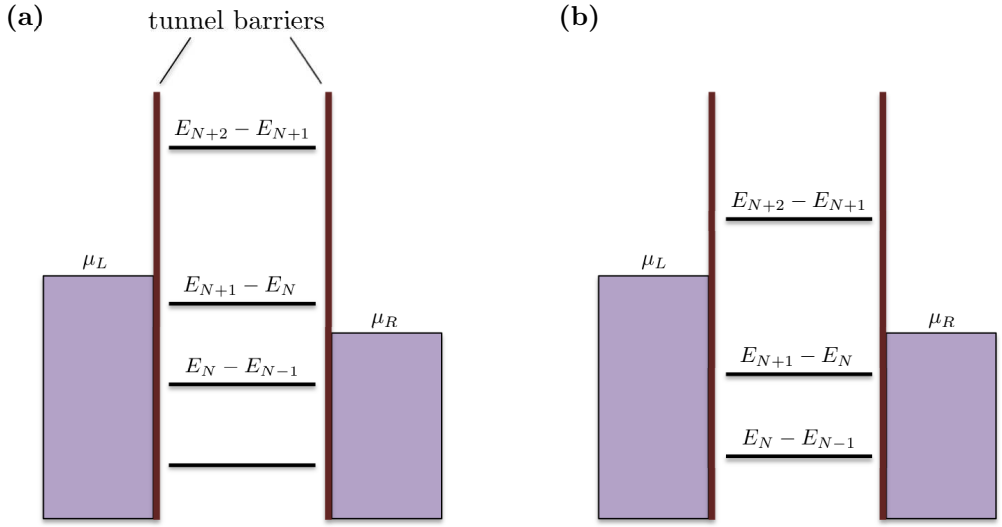

Figure 2.3: Schematic energy spectrum of a quantum dot (a) in resonance and (b) out of resonance with the leads.

sured from the leads' Fermi energy) lies between the chemical potentials of the two leads, $\mu_L > E_{N+1} - E_N > \mu_R$. A situation where the dot is in resonance and out of resonance with the leads is schematically shown in Fig. 2.3(a) and (b), respectively. The underlying tunneling processes are discussed in the following subsection.

Tunneling Processes

The transport through the dot is sustained by different tunneling processes which can be related to the different orders of a perturbation expansion in the tunnel-coupling strengths (Γ_L and Γ_R). Processes in first order describe *sequential tunneling*. In a sequential tunneling process an electron is transferred from the source lead onto the dot, see Fig. 2.4(a), changing its occupation from N to $N + 1$. For a net transfer from source to drain an electron tunnels in another process from the dot into the drain lead. These two tunneling processes are completely uncorrelated. This is described by the *orthodox theory*.[11,12] Sequential tunneling processes are the dominant transport processes as long as the dot is in resonance with the leads, see Fig. 2.3 (a). However, in an off-resonant transport regime, see Fig. 2.3 (b), sequential tunneling is exponentially suppressed for low temperatures due to the Coulomb blockade.

Inside the Coulomb blockade regime the dominant transport process is *cotunneling*. It is described by the second order contributions and, in contrast to sequential tunneling, is only algebraically suppressed. A cotunneling process consists of two tunneling events which are quantum mechanically correlated.[13] An electron tunnels onto the dot and an electron tunnels out of the dot. Between the two tunneling processes the dot is in an intermediate state which is determined by the chronological order in which the two tunneling events take place. In Fig. 2.4(b) a cotunneling process is shown where

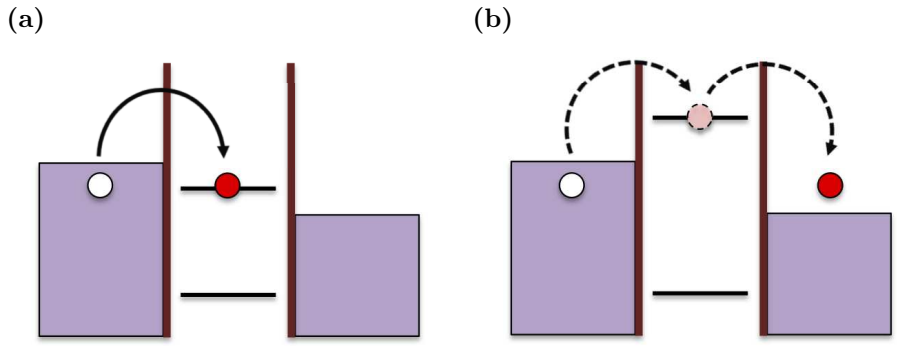

Figure 2.4: Tunneling processes through a quantum dot. (a) Sequential tunneling: An electron tunnels from the left lead onto the dot. (b) Cotunneling: Two quantum mechanically correlated tunneling events take place during one cotunneling process. First an electron tunnels from the left lead onto the dot leading to a virtual occupation, then an electron tunnels from the dot onto the right lead.

first an electron tunnels onto the dot. Energy conservation is not violated because the intermediate state is only virtually occupied, i.e., the time between the two tunneling events is sufficiently small to obey the uncertainty principle. In contrast to sequential tunneling, in cotunneling an electron may conserve its phase when it is transferred through a QD. A more detailed discussion is given in Sec. 2.1.2.

For very low temperatures or high tunnel coupling strengths arbitrary high orders have to be considered. They give rise to the *Kondo effect*. Whenever the dot's total spin is $S = 1/2$, i.e., a dot with sufficiently large level spacing is occupied with an odd number of electrons, dot and lead states near the Fermi surface hybridize to a Kondo liquid.[14] The consequence is an enhancement of the conduction.

In the following of this thesis we do not deal with the Kondo effect. We restrict ourselves to the sequential tunneling and cotunneling of electrons. In Chapter 6 we also allow for Cooper pair tunneling in higher orders.

2.1.2 Quantum Coherence

In transport situations where electrons interfere not only the transport properties described in the previous subsection but also quantum coherence play an important role. We start this subsection with a brief introduction to the Aharonov-Bohm effect which is crucial for an investigation of quantum coherence in transport through quantum dots.

Aharonov-Bohm Effect

The interference of propagating electrons can be influenced by a magnetic field enclosed by the trajectories of the electrons even if the field is spatially separated from the

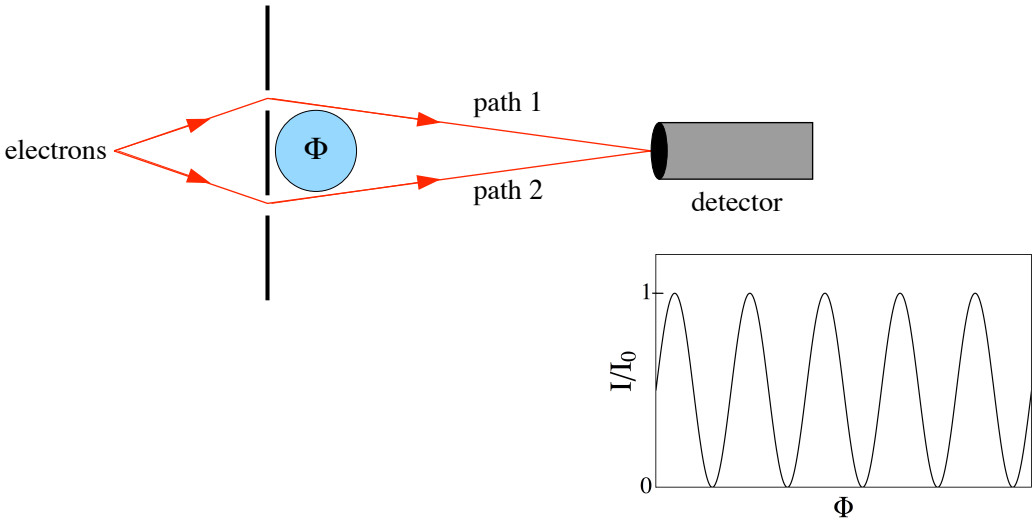

Figure 2.5: Double-slit experiment. The detected intensity oscillates with the enclosed magnetic flux.

trajectories themselves. This phenomenon was explored in 1959 by Yakir Aharonov and David Bohm and has been called *Aharonov-Bohm effect*[15] since then. In a double-slit experiment the Aharonov-Bohm effected can be illustrated in an easy way, see Fig. 2.5. Electrons impinge on the double slit, where a magnetic field is applied between the two slits. Interference effects can be observed by a detector placed behind the double-slit. The Aharonov-Bohm effect states that electrons which propagate along path 1 and path 2, respectively, experience a relative phase shift proportional to the enclosed magnetic flux. This phase difference is called *Aharonov-Bohm phase*,

$$\phi_{\mathrm{AB}} = 2\pi\Phi/\Phi_0\,, \tag{2.3}$$

where $\Phi_0 = 2\pi\hbar c/e$ is the flux quantum. Due to interference behind the double slit the detected intensity is strongly affected by the phase shift. The probability of observing a particle in the detector is then given by

$$|\Psi_{\mathrm{det}}|^2 = |\Psi_1 + \Psi_2 e^{i\phi_{\mathrm{AB}}}|^2 = |\Psi_1|^2 + 2|\Psi_2|^2 + |\Psi_1||\Psi_2|\cos\phi_{\mathrm{AB}} \tag{2.4}$$

with Ψ_i being the wavefunction for a transmission through path i. A variation of the magnetic flux, therefore, yields oscillations of the detected intensity, the *Aharonov-Bohm oscillations* (ABOs).

Quantum Coherence of Transport through Quantum Dots

Coherence of transport can be investigated in Aharonov-Bohm interferometers (ABIs) consisting of two reservoirs coupled to each other by two different arms. Quantum dots can be embedded in one or in both of the two arms, see Fig. 2.6. In these so called

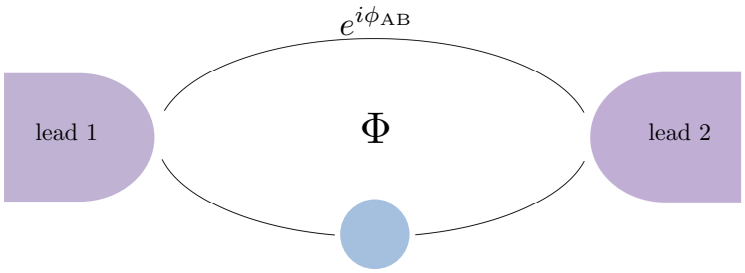

Figure 2.6: Setup of a single-quantum-dot Aharonov-Bohm interferometer. Propagation through different paths leads to a relative phase ϕ_{AB}, which is proportional to the enclosed magnetic flux Φ.

quantum-dot Aharonov-Bohm interferometers (QD-ABIs) the interplay between interference and Coulomb interaction has been extensively studied both experimentally[16–24] and theoretically.[25–45] Observed oscillations of the current through QD-ABIs as a function of the magnetic flux prove that transport through quantum dots is at least partially coherent.[16–24] The degree of coherence may be suppressed by interaction. This can, e.g., be studied in a controlled way by electrostatically coupling a quantum-point contact (QPC) to the quantum dot in the ABI. The current through the QPC serves as a which-path detector that diminishes the amplitude of the interference signal.[24–27] But even in the absence of any coupling to the outside world the degree of coherence may be limited by Coulomb interaction among the electrons within the QD-ABI. Then, the only source of decoherence is connected to the spin degree of freedom in the QD.[28,29] In general, transport through a QD can be divided into spin-flip and non-spin-flip processes. Only the non-spin-flip processes are coherent. Spin-flip processes due to spin-orbit coupling are neglected in the following considerations. For simplicity we assume a single-level quantum dot, i.e., the dot can only be empty, singly-occupied (with spin up or spin down), or doubly occupied (with spin up and spin down). This assumption is justified as long as the level spacing on the dot is larger than temperature and bias voltage in such a way that only one orbital participates in transport. When the dot is initially empty or doubly-occupied, transferred electrons keep their spin orientation, and the transport is fully coherent, see Fig. 2.7(a) and (b), respectively. In contrast, when the dot is occupied with a single electron, then the transferred electron may either keep, see Fig. 2.7(c) and (d), or flip its spin, see Fig. 2.7(e) and (f). The intermediate state can either be a doubly-occupied, see Fig. 2.7(c) and (f), or an empty dot, see Fig. 2.7(d) and (e). In the limit of noninteracting electrons spin flips do not appear and transport is completely coherent. This can be understood in two different ways. On the one hand the two spin channels do not interact and can hence be treated independently. Since spin degeneration does not have to be taken into account within one channel spin flips do not appear. On the other hand one could describe the spin-flip processes in Fig. 2.7(e) as particlelike and the process in Fig. 2.7(f) as holelike. Both processes come with opposite sign but have the same amplitude in the absence of any Coulomb repulsion. Therefore, both processes cancel each other exactly.[29]

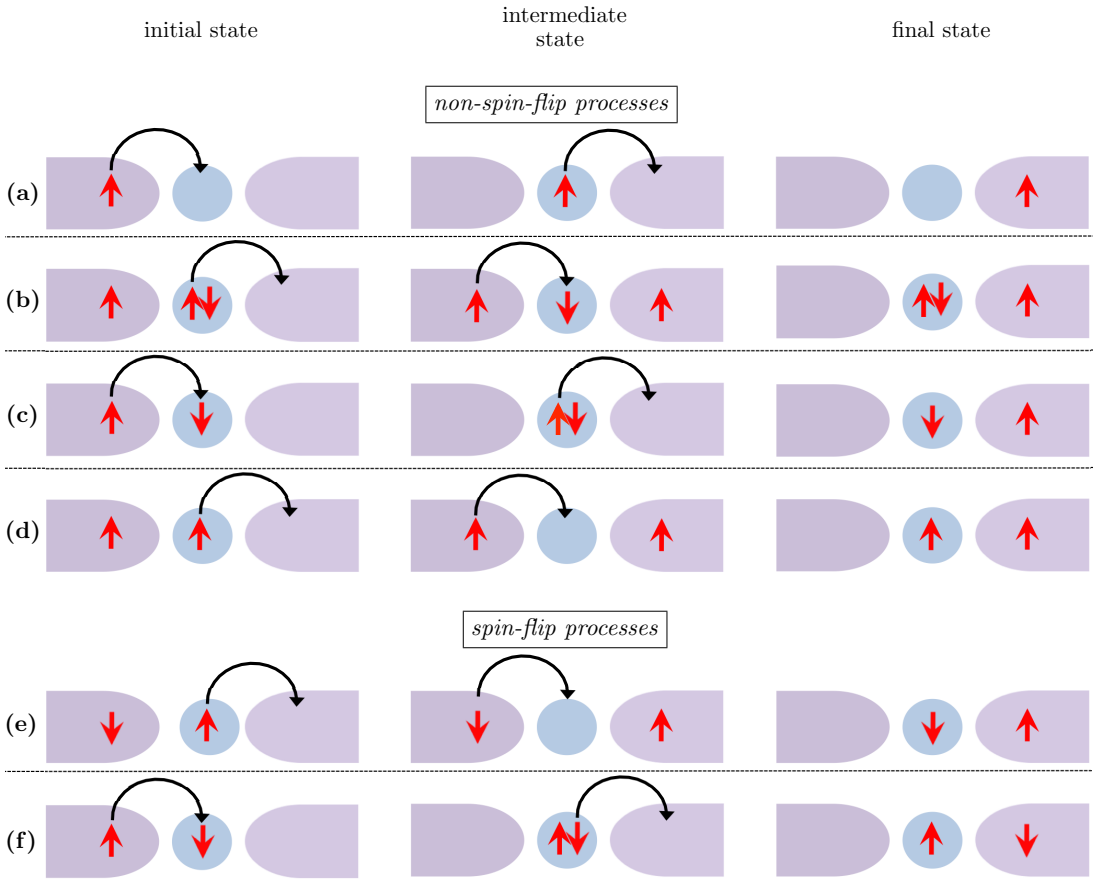

Figure 2.7: Cotunneling processes through a single-level quantum dot. For the dot being initially (a) empty, (b) doubly occupied or (c)-(f) singly occupied. The spin is flipped only in (e) and (f).

But what is the fraction of coherent transport processes to the total transport in the presence of any Coulomb repulsion? As long as the reservoirs are normal conductors and the intra-dot Coulomb repulsion is infinite excluding double occupation the fraction of the coherent to the total linear conductance is $c = 1/[1 + f(\varepsilon)]$. Here, $f(\varepsilon)$ is the Fermi function and ε the quantum-dot level, measured relative to the Fermi energy of the leads. It was theoretically predicted that this fraction c of coherent transport can be extracted from measuring the Aharonov-Bohm oscillation amplitude as a function of the level energy for a QD embedded in an Aharonov-Bohm ring.[28,29] This prediction was qualitatively confirmed in experiments.[16,17] Figure 2.8(a) shows a scanning electron micrograph of an ABI with QD embedded in the lower arm realized in a GaAs/AlGaAs two-dimensional electron gas.[16] The dot levels' energies and with it the number of electrons occupying the dot can be controlled by the gate voltage V_g. A variation of the magnetic flux leads to Aharonov-Bohm oscillations whose amplitude strongly depends on the gate voltage V_g, see Fig. 2.8(b). The amplitude averaged over

ten periods around $B = 0.485T$ as a function of the gate voltage V_g is shown in Fig. 2.8(c). An asymmetric double peak is visible around each resonance. At the center of the peak the amplitude is reduced because scattering processes experience a phase shift of π whenever a scattering region is tuned through resonance.[46] The asymmetry can be explained by the transport processes described above. Between the two double-peaks (peak 5 and 6 in Fig. 2.8) the dot is occupied with $2N + 1$ electrons, an odd number. This corresponds to a singly-occupied single-level quantum dot. On the left side of peak 5 the dot is occupied with $2N$ electrons and on the right side of peak 6 with $2N + 2$ electrons, which can be related to an empty and doubly-occupied dot, respectively. Each double peak has a side where an odd number and a side where an even number of electrons occupy the dot. Only for an odd occupation spin flip processes appear yielding dephasing. This explains the asymmetry of the peaks. Obviously, the

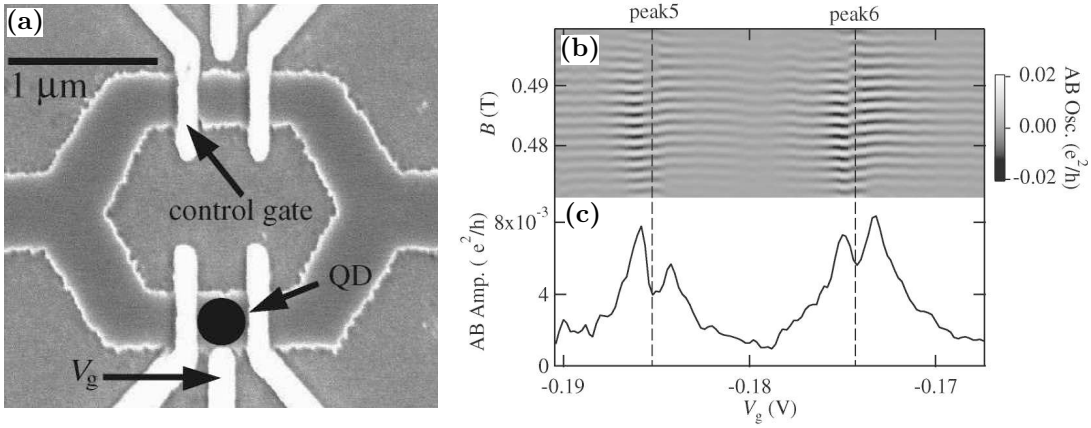

Figure 2.8: Experiment on coherence of transport through quantum dots. Reprinted figures with permission from H. Aikawa, K. Kobayashi, A. Sano, S. Katsumoto, and Y. Iye, Phys. Rev. Lett. **92**, 176802 (2004). Copyright 2004 by American Physical Society. (a) Scanning electron micrograph of the QD-ABI. (b) Gray-scale plot of the Aharonov-Bohm component of the current against the gate voltage V_g and the magnetic field B. (c) Averaged amplitude of ABOs as a function of the gate voltage.

spin plays a crucial role for the coherence of transport through quantum dots. In order to substantiate this role, in Chapter 5 we investigate a QD-ABI where spin-symmetry is broken by employing a lead with finite spin polarization.

2.1.3 Model of a Single-Level Quantum Dot

We describe a single-level quantum dot tunnel coupled to electron reservoirs as for a two-terminal setup shown in Fig. 2.1. In this thesis we restrict ourselves to a single level which is justified as long as level spacing is large enough that only one level

participates in transport. The total Hamiltonian consists of three building blocks.

$$H = H_{\rm dot} + H_{\rm leads} + H_{\rm tunn} \tag{2.5}$$

The QD accommodates a single, spin-degenerate level, i.e, the dot can be empty $|0\rangle$, singly occupied with spin up $|\uparrow\rangle$, singly occupied with spin down $|\downarrow\rangle$ or doubly occupied $|\uparrow\downarrow\rangle$. It is described by the Anderson-impurity model:[47]

$$H_{\rm dot} = \varepsilon \sum_{\sigma} n_\sigma + U n_\uparrow n_\downarrow \,. \tag{2.6}$$

with $n_\sigma = d_\sigma^\dagger d_\sigma$ and $d_\sigma^\dagger$ (d_σ) being the creation (annihilation) operator for an electron with spin σ on the QD. The dot-level position is denoted by ϵ and the onsite Coulomb-repulsion energy by U.

The leads are large reservoirs, which in principle can be normal conductors, ferromagnets, or superconductors. Superconductors and ferromagnets are introduced in Sec. 2.3.3 and Sec. 5.1, respectively. Here, we focus on noninteracting normal conductors whose Hamiltonian reads,

$$H_{\rm leads} \;=\; \sum_{rk\sigma} \varepsilon_{rk} c_{rk\sigma}^\dagger c_{rk\sigma} \,, \tag{2.7}$$

where $c_{rk\sigma}^\dagger$ ($c_{rk\sigma}$) is the creation (annihilation) operator for an electron in lead r with momentum k and spin σ. The energy of an electron ε_{rk} is spin-independent.

The tunnel coupling between the dot and the leads is modeled by the tunneling Hamiltonian:

$$H_{\rm tunn} \;=\; \sum_{rk\sigma} t_r c_{rk\sigma}^\dagger d_\sigma + \text{H.c.} \,. \tag{2.8}$$

We assume the tunnel-matrix elements t_r and the density of states of the leads ρ_r to be energy independent in the energy window relevant for transport. Tunnel-coupling strengths are then defined as $\Gamma_{\rm r} = 2\pi |t_{\rm r}|^2 \rho_{\rm r}$. The intrinsic line width of the dot level is the sum of the tunnel couplings, $\Gamma = \sum_r \Gamma_{\rm r}$.

2.2 Electron Pumping

The most common method to transfer charge through a scattering region is to apply a bias voltage. In this section we introduce a different transport mechanism: *pumping*. The principle of pumping is to generate transport in the absence of any bias voltage by varying certain system parameters as the potential of a scattering region or the coupling strengths to reservoirs periodically in time. It is therefore a mechanism converting an ac into a dc signal, which has been experimentally realized in different systems.[48–58] Whenever the pumping period is large compared to the dwell time of an electron in the scattering region one speaks of *adiabatic pumping*, where the system is in quasi equilibrium during the pumping process. Very often the distinction between

classical pumping and quantum pumping is made. In classical pumping electrons can be interpreted as particles without any wave properties while quantum pumping relies on coherent superposition of different electronic states.

Some formulations of Sec. 2.2.2 have already been published in Ref. 59.

2.2.1 Experimental Realization

The idea of electron pumping dates back on a theoretical work of Thouless from 1983,[60] where a quantized charge transfer is generated by varying the potential of a Schrödinger equation. Several proposals how an experimental setup could be realized followed. One idea is to place time-dependent potentials on a quantum wire.[61] Another proposal bases on inelastic absorption processes in a two-dimensional electron gas with two independent gates.[62]

One of the most prominent experiments on classical electron pumping was performed by Pothier *et al.* in 1992.[48] In this experiment two metallic islands are coupled to each other and each island is additionally coupled to a reservoir, see Fig. 2.9(a). The occupation number of the two islands N_1 and N_2 can be controlled by the gate voltages V_1 and V_2, respectively. In a so called *stability diagram*, see Fig. 2.9(b), the occupation as a function of the two gate voltages is illustrated. Inside one comb the occupation is constant. By variation of the gate voltages it is possible to propagate the charge state through different combs inside the stability diagram. The red circle in the diagram represents the cycle: $(0,0) \rightarrow (1,0) \rightarrow (0,1) \rightarrow (0,0)$, where an electron is transferred from the left into the right reservoir. The amplitude of the variation of the voltages has to be large enough to clearly propagate between the different combs (*strong pumping*). Measurements show that the pumped current is $I = e \cdot f$ with e being the elementary charge and f the pumping frequency. This result confirms that indeed one electron is transferred during one pumping cycle. Because the pumping mechanism of such a classical pump has many similarities to processes in macroscopic systems, e.g., inside the gastrointestinal tract, it is often referred to as *peristaltic pump*. Further experiments on classical pumping followed.[50–52]

In contrast to the pumping mechanism presented above, quantum pumping has no classical analogs but is a consequence of a coherent superposition of different quantum mechanical states. Experiments on quantum pumping are still very rare. The pioneering one was performed by Switkes *et al.* in 1999.[52] In this experiment a quantum dot is realized by a confined two-dimensional electron gas (2DEG), see Fig. 2.10(a). The shape of the dots' potential can be varied periodically in time by two different gate voltages, $V_{g1} \propto \sin \Omega t$ and $V_{g2} \propto \sin(\Omega t + \phi)$, where Ω is the pumping frequency. This variation is operated adiabatically, i.e., the period is large in comparison to the other time scales of the system, see Sec. 2.2.3. Additionally, a magnetic field is applied perpendicular to the 2DEG. The idea of this experiment is to induce a voltage, V_{dot}, across the quantum dot by means of pumping in absence of any bias current, $I_{\mathrm{bias}} = 0$. In good agreement with the theoretical predictions for adiabatic pumping the voltage V_{dot} shows a sinusoidal dependence on the phase difference ϕ between the two gate voltages, see Fig.2.10(b). However, the dependence on the magnetic flux as well as the amplitude strongly deviate from primal expectations. An explanation for this behavior

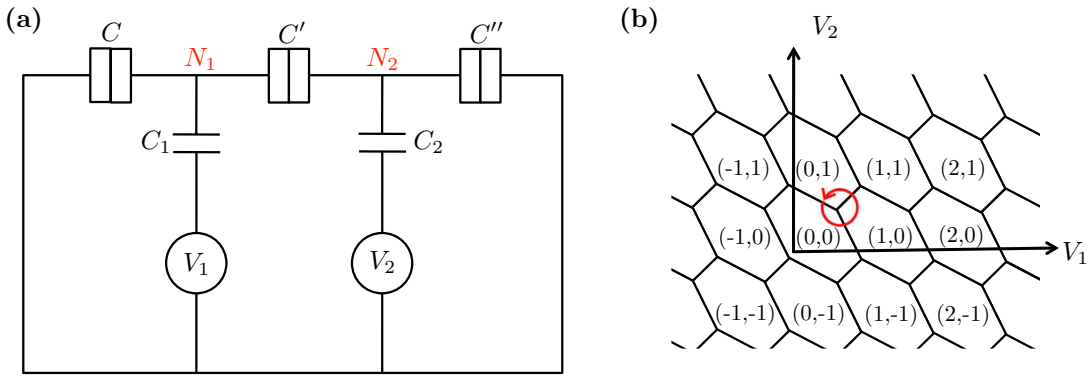

Figure 2.9: Experiment of Pothier *et al.*[48](a) Scheme of the setup. The numbers N_1 and N_2 indicate the occupation of the two islands which can be controlled by the gate voltages V_1 and V_2. Each coupling is described by a capacitance. (b) Stability diagram. The tuples (N_1, N_2) give the occupation of the two islands for the corresponding gate-voltage configuration.

is that in fact pumping is obscured by *rectification*.[63] The gate voltages capacitively couple to the reservoirs inducing an AC bias voltage. This AC signal is rectified by a time dependent conductance, i.e., a signal can be measured also averaged over one period.

The experiment of Switkes *et al.* shows that a realization of a quantum electron pump without any rectification effects is very challenging. In an experiment performed by Watson *et al.* electron transport was realized by a variation of two shape-defining gates of a GaAs quantum dot inside a Zeeman field.[53] As a result the pumped charge is again dominated by rectification effects while the spin transport relies on quantum pumping. Another very promising experiment on quantum electron pumping was performed by Giazotto *et al.* in 2011.[58] The setup consists of an InAs nanowire embedded in a superconducting quantum interference device (SQUID). Transport through the nanowire is generated by cyclic modulation of the phases of the superconductors' order parameters. The symmetry with respect to the enclosed magnetic flux and the bias current through the SQUID indicates that quantum pumping dominates rectification effects in this setup.

2.2.2 Theory of Pumping

Electron pumping has been in the focus of many theoretical works. A lot of the effort has been devoted to systems, where the Coulomb interaction can be treated within a mean-field approach.[64–74] In this regime, a well established theoretical framework for pumping, based on the dynamical scattering approach to mesoscopic transport, exists, where the pumping current can be expressed by Brouwer's formula.[64,65] It can be understood as an analogon to the Landau-Büttiker formula,[75,76] which relates small

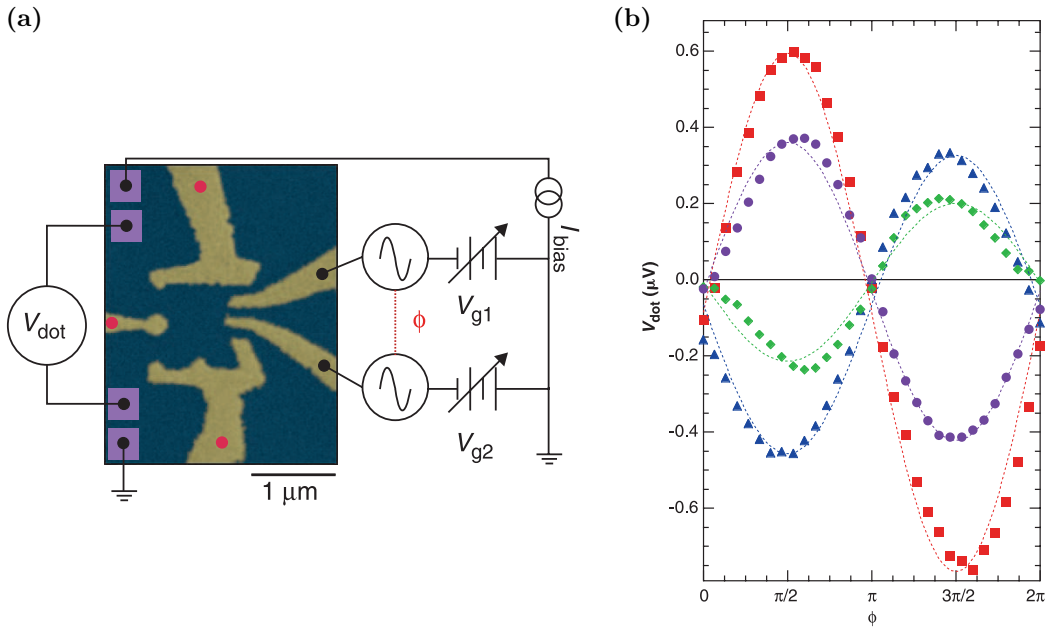

Figure 2.10: Experiment of Switkes *et al.*. From Science **283**, 1905 (1999). Reprinted with permission of AAAS. (a) Micrograph of the setup. (b) The voltage V_{dot} as a function of the phase difference between the two time dependent gate voltages ϕ. Different symbols indicate different magnetic fields. The dashed curves are fits of the form $V_{\mathrm{dot}} = A_0 \sin\phi + B_0$.

changes of bias voltage and current to each other. As an example we show the form of Brouwer's formula for weak adiabatic pumping which is the limit under investigation in this thesis. For noninteracting electrons with $X_1(t) = \overline{X}_1 + \Delta X_1 \sin(\Omega t)$ and $X_2(t) = \overline{X}_2 + \Delta X_2 \sin(\Omega t + \phi)$ being the pumping parameters, the charge pumped into lead η is then given by

$$Q_\eta = e \sin\phi \, \Delta X_1 \Delta X_2 \sum_{\alpha\in\eta} \sum_{\beta} \int_{-\infty}^{\infty} d\omega \frac{df_\eta(\omega)}{d\omega} \mathrm{Im}\left[\frac{\partial S^*_{\alpha\beta}(\omega)}{\partial X_1} \frac{\partial S_{\alpha\beta}(\omega)}{\partial X_2}\right] . \tag{2.9}$$

Here, e is the elementary charge, $f_\eta(\omega)$ is the Fermi function of lead η, and $S_{\alpha\beta}(\omega)$ is an element of the scattering matrix. The indices α and β denote all available transport channels where α only includes those of lead η.

In some nano-scale systems, such as few-electron quantum dots, Coulomb interaction can become very important, requiring a non-perturbative treatment. Pumping in strongly interacting systems has attracted a lot of theoretical interest in the last few years.[77–92] Such systems have, e.g., been investigated by means of the slave boson mean-field approximation,[77] an instantaneous linear response function calculated at every step along the contour in parameter space,[78] or a formalism using a controlled gradient expansion[79] .

In this thesis we use a diagrammatic perturbation expansion in the tunnel coupling

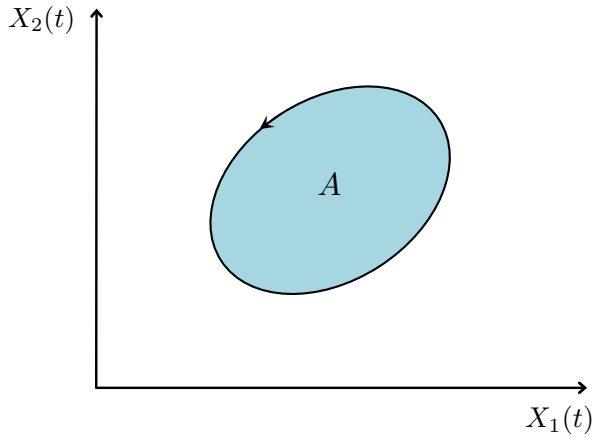

Figure 2.11: The time evolution of the pumping parameters, $X_1(t)$ and $X_2(t)$ in parameter space. The contour encloses the area A.

strengths between quantum dots and leads which are assumed to be small.[80] A more detailed introduction is given in Sec. 4.2.

2.2.3 Limit of Weak Adiabatic Pumping

In this subsection we introduce the limit of weak adiabatic pumping which is the limit under consideration in this thesis, see Chapters 4 and 6.

To generate a pumping current through a scattering region certain system parameters are varied periodically in time. This happens with the frequency Ω. The adiabatic limit is defined by the condition that this frequency is much smaller than the reciprocal dwell time τ_d of an electron in the scattering region,

$$\Omega \ll \frac{1}{\tau_d}\,. \tag{2.10}$$

In this limit at least two pumping parameters, $X_1(t)$ and $X_2(t)$, are required to transport charge on time average. The charge pumped in one period then only depends on the contour determined by $X_1(t)$ and $X_2(t)$ in parameter space, see Fig. 2.11, but not on the exact time evolution of the two parameters.[93] In order to generate a finite pumping current the area A enclosed by the contour has to be nonvanishing, i.e., the pumping parameters $X_1(t)$ and $X_2(t)$ must not have the same or by π differing phase. The reason is that in adiabatic pumping time-reversal symmetry has to be broken. The assumption of weak pumping is related to the amplitude of the time-dependent fraction of the pumping parameters. Weak pumping means that the pumping parameters only slightly deviate from their averages:

$$X_i(t) = \overline{X}_i + \delta X_i(t) \quad , i \in \{1, 2\} \tag{2.11}$$

with $\delta X_i(t)$ being small. In this context 'small' means that all functions F depending on $X_i(t)$ can be approximated by: $F(X_i(t)) \approx F(\overline{X_i}) + \frac{d}{dX_i(t)} F(X_i(t))|_{X_i(t)=\overline{X_i}} \delta X_i(t)$.

In this case of weak pumping the pumped charge only depends on the area A and not on the explicit shape of the contour.

2.3 Superconducting Heterostructures

In 1911 the Dutch physicist H. K. Onnes made a surprising discovery. Below a temperature of 4,2 K mercury looses its electrical resistance.[94] He discovered superconductivity. In the following decades further interesting properties of superconductors have been found.[95] One very important feature is that cooling a material below its critical temperature leads to an expulsion of the magnetic field from the superconductor. This phenomenon is known as Meissner effect. The transition from a normal into the superconducting state depends on two material-specific parameters. Below the critical temperature and the critical magnetic field materials become superconducting. And also the kind of transition is material specific. While type I superconductors can only be normal conducting or superconducting, type II superconductors can also be in a mixed state, the so called *Shubnikov phase*, where for a finite magnetic field normal conducting vortex lattices are formed inside the superconductor. For the practical use of superconductors, e.g., to realize high magnetic fields, the critical temperature is very important. In high temperature superconductors (HTSC) it can be above 77 K (temperature of fluid nitrogen) enabling a relatively cheap cooling. All HTSC are of type II.

A comprehensive theoretical description of superconductivity is given by the BCS theory.[96] Charge can be transferred in Cooper pairs consisting of two electrons. The pairing mechanisms of type I and type II superconductors seem to differ. It is commonly accepted, that in type I superconductors the attractive interaction between the two electrons is mediated by phonons. One electron excites a phonon which is absorbed by another electron at a later time. The distance between these two electrons is referred to as *coherence length*, which is typically $10^{-7} - 10^{-6}$ m. This formation of Cooper pairs is energetically favorably for electrons close to the Fermi energy. The consequence is a gap around the Fermi energy of the superconductor's density of state. Inside this gap only Cooper pairs and no single electrons exist. The Cooper pairs are described by two electrons forming a singlet state. All singlets inside a superconductor have the same quantum mechanical phase and hence this phase is a macroscopic property. In HTSC the temperature is too high for a phonon-based electron-electron attraction and the origin of attraction is still under discussion. However, the formation of Cooper pairs and the existence of an energy gap is beyond controversy.

In heterostructures containing superconductors and normal conductors interesting transport phenomena as *Andreev reflections* (ARs) or the *Josephson effect* occur, which will be presented in this subsection. Especially we focus on setups containing quantum dots (QDs). Advancements in nanofabrication enabled to contact superconductors with quantum dots (QDs), which can be formed in carbon nanotubes,[97–102] in InAs nanowires,[103–105] in graphene,[106] or by means of self-organization in InAs with Al electrodes.[107–109] There are several motivations to investigate such devices.[110,111] The most important ones are probably that in such QD-superconductor devices the inter-

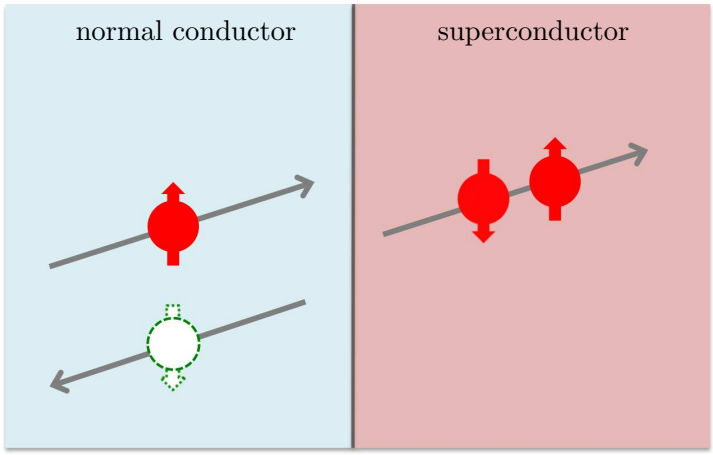

Figure 2.12: Andreev reflection. An electron from the normal conductor is retroreflected as hole and a Cooper pair is transferred into the superconductor.

play between superconducting correlations and Coulomb repulsion can be investigated and that transport properties of QDs can easily be tuned by external gate electrodes.

Some formulations of Sec. 2.3.1 and Sec. 2.3.2 have been published in Ref. 112.

2.3.1 Andreev Reflection

Charge transport through interfaces between superconductors and normal conductors takes place by different processes. Above the energy gap of the superconductor's density of states, mainly single electrons are transferred, while subgap transport is sustained by Andreev reflection (AR).[113,114] In an AR process, an electron in the normal conductor that impinges on the interface is retroreflected as a hole while a Cooper pair is transferred into the superconductor, see Fig. 2.12. In junctions, where two superconductors with different chemical potential are linked by a central region, see Sec. 2.3.2, also multiple Andreev reflection may occur. In such a process several Andreev reflections are correlated. An electron stemming from below the gap of superconductor $S1$ is Andreev reflected from superconductor $S2$ and approaches again superconductor $S1$ as a hole. There it is Andreev reflected again as an electron. In principle an arbitrary number of reflections can take place in this way. For each two reflections a Cooper pair is transferred from one superconductor to the other. The corresponding energy mismatch is gained by an electron to overcome the superconducting gap and to be transferred from below the gap of $S1$ to above the gap of $S2$. In junctions with more than one normal conductor also *crossed Andreev reflections* (CARs) may occur, i.e. the two electrons forming the Cooper pair stem from different normal conductors (or tunnel into different normal contacts in the opposite transport process). A requirement for the presence of CARs is that the distance between the contacts of the two normal conductors must not exceed the coherence length of the superconductor. This nonlocal transport mechanism has been extensively studied both theoretically[115–123] and experimentally.[124–127] In QD-superconductor devices (multiple) Andreev reflec-

tion[99,128–144] as well as crossed Andreev reflection[145–150] have been the focus of many theoretical works. Recently, CAR through QDs has also been observed in two very similar experiments. The setup consists of a superconducting lead tunnel coupled to two parallel quantum dots realized in an InAs semiconducting nanowire[105] and a carbon nanotube,[102] respectively. In both experiments each of the two quantum dots is additionally coupled to separate normal reservoirs, see Fig. 2.13(a). The energy levels

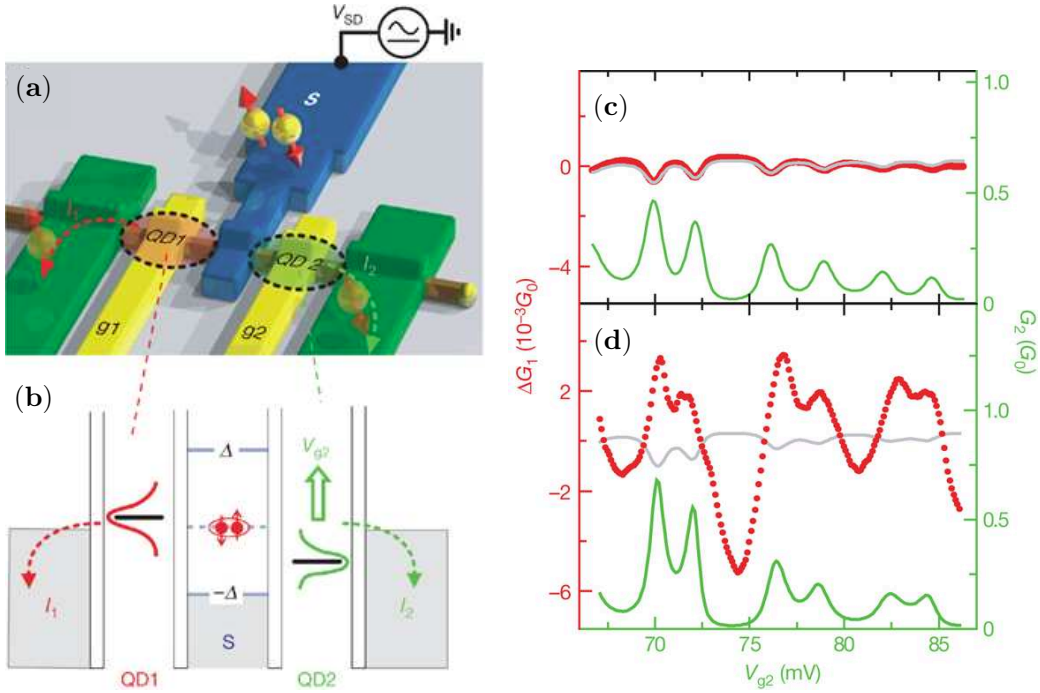

Figure 2.13: Experiment on CAR in QDs performed by Hofstetter *et* al.. Reprinted by permission from Macmillan Publishers Ltd: Nature **461**, 960, copyright 2009. (a) Setup of the experiment. (b) Energy scheme of the setup. (c)-(d) Linear conductance G_2 of QD2 (green line) and change ΔG_1 from QD1's average linear conductance (red line) in units of $G_0 \equiv \frac{2e^2}{h}$ as a function of the gate voltage V_{g2}. The gray line indicates the expected resistive cross-talk. (c) Normal conducting state with magnetic field $B = 120\text{mT}$. (d) Superconducting state with $B = 0$.

of the two dots, QD1 and QD2, can be independently tuned by the external gates g1 and g2, respectively. In the following we exemplary introduce one of the two very similar experiments which has been performed by Hofstetter *et al.*.[105] In this experiment a voltage between the superconductor and the two normal conductors is applied. QD1 is kept on a fixed level and only the gate voltage V_{g2} is varied. An energy scheme of one measurement configuration is shown in Fig. 2.13(b). The linear conductance G_2 of QD2 and the change ΔG_1 from QD1's average linear conductance are measured for different values of V_{g2}. This measurement was done for a magnetic field $B = 120\text{mT}$

bringing the superconductor in its normal state, see Fig. 2.13(c), and for $B = 0$, where it stays superconducting, see Fig. 2.13(d). In both cases correlations of G_2 (green line) and ΔG_1 (red line) appear. However, in the absence of any superconductivity the correlation are weak and peaks in G_2 lead to small dips in ΔG_1. This is in good agreement with the expected resistive cross talk (gray line). In the superconducting state the kind of correlations completely changes. The nonlocal signal ΔG_1 becomes a magnitude higher. Moreover, peaks and dips come together in ΔG_1 and G_2. This correlation strongly indicates the occurrence of CAR.

2.3.2 Josephson Effect

The Josephson effect describes a Cooper-pair tunneling current between two superconductors weakly linked by an insulator, a normal conductor, or a constriction in otherwise continuous superconducting material.[151,152] Such a device is called *Josephson junction*. Even in the absence of any bias voltage Cooper pairs can be transferred through a Josephson junction as long as the two superconductors have a different macroscopic phase. This phenomenon is called *DC Josephson effect*. The *supercurrent* is given by

$$I_S = I_C \sin \Delta\varphi \,, \tag{2.12}$$

where $\Delta\varphi$ is the phase difference between the two superconductors. The *critical current* I_C is the maximal supercurrent, which has no resistance. For external driven currents larger than the critical current also single electrons participate in transport. As a consequence a voltage across the Josephson junction builds up.
A voltage V across the Josephson junction yields a time dependence of the phase difference

$$\frac{\mathrm{d}}{\mathrm{d}t}\Delta\varphi = \frac{2eV}{\hbar} \,, \tag{2.13}$$

which is known as the *AC Josephson effect*. The current alternates with frequency $f = 2eV/h$. This makes a Josephson junction to an ideal voltage-frequency converter.

Many different devices can be used as weak links of the two superconductors in a Josephson junction. Using QDs enables the investigation of the influence of strong Coulomb repulsion on transport through Josephson junctions. Another advantage of QDs is the tuneability of the transport properties as the occupation of the dot by external gates. It has been theoretically predicted[153,154] and experimentally confirmed[100,103] that the two electrons forming a Cooper pair can tunnel coherently one by one through a strongly interacting quantum dot. The chronological order of the tunneling processes changes for the dot occupation being even and odd. This gives rise to a sign change of the transferred Cooper pair singlet referred to as *π-transition*. As a consequence the direction of the supercurrent can be controlled by an external gate. Whenever a bias voltage is applied between the two superconductors in a QD Josephson junction multiple Andreev reflection processes may arise. This causes that also higher harmonics contribute to the AC Josephson transport, i.e., $f = 2neV/h$ with n being integer. A more detailed discussion of this setup is given in Chapter 7.

2.3.3 BCS Hamiltonian

In the BCS theory[95,96] a superconducting lead r is described by the BCS Hamiltonian

$$H_r^{\mathrm{BCS}} = \sum_{k,\sigma} \varepsilon_k c_{rk\sigma}^\dagger c_{rk\sigma} - V \sum_{kk'} c_{rk'\uparrow}^\dagger c_{r-k'\downarrow}^\dagger c_{r-k\downarrow} c_{rk\uparrow}\,, \tag{2.14}$$

where $c_{rk\sigma}^\dagger$ ($c_{rk\sigma}$) is the creation (annihilation) operator for an electron with momentum k and spin σ. The first term describes free, noninteracting electrons as the Hamiltonian for normal conductors given in Eq. (2.7). The second term reflects the attractive electron-electron potential, which is mediated by phonons. Therefore, it only appears for $|\varepsilon_k - E_F| < \hbar\omega_D$ and $|\varepsilon_{k'} - E_F| < \hbar\omega_D$, where ω_D is the Debye frequency and E_F the lead's Fermi energy. In the following we take the Fermi energy as reference for other energies, $E_F = 0$.

In this thesis we treat the BCS Hamiltonian within a mean-field approximation. Then, it is given by

$$H_{\mathrm{r}}^{\text{mf-BCS}} = \sum_{k,\sigma} \varepsilon_k c_{rk\sigma}^\dagger c_{rk\sigma} - \Delta^* \sum_k S_r^\dagger c_{r-k\downarrow} c_{rk\uparrow} - \Delta \sum_k S_r c_{r-k\uparrow}^\dagger c_{rk\downarrow}^\dagger \tag{2.15}$$

with the order parameters $\Delta_r \equiv V \sum_{k'} \left\langle S_r^\dagger c_{r-k'\downarrow} c_{rk'\uparrow} \right\rangle$ and $\Delta_r^* \equiv V \sum_{k'} \left\langle S_r c_{rk'\uparrow}^\dagger c_{r-k'\downarrow}^\dagger \right\rangle$. The operators $S_r^\dagger$ (S_r) create (annihilate) a Cooper pair in lead r and hence allow for particle conservation.[151,155] (In contrast to other bosonic operators they do not generate prefactors as $1/\sqrt{n}$, where n is the number of Cooper pairs.) For setups containing only one superconductor a gauge can be chosen, where the Cooper pairs have a vanishing energy. Then, there is no need to consider the number of Cooper pairs explicitly, i.e., $S_r^\dagger = S_r = 1$.

In order to diagonalize $H_{\mathrm{r}}^{\mathrm{mf-BCS}}$ a Bogoliubov transformation can be performed.[95,139] The fermionic Bogoliubov quasiparticle operators $\gamma_{rk\sigma}$ can be obtained from the electron operators $c_{rk\sigma}$ by the relation

$$\begin{pmatrix} \gamma_{rk\uparrow} \\ \gamma_{r-k\downarrow}^\dagger \end{pmatrix} = \begin{pmatrix} u_{rk} & -v_{rk} S_r \\ v_{rk}^* S_r^\dagger & u_{rk}^* \end{pmatrix} \begin{pmatrix} c_{rk\uparrow} \\ c_{r-k\downarrow}^\dagger \end{pmatrix} \tag{2.16}$$

with coefficients

$$u_{kr} = \sqrt{\frac{1}{2}\left(1 + \frac{\varepsilon_k - \mu_k}{\sqrt{(\varepsilon_k - \mu_k)^2 + |\Delta_r|^2}}\right)} \tag{2.17}$$

and

$$v_{kr} = e^{i\Phi_r} \sqrt{\frac{1}{2}\left(1 - \frac{\varepsilon_k - \mu_k}{\sqrt{(\varepsilon_k - \mu_k)^2 + |\Delta_r|^2}}\right)}\,. \tag{2.18}$$

Here, Φ_r is the phase of order parameter Δ_r and μ_r is the chemical potential of reservoir r. The mean-field BCS Hamiltonian can then be written as

$$H_r^{\text{mf-BCS}} = \sum_{k\sigma} E_{rk} \gamma_{rk\sigma}^\dagger \gamma_{rk\sigma} + \mu_r N\,. \tag{2.19}$$

Here, $E_{rk} = \sqrt{(\varepsilon_k - \mu_r) + |\Delta|^2}$ is the quasiparticle energy and N is the total number of electrons which is the number of Bogoliubov quasiparticles plus twice the number of Cooper pairs. The superconductor's energy gap is reflected in the quasiparticle energy $E_{rk} \geq |\Delta|$.

3 Real-Time Transport Theory

In all setups under consideration in this thesis single-level quantum dots are weakly tunnel coupled to external leads. The basis of our used method for calculations is a diagrammatic real-time transport theory[156,157] where the degrees of freedom of the leads are traced out from the total density matrix. The resulting *reduced density matrix* can be treated explicitly. To this end the *generalized master equation* can be solved by performing a perturbation expansion in tunnel coupling taking into account the Coulomb repulsion nonperturbatively. The used assumptions are $k_BT \gg k_BT_{\mathrm{Kondo}}$ and $\Gamma \ll k_BT$ where Γ is the tunnel-coupling strength between dots and leads.

In this chapter we present the fundamentals of this method. Since the exact procedure of solution strongly depends on the problem under consideration, we do not discuss how to solve the generalized master equation in this chapter. Instead we give the details of the calculations in the corresponding result chapters 4, 5, 6 and 7.

3.1 Reduced Density Matrix

We consider a small number of single-level quantum dots (in this thesis always one or two) tunnel coupled to external leads. The corresponding Hamiltonian $H = H_{\mathrm{dots}} + H_{\mathrm{leads}} + H_{\mathrm{tunn}}$ is given in Sec. 2.1.3. While the leads can be treated as large noninteracting reservoirs, dot electrons repel each other but the dot's Hilbert space is small. The coupling between these two subsystems, H_T, is treated as perturbation which is *adiabatically switched on*[158] at time t_0 which we finally set to minus infinity ($t_0 \to -\infty$), i.e., $H(-\infty) = H_{\mathrm{dots}} + H_{\mathrm{leads}}$. As a consequence the density matrix factorizes,

$$\rho(-\infty) \equiv \rho_0 = \rho_{\mathrm{dots}} \otimes \rho_{\mathrm{leads}}\,. \tag{3.1}$$

The leads degree of freedom are traced out from the total density matrix to obtain the *reduced density matrix*

$$\rho^{\mathrm{red}} \equiv \mathrm{tr}_{\mathrm{leads}}(\rho)\,. \tag{3.2}$$

In the interaction picture the expectation value of a quantum-mechanical operator $\hat{A}(t)$ at a certain time is given by

$$A(t) = \left\langle T_K \left[\exp\left(-\mathrm{i} \int_K dt' H_T(t')_{\mathrm{I}} \right) A(t) \right] \right\rangle_0 . \tag{3.3}$$

The integration $\int_K ... \equiv \int_t^{t_0} ... + \int_{t_0}^{t} ...$ is performed along the Keldysh-contour,[159] see Fig. 3.1, and T_K is the time ordering operator along this contour. We introduce the notation $\langle ... \rangle_0 \equiv tr[\rho_0 ...]$ for the expectation value at time $t = t_0$. The reduced

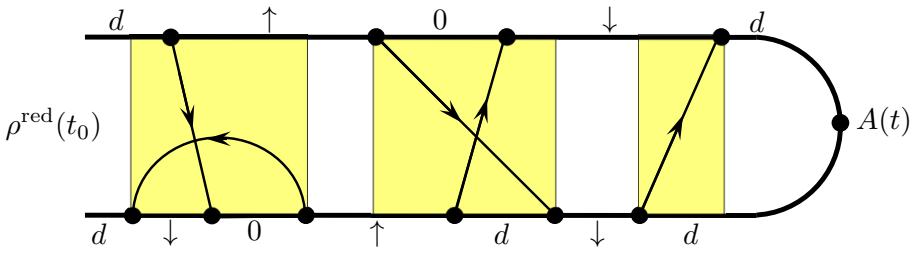

Figure 3.1: Example of a Keldysh-contour with initial time t_0. The contraction of lead operators are represented by tunneling lines between two vertices. The dot states are taken into account explicitly along the contour. *Irreducible* parts are colored yellow.

Planck constant is consequently set to one ($\hbar = 1$). An expansion of Eq. (3.3) yields for the expectation value of the reduced density matrix

$$\begin{aligned} P^{\chi_1}_{\chi_2}(t) &\equiv \langle \chi_1 | \rho^{\mathrm{red}} | \chi_2 \rangle (t) \\ &= \sum_{n=0}^{\infty} (-\mathrm{i})^n \underbrace{\int_K \mathrm{d}t_1 ... \int_K \mathrm{d}t_n}_{t_1 > ... > t_n} \langle T_K [H_T(t_1)_{\mathrm{I}} ... H_T(t_n)_{\mathrm{I}} | \chi_2 \rangle \langle \chi_1 | (t)] \rangle_0 \,, \end{aligned} \tag{3.4}$$

where χ_1 and χ_2 are dot states. The diagonal elements $P_\chi \equiv P^\chi_\chi$ give the probability for the dot being in the corresponding dot state χ. Each tunneling Hamiltonian $H_T(t_i)$ consists of summands which are proportional to $d^\dagger_\sigma c_{rk\sigma}$ or $c^\dagger_{rk\sigma} d_\sigma$. As a consequence the n-th order in the expansion shown in Eq. (3.4) contains summands with n creation and n annihilation operators. By means of Wick's theorem[158] lead operators can be contracted in pairs, i.e., only the expectation values of two lead operators have to be taken into account. The total expansion can completely be performed diagrammatically, see Fig. 3.1. The vertices on the contour symbolize the tunneling Hamiltonian at a certain time and the contractions are illustrated as tunneling lines between the vertices. Since a lead annihilation operator always comes with a dot creation operator and vice versa, each contraction of the lead operators also involves a change of the dot state, which is treated explicitly along the contour. The summation of all topological different contours corresponds to the expectation value of Eq. (3.4).

3.2 Generalized Master Equation

The time evolution of the reduced density matrix can generally be described by

$$P^{\chi_1}_{\chi_2}(t) = \sum_{\chi_1', \chi_2'} \Pi^{\chi_1 \chi_1'}_{\chi_2 \chi_2'}(t, t_0) P^{\chi_1'}_{\chi_2'}(t_0) \,, \tag{3.5}$$

where we introduced the full propagator $\Pi^{\chi_1 \chi_1'}_{\chi_2 \chi_2'}(t, t_0)$. It is represented by the sum of all diagrams with final and initial states as illustrated in Fig. 3.2 arising from Keldysh

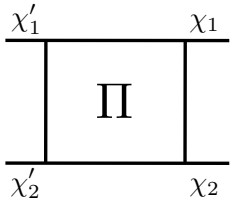

Figure 3.2: Diagrammatic illustration of the propagator $\Pi^{\chi_1\chi_1'}_{\chi_2\chi_2'}(t,t_0)$.

contours which are not closed. The ingredients of the full propagator are on the one hand the free propagator $\Pi^{(0)\,\chi_1}_{\quad\chi_2}(t_1,t_2)$ and on the other hand the *irreducible* diagrams $W^{\chi_1\chi_1'}_{\chi_2\chi_2'}(t_2,t_1)$. In this context irreducible means that a vertical cut through the diagram always involves cutting a tunneling line, see Fig. 3.1. The free propagator corresponds to the undisturbed system and, therefore, does not contain any tunneling lines. By means of these two ingredients the full propagator can be expressed self-consistently in a Dyson equation

$$\begin{aligned}\Pi^{\chi_1\chi_1'}_{\chi_2\chi_2'}(t,t_0) = {}& \Pi^{(0)\,\chi_1}_{\quad\chi_2}(t,t_0)\delta_{\chi_1\chi_1'}\delta_{\chi_2\chi_2'} \\ & + \sum_{\chi_1''\chi_2''}\int_{t_0}^{t}\mathrm{d}t_1\int_{t_0}^{t_1}\mathrm{d}t_2\;\Pi^{(0)\,\chi_1}_{\quad\chi_2}(t,t_1)W^{\chi_1\chi_1''}_{\chi_2\chi_2''}(t_1,t_2)\Pi^{\chi_1''\chi_1'}_{\chi_2''\chi_2'}(t_2,t_0)\end{aligned} \tag{3.6}$$

which is illustrated in Fig. 3.3.

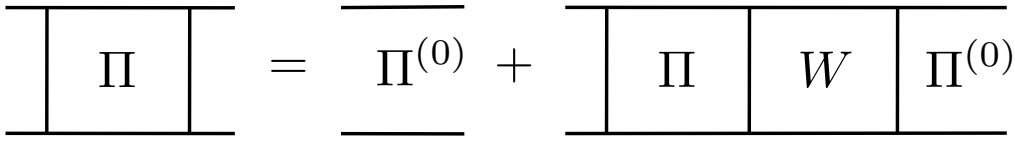

Figure 3.3: Dyson equation.

The free propagator is simply given by

$$\Pi^{(0)\,\chi_1}_{\quad\chi_2}(t,t_0) = e^{-\mathrm{i}(E_{\chi_1}-E_{\chi_2})(t-t_0)}\,, \tag{3.7}$$

where E_{χ_1} and E_{χ_2} are the eigenenergies of the corresponding dot states. From Eqs. (3.5), (3.6), and (3.7) follows the *generalized master equation*:

$$\frac{\mathrm{d}}{\mathrm{d}t}P^{\chi_1}_{\chi_2}(t) = -\mathrm{i}\left(E_{\chi_1(t)}-E_{\chi_2(t)}\right)P^{\chi_1}_{\chi_2}(t) + \sum_{\chi_1'\chi_2'}\int_{-\infty}^{t}\mathrm{d}t' W^{\chi_1\chi_1'}_{\chi_2\chi_2'}(t,t')P^{\chi_1'}_{\chi_2'}(t')\,, \tag{3.8}$$

where we inserted minus infinity as initial time $t_0=-\infty$. The reduced density matrix can be obtained from the generalized master equation together with the normalization condition

$$\sum_{\chi}P_{\chi} = 1\,. \tag{3.9}$$

Since in general the rates $W^{\chi_1\chi_1'}_{\chi_2\chi_2'}(t,t')$ can not be computed exactly a perturbation expansion is performed in tunnel coupling between dots and leads. Details of each calculation are given in the corresponding result chapters.

3.3 Current Formula

The electrical current out of lead r is governed by the change of numbers of electrons occupying the lead, i.e., $\frac{\mathrm{d}}{\mathrm{d}t}N_r$. The current operator is then given by

$$\hat{I}_r(t) = e\frac{\mathrm{d}}{\mathrm{d}t}N_r(t) = -\mathrm{i}e\sum_{k\sigma} t_{rk}c^\dagger_{rk\sigma}d_\sigma(t) - t^*_{rk}d^\dagger_\sigma c_{rk\sigma}(t)\,. \tag{3.10}$$

In order to calculate the expectation value of the current $I_r(t) \equiv \langle \hat{I}_r(t)\rangle$ by means of the Keldysh technique the current operator has to be the rightmost vertex on the contour. We contract this vertex with another vertex arising from the tunneling Hamiltonian. By shifting the rightmost vertex onto the upper or lower contour irreducible blocks similar to those introduced in the previous section arise, see Fig. 3.4.. Therewith the current can be expressed as

$$I_r(t) = e\sum_{\chi\chi'\chi''}\int_{-\infty}^{t}\mathrm{d}t'\, W^{I_r\,\chi\chi'}_{\chi\chi''}(t,t')P^{\chi'}_{\chi''}(t') \tag{3.11}$$

with the current rates $W^{I_r\,\chi\chi'}_{\chi\chi''}(t,t')$. As for the generalized master equation also the solution process of this integral strongly depends on the problem under consideration. Therefore, we give all details in the corresponding result chapters.

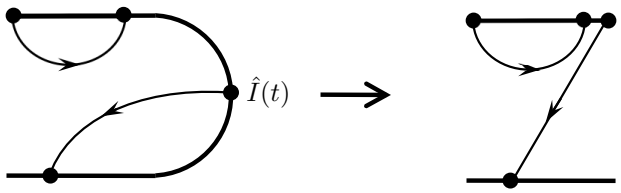

Figure 3.4: The diagrammatic illustration of a current rate $W^{I_r\,\chi\chi'}_{\chi\chi''}(t,t')$. It is obtained by shifting the rightmost vertex onto the upper or lower part of the contour.

4 Adiabatic Pumping through a Double-Dot ABI

In Section 2.2 we introduced the transport mechanism of adiabatic pumping and made the distinction between classical and coherent pumping. The goal of the present chapter is to address the issue of coherence in adiabatic pumping through systems with strong Coulomb interaction such as quantum dots. Recently, there have been several experiments on pumping in nano systems containing quantum dots,[55,160–163] where the influence of Coulomb repulsion has been studied. However, in this chapter we especially want to focus on the role of coherence. To this end, we consider pumping in an Aharonov-Bohm interferometer (ABI), with a quantum dot embedded in each of the two arms, see Fig. 4.1. An important issue when interpreting experimental data is to distinguish pumping from rectification.[63] In fact, due to the presence of stray capacitances, undesired ac bias voltages may appear across the time-dependent conductor, and can give rise to a dc current. Therefore, we compare pumping and rectification, analyze the different processes contributing to transport and discuss to which degree symmetry with respect to the magnetic field can be used to distinguish the two transport mechanisms.

In the diploma-thesis from Ref. 164 amongst other things adiabatic pumping through a double-dot ABI has been studied, but in the very special limits of completely symmetric coupling strengths and noninteracting electrons. The present work is a continuation. Most parts of this chapter have already been published in Ref. 59.

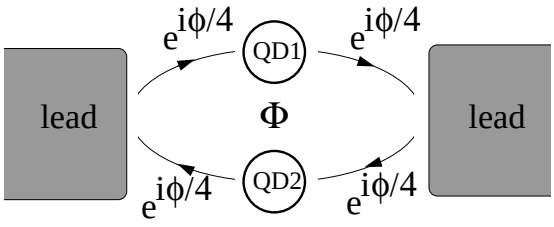

Figure 4.1: Setup of the double-dot Aharonov-Bohm interferometer.

4.1 Model

We start by reviewing the different building blocks of the quantum-dot Aharonov-Bohm interferometers which have already been introduced in Sec. 2.1.3. They are

given by

$$H_{\mathrm{dot},j} = \varepsilon_j \sum_\sigma n_{j\sigma} + U n_{j\uparrow} n_{j\downarrow} \,,$$

$$H_{\mathrm{leads}} = \sum_{rk\sigma} \varepsilon_{rk} c^\dagger_{rk\sigma} c_{rk\sigma} \,,$$

and

$$H_{\mathrm{tunn,j}} = \sum_{k\sigma r} t_{rj} \left(c^\dagger_{rk\sigma} d_{j\sigma} + \mathrm{H.c.} \right) .$$

The two quantum dots are numbered by index j. We assume the inter-dot charging energy to be negligible. Furthermore, we define $\Gamma_j \equiv \sum_r \Gamma_{rj} = \sum_r 2\pi |t_{rj}|^2 \rho_r$. The total Hamiltonian reads $H = \sum_{j=1,2} [H_{\mathrm{dot},j} + H_{\mathrm{tunn},j}] + H_{\mathrm{leads}}$. We choose the gauge in which $-\arg t_{\mathrm{L1}} = \arg t_{\mathrm{R1}} = -\arg t_{\mathrm{R2}} = \arg t_{\mathrm{R1}} = \phi/4$.

4.2 Real-Time Approach to Adiabatic Pumping

In Chapter 3 we derived the generalized master equation for the reduced density matrix and the corresponding current formula in its most general forms. In the following we demonstrate how to solve these equation in the adiabatic limit, i.e., for the pumping frequency Ω being much smaller than the inverse response time of the system. To this end, we follow the lines of Ref. 80 and extent the theory for a double-dot Aharonov-Bohm interferometer where also off-diagonal elements of the reduced density matrix appear accounting for coherent superpositions of the electrons in different quantum dots.[28,29] We introduce the vector $\boldsymbol{\pi} = (P^{\chi_1}_{\chi_1}, ..., P^{\chi_m}_{\chi_m}, ..., P^{\chi_i}_{\chi_j}, ...)^{\mathrm{T}}$, (with $i \neq j$), whose first m components are all diagonal elements of the reduced density matrix followed by all off-diagonal elements. In matrix notation the reduced density matrix can then be written as

$$\frac{d}{dt}\boldsymbol{\pi}(t) = -\mathrm{i}\mathbf{E}(t)\boldsymbol{\pi}(t) + \int_{-\infty}^{t} dt' \mathbf{W}(t,t')\boldsymbol{\pi}(t') \,. \tag{4.1}$$

The matrix elements of $\mathbf{E}(t)$ are given by $E^{\chi\chi''}_{\chi'\chi'''}(t) = \delta_{\chi\chi''}\delta_{\chi'\chi'''} \left(E_\chi(t) - E_{\chi'}(t)\right)$. [1]

We are interested in pumping, i.e., in transport due to the periodic variation of the system parameters, collectively denoted by X. The vector $\boldsymbol{\pi}(t)$ as well as the kernel $\mathbf{W}(t,t')$ depend in a functional way on the pumping parameters $X(\tau)$. To solve Eq. (4.1) we perform an adiabatic expansion. For this purpose, we first perform a Taylor expansion around the final time t of $\boldsymbol{\pi}(\tau) = \boldsymbol{\pi}(t) + (\tau - t)\frac{d\boldsymbol{\pi}}{d\tau}(\tau)\Big|_{\tau=t}$ in the integral on the right-hand side of Eq. (4.1). Furthermore, we need to perform the adiabatic

[1] The matrix elements of $\mathbf{W}(t,t')$ and $\mathbf{E}(t)$ are arranged in such a way that the matrix indices, characterized by two dot-state labels χ_1 and χ_2 each, match the order chosen for the vector $\boldsymbol{\pi}$. This ensures that $W^{\chi\,\chi''}_{\chi'\chi'''}(t,t')$ and $E^{\chi\,\chi''}_{\chi'\chi'''}(t)$ connect the initial $p^{\chi''}_{\chi'''}$ with the final $p^{\chi}_{\chi'}$ state.

expansion of the kernel $\mathbf{W}(t,t')$. In order to do so, we expand the parameters around the time t, i.e., $X(\tau) = X(t) + (\tau - t)\frac{d}{d\tau}X(\tau)\Big|_{\tau=t}$. We write the kernel expansion as

$$\mathbf{W}(t,t') = \mathbf{W}_t^{(\mathrm{i})}(t-t') + \mathbf{W}_t^{(\mathrm{a})}(t-t'). \tag{4.2}$$

The subscript t denotes the time t around which the adiabatic expansion is performed. The instantaneous part with superscript (i) is obtained by freezing all parameters at time t. The adiabatic correction term with superscript (a) contains only terms which are linear in time derivatives of the pumping parameters $\frac{d}{d\tau}X(\tau)\Big|_{\tau=t}$. Finally, we perform an adiabatic expansion of the reduced density matrix,

$$\boldsymbol{\pi}(t) = \boldsymbol{\pi}_t^{(\mathrm{i})} + \boldsymbol{\pi}_t^{(\mathrm{a})}\,. \tag{4.3}$$

The instantaneous part can be obtained by solving the generalized master equation in the stationary limit

$$0 = \left(-\mathrm{i}\mathbf{E}(t) + \mathbf{W}_t^{(\mathrm{i})}\right)\boldsymbol{\pi}_t^{(\mathrm{i})} \tag{4.4}$$

together with the normalization condition $\boldsymbol{n}\boldsymbol{\pi}_t^{(\mathrm{i})} = 1$ with $\boldsymbol{n} = (1,...1,0,...,0)$, i.e., the first m components of $\boldsymbol{n}$ are 1 and the other components are 0. In Eq. (4.4), we have introduced the generalized rates as the Laplace transform of the Kernel computed at zero frequency: $\mathbf{W}_t^{(\mathrm{i/a})} = \lim\limits_{z\to 0^+}\int\limits_{-\infty}^{t} dt' e^{-z(t-t')}\mathbf{W}_t^{(\mathrm{i/a})}(t-t')$.

The first adiabatic correction of the generalized master Eq. (4.1) reads

$$\frac{d}{dt}\boldsymbol{\pi}_t^{(\mathrm{i})} = \left(-\mathrm{i}\mathbf{E}(\mathbf{t}) + \mathbf{W}_{\mathbf{t}}^{(\mathrm{i})}\right)\boldsymbol{\pi}_t^{(\mathrm{a})} + \mathbf{W}_t^{(\mathrm{a})}\boldsymbol{\pi}_t^{(\mathrm{i})} + \partial\mathbf{W}_t^{(i)}\frac{d}{dt}\boldsymbol{\pi}_t^{(\mathrm{i})}\,, \tag{4.5}$$

with $\partial\mathbf{W}_t^{(\mathrm{i})} = \lim\limits_{z\to 0^+}\frac{d}{dz}\int\limits_{-\infty}^{t} dt' e^{-z(t-t')}\mathbf{W}_t^{(\mathrm{i})}(t-t')$. Equation (4.5) together with the normalization condition $\boldsymbol{n}\boldsymbol{\pi}_t^{(\mathrm{a})} = 0$ allows to determine the adiabatic correction of the reduced density matrix $\boldsymbol{\pi}_t^{(a)}$.

In the following, we concentrate on the limit of weak tunnel couplings. Therefore, we perform a perturbation expansion in the tunnel-coupling strength Γ between dot and leads. The kth order contribution to the reduced density matrix is denoted by $\boldsymbol{\pi}_t^{(\mathrm{i/a},k)}$. Matching the orders in Eq. (4.5), it is easy to see that the expansion of the instantaneous term of the reduced density matrix $\boldsymbol{\pi}_t^{(\mathrm{i},k)}$ starts in zeroth order ($k=0$), while the adiabatic correction $\boldsymbol{\pi}_t^{(\mathrm{a},k)}$ starts in minus first order in Γ ($k=-1$). This does not invalidate the expansion, since due to the low-frequency condition $\Omega \ll \Gamma$ the correction $\boldsymbol{\pi}_t^{(\mathrm{a},-1)} \propto \Omega/\Gamma$ still remains small.

The expectation value of the current flowing into lead r consists of an instantaneous part and its adiabatic correction. The instantaneous part reads

$$J_r^{(\mathrm{i})}(t) = e\boldsymbol{n}\mathbf{W}_t^{r,(\mathrm{i})}\boldsymbol{\pi}_t^{(\mathrm{i})}\,, \tag{4.6}$$

with the current rates $\mathbf{W}^r$. The latter are calculated similar to $\mathbf{W}$ but are weighted with the number of electrons transferred to lead r. Without applied bias voltage the instantaneous part vanishes. Hence, the pumped current is given by the adiabatic correction

$$J_r^{(\mathrm{a})}(t) = e\boldsymbol{n}\left(\mathbf{W}_t^{r,(\mathrm{a})}\boldsymbol{\pi}_t^{(\mathrm{i})} + \mathbf{W}_t^{r,(\mathrm{i})}\boldsymbol{\pi}_t^{(\mathrm{a})} + \partial\mathbf{W}_t^{r,(\mathrm{i})}\frac{d}{dt}\boldsymbol{\pi}_t^{(\mathrm{i})}\right), \tag{4.7}$$

where the superscript r points out that the rates, both the instantaneous ones and their adiabatic corrections, are current rates and the number of transferred electrons needs to be accounted for. The rules how to calculate all rates $\mathbf{W}$ are given in Appendix A.

4.3 Results

Using the real-time perturbation theory we compute the pumped current through an AB interferometer with a quantum dot embedded in both arms. We concentrate on the limit of weak tunnel coupling and we expand the pumped current up to the lowest order that is AB-flux dependent, which is associated with AB interference. Furthermore, we calculate the dc current driven through the AB interferometer by an applied ac bias voltage and rectified by the time dependence of the instantaneous conductance of the system. We identify the characteristic features for both transport mechanisms. This helps us to deepen our understanding of pumping, but more importantly, to distinguish pumping from rectification in experiments. We consider two different limits regarding the Coulomb-interaction strength: (i) fully noninteracting case and (ii) infinite intra-dot interaction, which forbids double occupation of a single dot, and negligible inter-dot interaction.

4.3.1 Weak Adiabatic Pumping

We consider the tunneling barriers between dot and lead to be the same for both dots: $\Gamma_{\mathrm{L}1} = \Gamma_{\mathrm{L}2} = \Gamma_{\mathrm{L}}$ and $\Gamma_{\mathrm{R}1} = \Gamma_{\mathrm{R}2} = \Gamma_{\mathrm{R}}$. We assume the difference $\Delta\varepsilon = \varepsilon_1 - \varepsilon_2$ between the dot level of the upper and of the lower dots to be of the same order as Γ. The average level is defined as $\varepsilon = (\varepsilon_1 + \varepsilon_2)/2$. We calculate the current in first order in Γ. This order of perturbation theory is already flux dependent. In the noninteracting case, we can consider spinless electrons and take into account spin degeneracy by multiplying the current by a factor of 2. The dot Hilbert space for spinless electrons is spanned by the states $\{|0\rangle, |1\rangle, |2\rangle, |12\rangle\}$, corresponding, respectively, to both dots being empty, only upper dot occupied, only lower dot occupied, and both dots occupied. On the other hand, for infinite intra-dot interaction the dot Hilbert space has dimension 9 and it is spanned by the states $\{|0\rangle, |j\sigma\rangle, |1\sigma 2\sigma'\rangle\}$, with $j = 1, 2$ and $\sigma, \sigma' = \uparrow, \downarrow$. These states correspond, respectively, to both dots being empty, dot j occupied with spin σ and both dots occupied with spin σ in dot 1 and spin σ' in dot 2. For the interacting system, we introduce the abbreviation $p_j^{j'} \equiv p_{j\sigma}^{j'\sigma}$. In both cases addressed here, the

pumped current is written conveniently as a function of the isospin's expectation value

$$\mathbf{I} = \begin{pmatrix} I_x \\ I_y \\ I_z \end{pmatrix} = \frac{1}{2} \begin{pmatrix} p_2^1 + p_1^2 \\ \mathrm{i}(p_1^2 - p_2^1) \\ p_2^2 - p_1^1 \end{pmatrix}.$$

Notice that if the isospin lies in the xy plane, it indicates that the system is in a superposition of two states: one with only an electron in the first dot and a second with only an electron in the second dot (both states with the same spin).

Computing the adiabatic correction to the reduced density matrix and inserting it in Eq. (4.7) in isospin notation, we obtain for noninteracting electrons

$$J^{(\mathrm{a},0)}_{\mathrm{L}(U=0)} = -4e\frac{\Gamma_\mathrm{L}}{\Gamma}\frac{2\Gamma_\mathrm{R}\sin\frac{\phi}{2}\left(\Gamma\sin\frac{\phi}{2} + \Delta\varepsilon\cos\frac{\phi}{2}\right) + \Delta\varepsilon^2}{4\Gamma_\mathrm{L}\Gamma_\mathrm{R}\sin^2\frac{\phi}{2} + \Delta\varepsilon^2}\frac{df(\varepsilon)}{d\varepsilon}\frac{d\varepsilon}{dt}. \tag{4.8}$$

In the case of infinite interaction within one dot and vanishing interaction between the dots the expression for the current is quite long. For symmetric tunnel-coupling strengths ($\Gamma_\mathrm{L} = \Gamma_\mathrm{R}$) it simplifies to

$$J^{(\mathrm{a},0)}_{\mathrm{L}(U\to\infty)} = -2e\frac{df(\varepsilon)}{d\varepsilon}\frac{d\varepsilon}{dt}\frac{\Gamma^2\sin^2\frac{\phi}{2}\left[1+f(\varepsilon)\right]^3 + \Delta\varepsilon^2[1+f(\varepsilon)] + \Gamma\Delta\varepsilon\cos\frac{\phi}{2}\sin\frac{\phi}{2}}{[1+f(\varepsilon)]^3\left\{(\Gamma^2\sin\frac{\phi}{2}[1+f(\varepsilon)]^2 + \Delta\varepsilon^2\right\}}. \tag{4.9}$$

Now we consider weak pumping and compute the pumped charge in bilinear order of the pumping parameters $\varepsilon(t) = \bar{\varepsilon} + \delta\varepsilon(t)$ and $\Delta\epsilon(t) = \overline{\Delta\varepsilon} + \delta\Delta\varepsilon(t)$. The area of the pumping cycle in the parameter space is

$$\eta_{\Delta\varepsilon,\varepsilon} = \int_0^{2\pi/\Omega} \frac{\partial\delta\varepsilon}{\partial t}\delta\Delta\varepsilon dt.$$

For noninteracting electrons the pumped charge per period reads

$$Q^{(\mathrm{a},0)}_{\Delta\varepsilon,\varepsilon(U=0)} = 8e\eta_{\Delta\varepsilon,\varepsilon}\frac{\Gamma_\mathrm{L}\Gamma_\mathrm{R}}{\Gamma}\sin\frac{\phi}{2}\frac{df(\bar{\varepsilon})}{d\bar{\varepsilon}}\frac{\cos\frac{\phi}{2}(\overline{\Delta\varepsilon}^2 - 4\Gamma_\mathrm{L}\Gamma_\mathrm{R}\sin^2\frac{\phi}{2}) - 2(\Gamma_\mathrm{L}-\Gamma_\mathrm{R})\sin\frac{\phi}{2}\,\overline{\Delta\varepsilon}}{\left(4\Gamma_\mathrm{L}\Gamma_\mathrm{R}\sin^2\frac{\phi}{2} + \overline{\Delta\varepsilon}^2\right)^2}. \tag{4.10}$$

For an infinite Coulomb interaction we give, again, the expression for symmetric tunnel coupling,

$$Q^{(\mathrm{a},0)}_{\Delta\varepsilon,\varepsilon(U\to\infty)} = 2e\eta_{\Delta\varepsilon,\varepsilon}\Gamma\frac{df(\bar{\varepsilon})}{d\bar{\varepsilon}}\frac{\cos\frac{\phi}{2}\sin\frac{\phi}{2}\{\overline{\Delta\varepsilon}^2 - \Gamma^2\sin^2\frac{\phi}{2}\left[1+f(\bar{\varepsilon})\right]^2\}}{[1+f(\varepsilon)]^3\left\{\Gamma^2\sin^2\frac{\phi}{2}\left[1+f(\varepsilon)\right]^2 + \overline{\Delta\varepsilon}^2\right\}^2}. \tag{4.11}$$

The pumped charge for $\Gamma_\mathrm{L} \neq \Gamma_\mathrm{R}$ as a function of $\bar{\varepsilon}$ and $\overline{\Delta\varepsilon}$ is shown in Figs. 4.2(a) and 4.2(b). We find a sign change in the pumped charge which in the noninteracting case

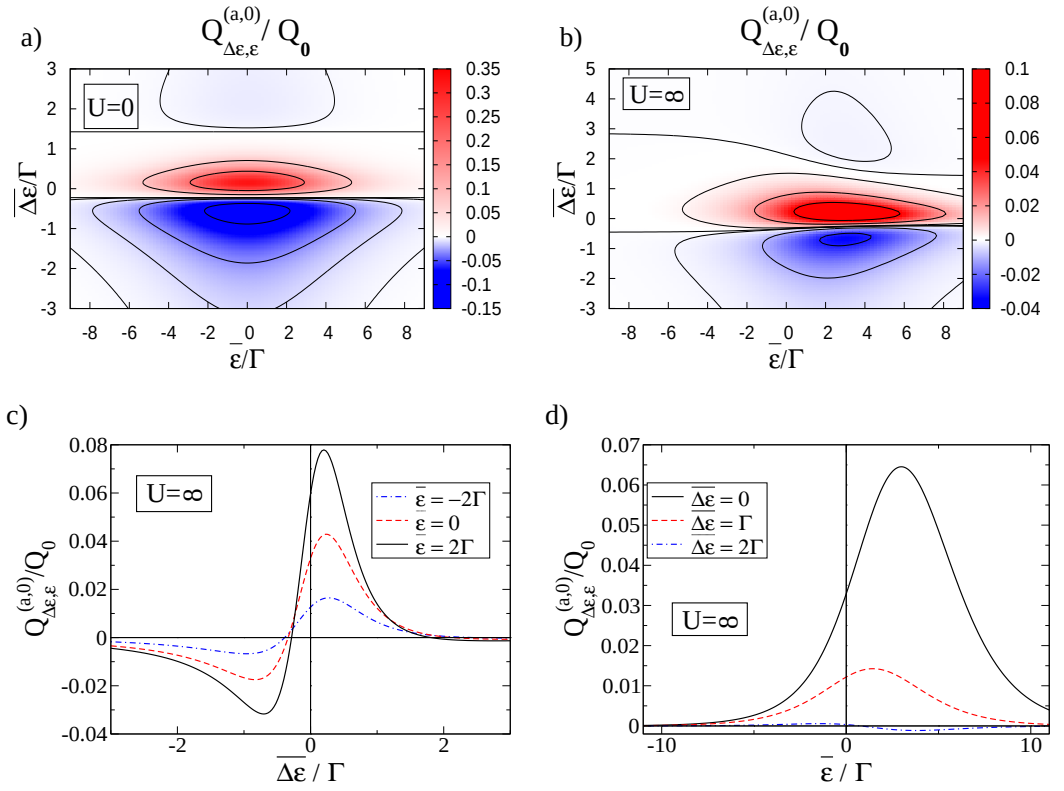

Figure 4.2: Pumped charge $Q^{(a,0)}_{\Delta\varepsilon,\varepsilon}$ in units of $Q_0 = e\eta(\varepsilon, \delta\varepsilon)/\Gamma^2$ for $\Gamma_L = 0.8\Gamma$, $\Gamma_R = 0.2\Gamma$, $\phi = \pi/2$, and $k_BT = 2\Gamma$. (a) and (b) show a density plot where $Q^{(a,0)}_{\Delta\varepsilon,\varepsilon}$ is a function of $\bar{\varepsilon}$ and $\overline{\Delta\varepsilon}$ for (a) vanishing and (b) infinite Coulomb interaction. Cuts through (b) are shown in (c) and (d). In (c) $Q^{(a,0)}_{\Delta\varepsilon,\varepsilon}$ is plotted as a function of $\overline{\Delta\varepsilon}$ for different $\bar{\varepsilon}$. In (d) $Q^{(a,0)}_{\Delta\varepsilon,\varepsilon}$ is plotted as a function of $\bar{\varepsilon}$ for different $\overline{\Delta\varepsilon}$.

only depends on $\overline{\Delta\varepsilon}$ but for an infinite interaction also depends on $\overline{\varepsilon}$. Equation 4.11 suggests an even symmetry concerning $\overline{\Delta\varepsilon}$. Figure 4.2(c) shows that this symmetry is not general but only valid for symmetric tunneling barriers. As a function of $\bar{\varepsilon}$, the pumped charge is even only in the noninteracting but not in the interacting case, Fig. 4.2(d).

The fact that we find a nonvanishing pumped charge at all is not self-evident. The two pumping parameters are associated with the different arms of the interferometer. This suggests that pumping relies on coherent superposition of states localized in the different arms described by the isospin components I_x and I_y. Therefore, one can view pumping in this case as fully quantum mechanical.

4.3.2 Comparison with Rectification

Adiabatic pumping may be obscured by rectification. A time-dependent gate voltage may not only change the level position of the quantum dot but, due to a parasitic capacitive coupling to the leads, give rise to an effective (in-phase) ac bias voltage. This ac bias voltage can, in turn, cause a dc current component due to the time dependence of the dot-level position. In Ref. 63, symmetry with respect to magnetic field has been used to discriminate pumping from rectification. Assuming that the lever arms between gates and reservoirs are small, one can neglect rectification contributions quadratic in $V(t)$ but to zeroth order in time variation of the system parameters of the pumping region ($\delta\epsilon$ in our case). This is because the effect of the gate-voltage modulation on the dot-level position dominates over the ac voltage due to the parasitic stray capacitance. In this limit, the charge transferred in one period by rectification can be computed as $Q_{\mathrm{rec},X} = \int_0^{2\pi/\Omega} G_{\mathrm{L}}(t)V(t)dt$, where $G_{\mathrm{L}}(t)$ is the instantaneous linear conductance and $V(t)$ is the undesired oscillating bias voltage. Due to Onsager relations the linear conductance, and, therefore, also the rectification contribution to the transferred charge, is an even function of the magnetic field. This reasoning, however, is no longer valid when contributions to the rectified current that are nonlinear in the parasitic ac bias voltage have to be taken into account. In fact, magnetic field symmetries for different transport regimes have been extensively investigated experimentally[165–167] as well as theoretically.[168,169] In nonlinear response it has been measured that Coulomb interaction may yield an odd part also in rectification.[167] The ratio between odd and even parts strongly depends on the bias mode and the frequency. Especially, in the adiabatic regime the odd part is in general not negligible.[169]

We consider rectification in the linear-response regime, in which the linear conductance, and, therefore, also the transferred charge, is an even function of the magnetic flux. The linear conductance for vanishing interaction reads

$$G^{(1)}_{\mathrm{L}(U=0)} = -4e^2 \frac{\Gamma_{\mathrm{L}}\Gamma_{\mathrm{R}}}{\Gamma} \frac{df}{d\varepsilon} \frac{\Delta\varepsilon^2 + \Gamma_{\mathrm{L}}\Gamma_{\mathrm{R}} \sin^2\phi}{\Delta\varepsilon^2 + \Gamma_{\mathrm{L}}\Gamma_{\mathrm{R}} \sin^2\frac{\phi}{2}}\,, \tag{4.12}$$

while for infinite intra-dot interaction it is

$$G^{(1)}_{\mathrm{L}(U\to\infty)} = -4e^2 \frac{\Gamma_{\mathrm{L}}\Gamma_{\mathrm{R}}}{\Gamma} \frac{1}{1+f(\varepsilon)} \frac{df}{d\varepsilon} \frac{\Gamma_{\mathrm{L}}\Gamma_{\mathrm{R}}(1-\cos\phi)\left[1+\cos\phi+2f(\varepsilon)\left(2+f(\varepsilon)\right)\right]+\Delta\varepsilon^2}{2\Gamma_{\mathrm{L}}\Gamma_{\mathrm{R}}(1-\cos\phi)\left(1+f(\varepsilon)\right)^2+\Delta\varepsilon^2}\,. \tag{4.13}$$

The pumping, on the other hand, has no definite symmetry with respect to magnetic field (Fig. 4.3) unless a symmetric choice of the tunnel-coupling strengths is assumed. Furthermore, we remark that the pumped charge vanishes for zero flux.

4.4 Conclusions

We have investigated adiabatic pumping through an AB interferometer with a quantum dot embedded in both arms by means of a diagrammatic real-time approach to

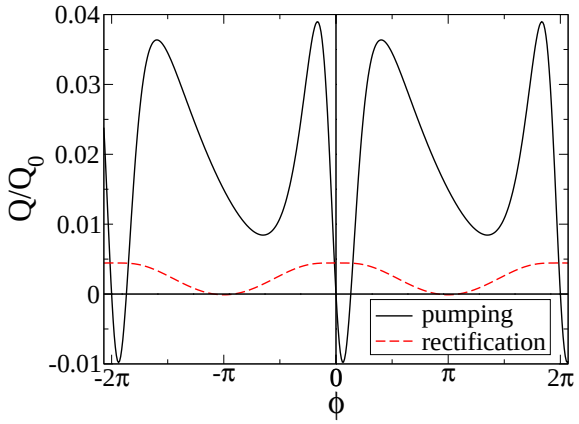

Figure 4.3: Pumped charge $Q^{(\mathrm{a},0)}_{\Delta\varepsilon,\bar{\varepsilon}}$ in units of $Q_0 = e\eta(\varepsilon,\delta\varepsilon)/\Gamma^2$ and rectified charge $Q^{(i,1)}_{\mathrm{rec},\bar{\varepsilon}}$ in units of $Q_0 = e^2\eta_{\mathrm{rec},\varepsilon}/\Gamma$ as a function of ϕ for $U = \infty$, $\Gamma_\mathrm{L} = 0.8\Gamma$, $\Gamma_\mathrm{R} = 0.2\Gamma$, $\bar{\varepsilon} = 0$, $\overline{\Delta\varepsilon} = 0.5\Gamma$, and $k_\mathrm{B}T = 2\Gamma$.

pumping. Adiabatic pumping with the levels of the two dots is a pure quantum-mechanical transport mechanism, since it relies on the system being in a coherent superposition of eigenstates of the dots in the upper and lower arms. Therefore, a nonvanishing pumping signal is not self-evedent. Finally, we found that the symmetry of the pumped charge with respect to the magnetic flux may help to distinguish pumping from rectification, at least in the linear-response regime.

5 Spin-Dependent Transport through Quantum-Dot ABIs

In Sec. 2.1.2 we discussed the coherence of transport through quantum dots which can be investigated in quantum-dot Aharonov-Bohm interferometers (QD-ABIs). If any coupling of the quantum dot to some bath is negligibly small then the only source of decoherence is connected to the spin degree of freedom in the quantum dot. In general, transport through the quantum dot can be divided into spin-flip and non-spin-flip processes. Only the non-spin-flipping ones are coherent. It was theoretically predicted[28,29] and experimentally confirmed[16,17] that the fraction $c = I^{\mathrm{coh}}/I^{\mathrm{total}}$ of coherent transport can be extracted from measuring the Aharonov-Bohm-oscillation amplitude as a function of level energy for a quantum dot embedded in an Aharonov-Bohm ring. For exclusively normal conducting leads the fraction of coherent to total linear conductance in the limit of weak tunnel coupling has been found to be $c = 1/[1 + f(\epsilon)]$, where $f(\epsilon)$ is the Fermi function and ϵ the quantum dot level, measured relative to the Fermi energy of the leads.

In order to substantiate the role played by the spin, we suggest in this chapter to consider one of the electrodes to be a lead with a finite degree of spin polarization p, see Fig. 5.1. The main idea behind this proposal is that a large degree of spin polarization should, in general, increase the fraction of coherent transport since spin-flip processes are less frequent. However, introducing a spin-polarized lead breaks the spin symmetry and, thus, changes the transport characteristics in a non-trivial way. This includes the possibility of spin accumulation on the dot,[170–173] tunnel magneto resistance,[174,175] or a negative differential conductance.[171,176–178] Especially we are interested in the two questions (1) What fraction c of the total current through a single-level quantum dot weakly coupled to the electrodes is coherent? (2) How and under which circumstances can this fraction c be extracted from a current measurement in an Aharonov-Bohm setup? Since the physics of spin accumulation may introduce an asymmetry of the current between the cases $\epsilon > 0$ and $\epsilon < 0$, that is not related to decoherence, an asymmetry of the AB oscillation amplitude does not necessarily indicate decoherence. The measurable quantity to compare c with is the visibility v. In case of weak tunneling, where only one Fourier component of the flux-dependent current needs to be considered, the visibility v (with $v > 0$) is defined via

$$I^{\mathrm{total}}(\varphi) = I^{\mathrm{av}} \left[1 + v \cos(\varphi + \varphi_0)\right] , \tag{5.1}$$

where I^{av} is the flux-averaged current and φ the AB phase. Spin-flip processes due to spin-orbit coupling are neglected in the following considerations. Furthermore, we restrict our analysis to temperatures larger than the Kondo temperature. For temperatures below the Kondo temperature, the lead electrons screen the local spin

on the quantum dot, and, as a consequence, no spin-flip scattering occurs anymore, see, e.g., Ref. 179.

The most parts of this chapter have already been published in Ref. 10.

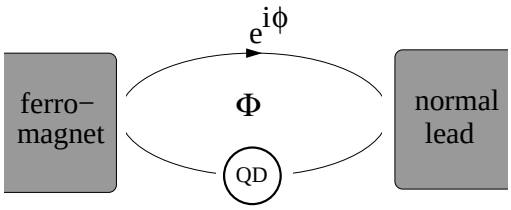

Figure 5.1: Setup of single-dot Aharonov-Bohm interferometer with one spin-polarized lead.

5.1 Model

We consider a closed single-dot ABI, i.e., a two-terminal ABI with a single-level quantum dot embedded in one of the arms, see Fig 5.1. The total Hamiltonian of our system consists of four parts,

$$H = H_{\rm dot} + H_{\rm leads} + H_{\rm tunn} + H_{\rm ref}\,. \tag{5.2}$$

The first three summands of the Hamiltonian are the same as introduced in Sec. 2.1.3

$$\begin{aligned} H_{\rm dot} &= \varepsilon \sum_\sigma n_\sigma + U n_\uparrow n_\downarrow \\ H_{\rm leads} &= \sum_{rk\sigma} \varepsilon_{rk\sigma} c^\dagger_{rk\sigma} c_{rk\sigma} \\ H_{\rm tunn} &= \sum_{rk\sigma} t_r c^\dagger_{rk\sigma} d_\sigma + \text{H.c.}\,. \end{aligned}$$

In the ferromagnetic lead we have to distinguish between the density of states of electrons with majority ($\sigma = +$) and minority spin ($\sigma = -$). For the normal lead this distinction is not necessary ($\rho_{\rm N}/2 \equiv \rho_{\rm N+} = \rho_{\rm N-}$). The spin polarization $p = (\rho_{\rm F+} - \rho_{\rm F-})/(\rho_{\rm F+} + \rho_{\rm F-})$ characterizes the asymmetry of the density of states. Tunnel-coupling strengths are then defined as $\Gamma_{\rm N} = 2\pi|t_{\rm N}|^2\rho_{\rm N}$ and $\Gamma_{\rm F\pm} = 2\pi|t_{\rm F}|^2\rho_{\rm F\pm} = (1 \pm p)\Gamma_{\rm F}$.

The second ("reference") interferometer arm is modeled by a direct tunnel coupling between the leads. The Hamiltonian of the reference arm reads

$$H_{\rm ref} = \sum_{k,q,\sigma} (\tilde{t} c^\dagger_{{\rm N}k\sigma} c_{{\rm F}q\sigma} + \text{H.c.}) \tag{5.3}$$

with transmission amplitude $t^{\rm ref}_\sigma = 2\pi\tilde{t}\sqrt{\rho_{{\rm F}\sigma}\rho_{\rm N}}$. The magnetic flux Φ threading the interferometer is included in the phases of the tunneling amplitudes. We choose the

gauge in which $t_\mathrm{F}, t_\mathrm{N} \in \Re^+$ and $\arg \tilde{t} = \varphi = 2\pi\Phi/\Phi_0$, where Φ is the magnetic flux and Φ_0 the flux quantum. In analogy to the tunnel coupling to the dot, we define the total transmission probability $|t^\mathrm{ref}|^2 = |t_+^\mathrm{ref}|^2 + |t_-^\mathrm{ref}|^2$.

5.2 Method

In the following considerations spin-flip processes occur in cotunneling but we assume the spin to be always conserved during a single tunneling event. As a consequence superpositions of different dot states are absent. The dynamics of the quantum dot's degree of freedom, i.e., the probabilities P_χ to find the dot in state $\chi = 0, \uparrow, \downarrow, d$, is governed by a generalized master equation, see Eq. (3.8). In the stationary limit, it simplifies to

$$0 = \sum_{\chi'} W_{\chi\chi'} P_{\chi'} \,. \tag{5.4}$$

Here, $W_{\chi\chi'} \equiv \lim\limits_{z\to 0^+} \int\limits_{-\infty}^{t} dt' e^{-z(t-t')} W_{\chi\chi'}(t,t')$ is the transition rate Fourier transformed at zero frequency, which is time-independent. Analogously the stationary current can be written as

$$I = \mathrm{e} \sum_{\chi'} W^I_{\chi\chi'} P_{\chi'} \,, \tag{5.5}$$

where the current transition rates $W^I_{\chi\chi'}$ are obtained from the transition rates $W_{\chi\chi'}$ by multiplying with the net number of transferred electrons in the transition described by $W_{\chi\chi'}$.

Our method is applicable for arbitrary values of the Coulomb repulsion U. However, in this chapter for simplicity we only consider the two limits $U = 0$ and $U = \infty$ from now on. In the latter case, double occupancy of the dot is prohibited. We aim at a systematic perturbation expansion for weak coupling ($\Gamma \lesssim k_\mathrm{B}T$ and $|t^\mathrm{ref}| \ll 1$) of the current $I = \sum_{m,n} I^{(m,n)}$, where m indicates the power in the tunnel coupling Γ between dot and leads and n the power in the direct tunnel coupling $|t^\mathrm{ref}|$ between the two leads. A direct coupling between the leads can be made small in experiments with the help of a tunable barrier in the reference arm. We perform a corresponding expansion for the probabilities and the transition rates. We restrict ourselves to the lowest-order contributions. This means, we include the current through the reference arm in the absence of the quantum dot, $I^{(0,2)}$, the interference term $I^{(1,1)}(\varphi)$, which is the lowest-order contribution that depends on the Aharonov-Bohm phase φ, and the current through the quantum dot in the absence of the reference arm.

For the last contribution, it is important to distinguish two different transport regimes. If the dot level ε lies inside the energy window for which occupied states in the source electrode and simultaneously empty states in the drain are available, i.e., $|\varepsilon| \lesssim \max\{k_\mathrm{B}T, |\mathrm{e}V/2|\}$, then transport is dominated by transition rates $W^{(1,0)}$ (and $W^{I(1,0)}$) that are first order in Γ. It is clear that in this case only first-order rates are required to evaluate the zeroth-order probability distribution $P_\chi^{(0,0)}$. We refer to this procedure as calculation scheme 1.

The situation is different in the cotunneling regime, $|\varepsilon| \gg \max\{k_\mathrm{B}T, |eV/2|\}$, for which some of the rates $W^{(1,0)}$ are exponentially suppressed and the lowest-order contribution is $W^{(2,0)}$. Then, as discussed e.g. in Ref. 180, some second-order rates are required to evaluate the zeroth-order probability distribution $P_\chi^{(0,0)}$. This we call calculation scheme 2. The details of matching the different orders in the generalized master equation for the two schemes are presented in Appendix B.

For scheme 1, we use a real-time diagrammatic technique to perform the perturbation expansion in the tunnel-coupling strengths.[156,157] The rules for a diagrammatic calculation of a rate are given in Appendix A. The advantage of this technique is that it is systematic in the sense that all contributions of given order are properly taken into account. The downside is that including higher-order contributions becomes increasingly cumbersome. In the cotunneling regime, where scheme 2 needs to be used, the expressions for the rates obtained from the diagrammatic technique drastically simplify. In that case it is easier to directly identify all the cotunneling processes and evaluate the corresponding rates by second-order perturbation theory rather than employing the real-time diagrammatics.

To discuss the results obtained by scheme 1, we will only provide the final expressions for the current. As we will discuss below, for connecting the degree of coherence with the visibility of the Aharonov-Bohm oscillations, the cotunneling regime is more important. In this case, we use scheme 2 with the cotunneling rates $W_{\chi\chi'}^{(2,0)} = \sum_{r,r'} \gamma_{rr'}^{\chi\chi'(2,0)}$, where $\gamma_{rr'}^{\chi\chi'}$ is the rate of a transition where an electron is transferred from reservoir r' to reservoir r, accompanied by a change of the dot state from χ' to χ. An example for the calculation of such a cotunneling rate, as introduced in Refs. 181, 182 for metallic islands and applied for single-level quantum dots, e.g., in Ref. 183, is given in Appendix C. For $|\varepsilon| \gg \max\{k_\mathrm{B}T, |eV/2|\}$ and $U = 0$, the cotunneling rates simplify to

$$\gamma_{rr'}^{00(2,0)} = \gamma_{rr'}^{\sigma\sigma(2,0)} = \gamma_{rr'}^{dd(2,0)} = \sum_{\sigma'} \frac{\Gamma_r^{\sigma'}\Gamma_{r'}^{\sigma'}}{2\pi\varepsilon^2} F(\mu_r - \mu_{r'}) \tag{5.6}$$

$$\gamma_{rr'}^{\bar{\sigma}\sigma(2,0)} = 0 \tag{5.7}$$

with $F(x) = x/[\exp(x/k_\mathrm{B}T) - 1]$. For $U = \infty$, we obtain

$$\gamma_{rr'}^{00(2,0)} = \sum_{\sigma} \frac{\Gamma_r^{\sigma}\Gamma_{r'}^{\sigma}}{2\pi\varepsilon^2} F(\mu_r - \mu_{r'}) \tag{5.8}$$

$$\gamma_{rr'}^{\sigma\sigma(2,0)} = \frac{\Gamma_r^{\sigma}\Gamma_{r'}^{\sigma}}{2\pi\varepsilon^2} F(\mu_r - \mu_{r'}) \tag{5.9}$$

$$\gamma_{rr'}^{\bar{\sigma}\sigma(2,0)} = \frac{\Gamma_r^{\sigma}\Gamma_{r'}^{\bar{\sigma}}}{2\pi\varepsilon^2} F(\mu_r - \mu_{r'})\,. \tag{5.10}$$

The rates in Eqs. (5.8) and (5.9) are associated with non-spin-flip processes while Eq. (5.10) describes spin-flip processes.

Finally, we also need the rates to first order in Γ and first order in $|t^\mathrm{ref}|$. Only those

contributions with $r \neq r'$ exist. We obtain

$$\gamma_{rr'}^{00(1,1)} = \delta_{r,\bar{r}'} \sum_{\sigma} \frac{|t_\sigma^{\mathrm{ref}}| \sqrt{\Gamma_r^\sigma \Gamma_{r'}^\sigma}}{\pi\varepsilon} F(\mu_r - \mu_{r'}) \cos\varphi \tag{5.11}$$

$$\gamma_{rr'}^{\sigma\sigma'(1,1)} = 2\delta_{\sigma,\sigma'}\delta_{r,\bar{r}'} \frac{|t_\sigma^{\mathrm{ref}}| \sqrt{\Gamma_r^\sigma \Gamma_{r'}^\sigma}}{\pi\varepsilon} F(\mu_r - \mu_{r'}) \cos\varphi \tag{5.12}$$

$$\gamma_{rr'}^{dd(1,1)} = -\gamma_{rr'}^{00(1,1)} \tag{5.13}$$

for $U = 0$ and

$$\gamma_{rr'}^{00(1,1)} = \delta_{r,\bar{r}'} \sum_{\sigma} \frac{|t_\sigma^{\mathrm{ref}}| \sqrt{\Gamma_r^\sigma \Gamma_{r'}^\sigma}}{\pi\varepsilon} F(\mu_r - \mu_{r'}) \cos\varphi \tag{5.14}$$

$$\gamma_{rr'}^{\sigma\sigma'(1,1)} = \delta_{r,\bar{r}'} \frac{|t_\sigma^{\mathrm{ref}}| \sqrt{\Gamma_r^\sigma \Gamma_{r'}^\sigma}}{\pi\varepsilon} F(\mu_r - \mu_{r'}) \cos\varphi \tag{5.15}$$

for $U = \infty$. Here, $\bar{r}'$ indicates the lead other than r'.

5.3 Results

5.3.1 Charge Current

The quantity that is directly measured in experiment is the charge current. As indicated above, the total current can be split into three contributions: the current through the reference arm in the absence of the quantum dot, $I^{(0,2)}$, the current through the quantum dot in the absence of the reference arm, $I^{(1,0)}$ or $I^{(2,0)}$ (for scheme 1 and 2, depending on the level position ϵ, respectively), and the interference term, $I^{(1,1)}(\varphi)$. Only the last one depends on the Aharonov-Bohm phase φ.

Direct tunneling through the reference arm can be calculated with Fermi's golden rule and contributes to the current with

$$I^{(0,2)} = \frac{e^2}{\pi} V |t^{\mathrm{ref}}|^2, \tag{5.16}$$

where V is the bias voltage applied between the ferromagnet and the normal conductor.

We now consider the transport through the quantum dot in the absence of the direct interferometer arm. If the dot level lies in between the transport voltage defined by the Fermi energies of the electrodes then transport through the dot will be dominated by first-order tunneling, $I^{(1,0)}$, and we use scheme 1. We find

$$I^{(1,0)} = -2\mathrm{e} \frac{\Gamma_\mathrm{F}\Gamma_\mathrm{N}\left(\Gamma - p^2\Gamma_\mathrm{F}\right)}{\Gamma^2 - p^2\Gamma_\mathrm{F}^2} \left[f_\mathrm{F}(\varepsilon) - f_\mathrm{N}(\varepsilon)\right], \tag{5.17}$$

for noninteracting electrons, $U = 0$, where $f_{\mathrm{F/N}}$ is the Fermi function of the normal/ferromagnetic lead. For an infinite interaction, $U = \infty$, we obtain

$$I^{(1,0)} = -2\mathrm{e}A^{-1}\Gamma_\mathrm{F}\Gamma_\mathrm{N}\left[f_\mathrm{F}(\varepsilon) - f_\mathrm{N}(\varepsilon)\right]\left[\Gamma_\mathrm{F}\left(1 - p^2\right)\left(1 - f_\mathrm{F}(\varepsilon)\right) + \Gamma_\mathrm{N}\left(1 - f_\mathrm{N}(\varepsilon)\right)\right], \tag{5.18}$$

with

$$A = \Gamma^2 - p^2\Gamma_\mathrm{F}^2 - [\Gamma_\mathrm{F} f_\mathrm{F}(\varepsilon) + \Gamma_\mathrm{N} f_\mathrm{N}(\varepsilon)]^2 + p^2\Gamma_\mathrm{F}^2 f_\mathrm{F}^2(\varepsilon)\,.$$

If the dot level lies outside the energy window defined by the Fermi energies of the leads ($|\varepsilon| \gg \max\{k_\mathrm{B}T, |\mathrm{e}V/2|\}$) then $I^{(1,0)}$ is exponentially suppressed and transport through the dot is dominated by cotunneling, $I^{(2,0)}$. In this case, we employ scheme 2, see Sec. 5.2. In this regime the current for noninteracting electrons ($U = 0$) reads,

$$I^{(2,0)} = \mathrm{e}^2 \frac{\Gamma_\mathrm{F}\Gamma_\mathrm{N}}{\pi\varepsilon^2} V\,. \tag{5.19}$$

In the case of an infinite Coulomb interaction on the dot ($U = \infty$) we have to distinguish different cases. For a dot-level position well above the Fermi energy of the leads, $\varepsilon > 0$, the current through the quantum dot is the same as for noninteracting electrons. The reason is that the dot is never doubly occupied anyway. In the opposite case, $\varepsilon < 0$, we get

$$I^{(2,0)} = \mathrm{e}^2 \frac{\Gamma_\mathrm{F}\Gamma_\mathrm{N}}{\pi\varepsilon^2} V \left[1 + \frac{pm}{1 - \exp(-\mathrm{e}V/k_\mathrm{B}T)}\right], \tag{5.20}$$

where m is the spin accumulation on the dot, which depends on the transport direction. In the regime of unidirectional cotunneling, $|\varepsilon| \gg |\mathrm{e}V/2| \gg k_\mathrm{B}T$, it simplifies to $m = p$ for transport from the ferromagnetic into the normal lead ($V < 0$) and $m = -p$ for the opposite transport direction ($V > 0$).

The flux-dependent part is given by $I^{(1,1)}(\varphi) = I^{(1,1)}_\mathrm{even}\cos\varphi + I^{(1,1)}_\mathrm{odd}\sin\varphi$. For noninteracting electrons, the coefficients are

$$I^{(1,1)}_\mathrm{odd} = 0 \tag{5.21}$$

and

$$I^{(1,1)}_\mathrm{even} = 2\mathrm{e}|t^\mathrm{ref}|\sqrt{\Gamma_\mathrm{N}\Gamma_\mathrm{F}}\sigma(\varepsilon) \tag{5.22}$$

with

$$\sigma(\varepsilon) = \frac{1}{\pi}\mathrm{Re}\left[\int d\omega \frac{f_\mathrm{F}(\omega) - f_\mathrm{N}(\omega)}{\varepsilon - \omega + \mathrm{i}0^+}\right],$$

independent of the polarization p.

For an infinitely strong charging energy, both the contributions even and odd in the flux are present. They read in the sequential tunneling regime (scheme 1)

$$\begin{aligned} I^{(1,1)}_\mathrm{odd} &= 2\mathrm{e}A^{-2}|t^\mathrm{ref}|(\Gamma_\mathrm{N}\Gamma_\mathrm{F})^{3/2}\left(f_\mathrm{F}(\varepsilon) - f_\mathrm{N}(\varepsilon)\right)^2 \\ &\quad\times\left\{\left[\Gamma_\mathrm{F}(1-p^2)(1 - f_\mathrm{F}(\varepsilon)) + \Gamma_\mathrm{N}(1 - f_\mathrm{N}(\varepsilon))\right]^2 - \Gamma_\mathrm{N}^2\left[p^2\left(1 - f_\mathrm{N}^2(\varepsilon)\right)\right]\right\} \end{aligned} \tag{5.23}$$

and

$$\begin{aligned} &I^{(1,1)}_\mathrm{even} = 2\mathrm{e}A^{-1}|t^\mathrm{ref}|\sqrt{\Gamma_\mathrm{N}\Gamma_\mathrm{F}}\sigma(\varepsilon) \\ &\times\left\{\Gamma_\mathrm{F}^2(1 - f_\mathrm{F}(\varepsilon))(1-p^2) + \Gamma_\mathrm{N}^2(1 - f_\mathrm{N}(\varepsilon))\Gamma_\mathrm{F}\Gamma_\mathrm{N}\left(2 - f_\mathrm{F}(\varepsilon)(1-p^2) - f_\mathrm{N}(\varepsilon)(1+p^2)\right)\right\}, \end{aligned} \tag{5.24}$$

respectively.

In the cotunneling regime (scheme 2) the odd contribution drops out, $I^{(1,1)}_{\text{odd}} = 0$ while the even part is given by

$$I^{(1,1)}_{\text{even}} = -\frac{\mathrm{e}^2 V}{\pi\varepsilon}\sqrt{\Gamma_{\text{F}}\Gamma_{\text{N}}}|t^{\text{ref}}|(1+pm)\ . \tag{5.25}$$

The odd and even parts of the first flux dependent correction differ in many respects. The odd part $I^{(1,1)}_{\text{odd}}$ describes transport processes where an electron cotunnels through a lead.[44] It only occurs for a nonvanishing Coulomb interaction. Figure 5.2 shows both transport directions of $I^{(1,1)}_{\text{odd}}$ as a function of the dot-level position ε for an infinite Coulomb interaction. The current has its maximum value where the dot level lies

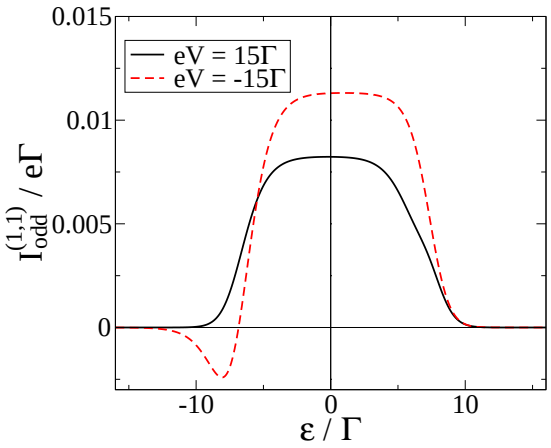

Figure 5.2: Odd part of the first flux dependent order of the current $I^{(1,1)}_{\text{odd}}$ for polarization $p = 0.7$ and Coulomb interaction $U = \infty$ as a function of ε. In the total current a negative bias voltage corresponds to a transport from the ferromagnet into the normal conductor. The value of the parameters used in the calculations are: $\varphi = \pi/2$, $|t^{\text{ref}}| = 0.1$, $k_{\text{B}}T = \Gamma$, $\Gamma_{\text{F}} = \Gamma_{\text{N}} = \Gamma/2$.

between the chemical potential of the two leads. Beside this range the current decreases exponentially.

Figure 5.3 shows $I^{(1,1)}_{\text{even}}$ as function of dot-level position for vanishing and infinite Coulomb interaction. For an infinite Coulomb interaction two different lines are shown. The red, dashed line is calculated by means of scheme 1 while the blue, dashed-dotted line is obtained by means of scheme 2, see Sec. 5.2. Figure 5.3a) shows the current of electrons from the ferromagnetic into the normal lead. For noninteracting electrons the current $I^{(1,1)}$ is an odd function of the dot level position ε. The sign change around $\varepsilon = 0$ relies on a phase shift of the transmission amplitude of the quantum dot. An infinite Coulomb interaction excludes the double occupation of the dot. Hence it has a higher influence for negative than for positive values of ε. The transport from the normal conductor into the ferromagnet is for $\varepsilon < 0$ strongly suppressed, see Fig. 5.3b). Transport through the quantum dot is blocked by an accumulation of the minority spin on the dot.

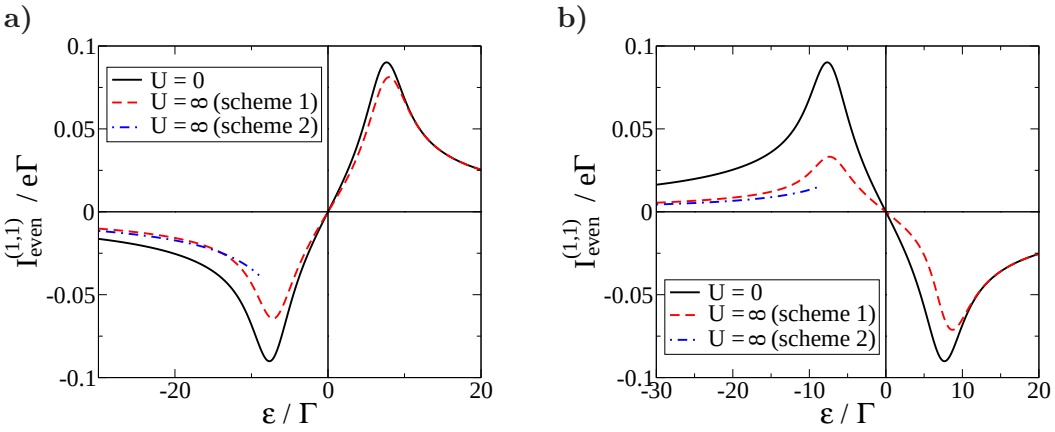

Figure 5.3: Even part of the first flux dependent order of the current $I^{(1,1)}_{\mathrm{even}}$ for polarization $p = 0.7$ as a function of ε for vanishing (solid line) and infinite Coulomb interaction for two different calculation schemes (see text). Scheme 1 (dashed line) is more accurate for $\varepsilon \gtrsim -\max\{k_{\mathrm{B}}T, |eV/2|\}$ while scheme 2 (dashed-dotted line) is more accurate for $\varepsilon \ll -\max\{k_{\mathrm{B}}T, |eV/2|\}$. **a)** Electrons are transported from ferromagnet into normal lead ($eV = -15\Gamma$). **b)** Electrons are transported from normal lead into ferromagnet ($eV = 15\Gamma$). The value of the parameters used in the calculations are: $\varphi = 0$, $|t^{\mathrm{ref}}| = 0.1$, $k_{\mathrm{B}}T = \Gamma$, $\Gamma_{\mathrm{F}} = \Gamma_{\mathrm{N}} = \Gamma/2$.

What can we conclude from this for the fraction c of coherent transport through a quantum dot? Not much, as long as the dot's level is inside the energy window of lowest-order transport. And even for the cotunneling regime, an interpretation is difficult for $|eV/2| \lesssim k_{\mathrm{B}}T$, i.e., when transport processes from source to drain are partially compensated by processes from drain to source. For the further discussion, we will, therefore, turn to the regime of unidirectional cotunneling, $|\varepsilon| \gg |eV/2| \gg k_{\mathrm{B}}T$. We emphasize that our method is applicable to arbitrary values of U. For $U = 0$, no spin-flip processes occur since contributions with intermediate empty and double occupation of the dot cancel out each other. As long as $U \ll \min\{|eV|, k_{\mathrm{B}}T\}$ this also holds for a finite U. In the opposite limit, $U = \infty$, double occupancy is fully suppressed, and this cancellation does not occur anymore. This will remain true as long as $U \gg \max\{|eV|, k_{\mathrm{B}}T\}$. Between these two limits there will be a smooth crossover. Therefore, we focus on the limits $U = 0$ and $U = \infty$ only. In particular we will distinguish the four different cases summarized in the Table 5.1. For reference, we always compare to the non-interacting limit (case 1). For strong Coulomb interaction, the dot level may either lie well above the Fermi level of the leads (case 2a), or it may lie well below. In the latter case, the results will strongly depend on the polarity of the applied transport voltage. Case 2b refers to the limit when electrons are transported from the ferromagnet to the normal lead, and case 2c describes the opposite transport direction.

Table 5.1: The considered cases

case 1	$U = 0$
case 2a	$U = \infty$, $\varepsilon \gg \lvert eV/2\rvert \gg k_B T$
case 2b	$U = \infty$, $-\varepsilon \gg \lvert eV/2\rvert \gg k_B T$, $F \to N$
case 2c	$U = \infty$, $-\varepsilon \gg \lvert eV/2\rvert \gg k_B T$, $N \to F$

5.3.2 Fraction of Coherent Transport

How can the fraction of coherent transport be measured in an experiment? Coherence can be tested by interferometry. We consider here an Aharonov-Bohm interferometer in which a single-level quantum dot is embedded in one of the arms. Electrons entering from the source electrode can either travel through the quantum dot or through the direct arm to the drain. If no spin flip occurs, there will be an interference of both paths, which gives rise to a flux-dependent current. The amplitude of the Aharonov-Bohm oscillations relative to the flux-averaged current contains information about the degree of coherence.

There is, however, a major problem in quantitatively connecting the degree of coherence c and the visibility v. A quantum-dot Aharonov-Bohm interferometer probes many different transport channels, distinguished by the energy of the incoming electron, simultaneously. If for the participating electrons the transmission through the quantum dot is strongly energy dependent, then the expected visibilities for the individual channels will be very different from each other. This is the case, when the dot's level position lies inside the energy window defined by the Fermi energies of the leads. For establishing a connection between visibility and fraction of coherent transport, we need to identify a situation in which for all participating electrons the transmission through the dot is the same. This is possible in the cotunneling regime, i.e., when the energy level of the quantum dot is outside this energy window, $|\varepsilon| \gg \max\{|eV/2|, k_B T\}$. Furthermore, for the case when the fraction of coherent transport depends on the transport direction, we need $|eV| \gg k_B T$, i.e., unidirectional cotunneling, as an extra condition to separate the two directions.

What do we expect for the fraction c of coherent transport in this regime of unidirectional cotunneling from lead r to lead $\bar{r}$? We assume that flipping the spin in the quantum dot provides the only source of decoherence. The coherence fraction c is the ratio

$$c = \frac{\sum_{\chi} \gamma_{\bar{r}r}^{\chi\chi(2,0)} P_{\chi}^{(0,0)}}{\sum_{\chi,\chi'} \gamma_{\bar{r}r}^{\chi\chi'(2,0)} P_{\chi'}^{(0,0)}}\,, \tag{5.26}$$

with $P_{\chi}^{(0,0)}$ being the probability to find the dot in state χ and $\gamma_{\bar{r}r}^{\chi\chi'(2,0)}$ the transition rate from initial dot state χ' to final dot state χ where an electron is transferred from lead r to lead $\bar{r}$. In the numerator, only rates are taken into account that do not change the dot state. In particular, no spin-flip processes are included. This contrasts with the expression in the denominator, in which spin-flip processes, i.e. $\chi = \sigma$ and $\chi' = \bar{\sigma}$

are taken into account.

In the limit of vanishing Coulomb interaction, $U = 0$ (case 1), no spin-flip processes occur, which yields $c = 1$. Now we consider the limit of strong Coulomb interaction, $U = \infty$. If the dot's level lies well above the Fermi energies of the leads, $\varepsilon \gg |\mathrm{e}V/2|$ (case 2a), then the dot will be predominately empty. Electrons passing through the quantum dot cannot flip their spin, and therefore $c = 1$. The situation becomes different for $-\varepsilon \gg |\mathrm{e}V/2|$. Then the dot is mostly singly occupied with either spin with probabilities $p_\uparrow$ and $p_\downarrow$ (such that $p_\uparrow^{(0,0)} + p_\downarrow^{(0,0)} = 1$). If the electrons travel from the ferromagnet to the normal lead (case 2b) we get $c = (1+p^2)/2$. In the opposite case (case 2c), transport from the normal lead to the ferromagnet, we get always $c = 1/2$ since an electron enters the dot from the normal lead and hence carries in one half of the cases the same spin as the electron initially occupying the dot.

These results are given in the last column of Table 5.2. The remaining question now is whether and how they are reflected in the visibility of the Aharonov-Bohm oscillations.

5.3.3 Visibility

In the regime of unidirectional cotunneling, the leading order of transport through the quantum dot is $I^{(2,0)}$. In this limit the transmission through the QD is for all energies in good approximation the same. Furthermore, the $\sin\varphi$ part of the current which describes cotunneling through the lead but not through the quantum dot[44] vanishes. The total current then is

$$I^{\mathrm{total}} = I^{(2,0)} + I^{(0,2)} + I^{(1,1)} = I^{\mathrm{av}}\left(1 + v\cos\varphi\right) , \tag{5.27}$$

where v is the visibility and I^{av} the flux averaged current.

For the average current, measured in units of $I_0 = \mathrm{e}^2V/\pi$ we find

$$\frac{I^{\mathrm{av}}}{I_0} = \begin{cases} |t^{\mathrm{ref}}|^2 + \dfrac{\Gamma_{\mathrm{F}}\Gamma_{\mathrm{N}}}{\varepsilon^2} & \text{for cases 1,2a,2b} \\ |t^{\mathrm{ref}}|^2 + (1-p^2)\dfrac{\Gamma_{\mathrm{F}}\Gamma_{\mathrm{N}}}{\varepsilon^2} & \text{for case 2c} \end{cases} . \tag{5.28}$$

We express the visibility in terms of

$$v_0 = \frac{2\frac{\sqrt{\Gamma_{\mathrm{F}}\Gamma_{\mathrm{N}}}}{|\varepsilon|}|t^{\mathrm{ref}}|}{|t^{\mathrm{ref}}|^2 + \frac{\Gamma_{\mathrm{F}}\Gamma_{\mathrm{N}}}{\varepsilon^2}} . \tag{5.29}$$

We obtain

$$\frac{v}{v_0} = \begin{cases} 1 & \text{for cases 1,2a} \\ \dfrac{1+p^2}{2} & \text{for case 2b} \\ \dfrac{1}{2} - \dfrac{p^2|t^{\mathrm{ref}}|^2}{2|t^{\mathrm{ref}}|^2 + 2(1-p^2)\frac{\Gamma_{\mathrm{F}}\Gamma_{\mathrm{N}}}{\varepsilon^2}} & \text{for case 2c} \end{cases} . \tag{5.30}$$

In the cases 1, 2a, and 2b, the visibility can be maximized by tuning $|t^{\mathrm{ref}}|$ to $\frac{\sqrt{\Gamma_{\mathrm{F}}\Gamma_{\mathrm{N}}}}{|\varepsilon|}$. Then, $v_0 = 1$ and $v = v_{\max}$, independent of the degree of spin polarization p. However,

for the case 2c, the maximal visibility $v_{\max}$ can only be obtained by tuning $|t^{\mathrm{ref}}|$ in a p-dependent way to $\frac{\sqrt{\Gamma_F \Gamma_N}}{|\varepsilon|}\sqrt{1-p^2}$. In this case $v_{\max}$ turns out to be $v_{\max} = \frac{\sqrt{1-p^2}}{2}$.

The visibility of the total current is a quantity that can be measured in an experiment. To what extent the visibility provides information about coherence of transport is discussed in the next subsection.

5.3.4 Visibility versus Coherence

In order to investigate the measurability of coherence we compare the fraction c with the maximal visibility $v_{\max}$. Because coherence is an essential assumption for flux dependence in general $c \geq v_{\max}$. In the case of a vanishing Coulomb interaction (case 1) or a very high dot's level position (case 2a) $v_{\max} = 1$ and, hence, $c = 1$, see Fig.5.4a). If the dot level is very low and electrons are transferred from the ferromagnet into the

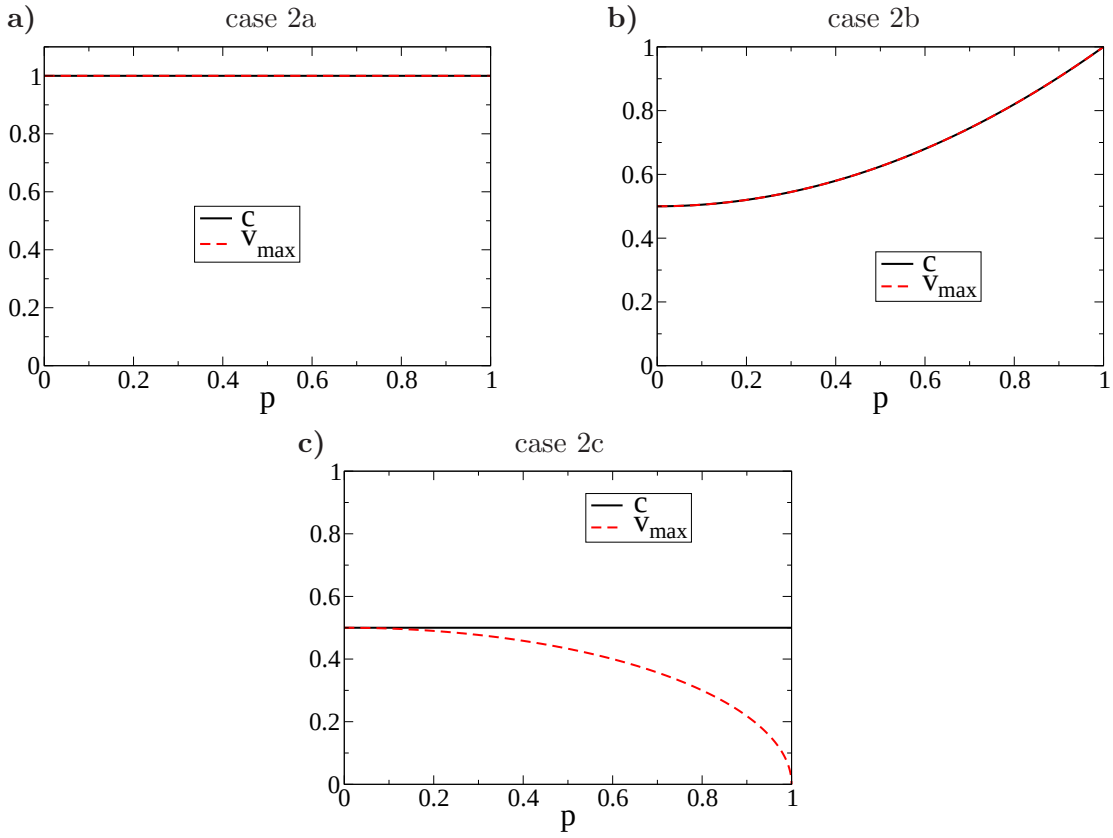

Figure 5.4: Maximal visibility and coherent fraction of the total current for the two different transport directions.

normal conductor (case 2b) the coherent fraction c is equal to the maximal visibility $v_{\max}$, see Fig. 5.4b). For a vanishing polarization 1/2 of the electrons leaving the source carry the same spin as the electron initially occupying the dot. Hence, in one half of the cases the spin on the dot is not flipped and transport is coherent. The

higher the polarization the more electrons with majority spin take part in transport and, thus, less spin-flip processes take place.
For reversed transport voltages (case 2c) independent of the polarization one half of the processes are coherent. The source is a normal lead and, hence, one half of the electrons which tunnel onto the dot carry the same spin as the electron which initially occupied the dot. On the other hand the visibility is low for a high polarization, see Fig. 5.4(c), due to spin blockade on the dot. While transport through the reference arm is spin independent transport through the quantum dot is not. This prevents the possibility to tune the transmission through the reference arm and the transmission through the quantum dot to the same value.
In all cases the maximal visibility is obtained by tuning $|t^{\mathrm{ref}}|$ to a certain value. While in the cases 1, 2a and 2b this value is independent of the polarization p, in case 2c $|t^{\mathrm{ref}}|$ has to be tuned in a p-dependent way, see Sec. 5.3.3.

Table 5.2: Summary of results

	v/v_0	$v_{\max}$	c
$U=0$	1	1	1
$U=\infty$, $\varepsilon \gg \lvert eV/2\rvert \gg k_{\mathrm{B}}T$	1	1	1
$U=\infty$, $-\varepsilon \gg \lvert eV/2\rvert \gg k_{\mathrm{B}}T$,$F\to N$	$\frac{1+p^2}{2}$	$\frac{1+p^2}{2}$	$\frac{1+p^2}{2}$
$U=\infty$, $-\varepsilon \gg \lvert eV/2\rvert \gg k_{\mathrm{B}}T$,$N\to F$	$\frac{1}{2}-\frac{p^2\lvert t^{\mathrm{ref}}\rvert^2}{2\lvert t^{\mathrm{ref}}\rvert^2+2(1-p^2)\frac{\Gamma_{\mathrm{F}}\Gamma_{\mathrm{N}}}{\varepsilon^2}}$	$\frac{\sqrt{1-p^2}}{2}$	$\frac{1}{2}$

5.4 Conclusions

We have investigated the current through an AB interferometer coupled to one normal and one ferromagnetic lead with a quantum dot embedded in one of the arms. In particular we elucidated the influence of polarization on the visibility of transport and studied the relation between visibility and coherence. We found that in the lowest flux-dependent order transport of noninteracting electrons is fully coherent and the maximal visibility is 1. In the case of an infinite intra-dot Coulomb repulsion the coherence as well as the visibility of the current are strongly influenced by the polarization and the transport direction. As long as no spin blockade on the dot occurs the maximal visibility is equal to the coherent fraction of the current and can be obtained by tuning the transmission through the reference arm $|t^{\mathrm{ref}}|$ in a p-independent way.

6 Adiabatic Pumping in a Double-Dot Cooper-Pair Beam Splitter

The processes of charge transport through interfaces between superconductors and normal conductors have been introduced in Sec. 2.3.1. In the present chapter we mainly focus on crossed Andreev reflection (CAR), where a Cooper pair is formed by two electrons stemming from different normal conductors (or a Cooper pair breaks up and two electrons are transferred into different normal conductors in the opposite transport process). The presence of CAR in quantum dots has been observed in experiment.[102,105] The setup consists of a superconducting lead tunnel coupled to two parallel quantum dots and each of the two quantum dots is additionally coupled to separate normal reservoirs, see Fig. 6.1. As a result the dependence of the current in one arm of the beam splitter on the parameters of the other arm indicates the occurrence of CAR, see Sec 2.3.1. In this experiment a bias voltage is applied to generate dc transport. Here, we propose to use adiabatic pumping in order to investigate features of CAR, see Sec. 2.2. In the experiments performed so far, the CAR and AR signals coexist. This happens even though strong Coulomb interaction within each dot tends to suppress AR, therefore enhancing the visibility of CAR. Adiabatic pumping requires two out-of-phase time-dependent parameters in order to obtain a finite dc current. Choosing gates applied to the two dots, belonging to two different arms of the beam splitter, as pumping parameters, only transport mechanisms relying on nonlocal correlations between the two arms contribute to the pumped charge. Therefore, such a type of pumping cycle has the advantage with respect to biased transport that it singles out CAR, while local effects do not yield any finite dc current.

Theoretically, in noninteracting systems, the influence of the superconducting proximity effect on pumping was studied in Refs. 184–186. However, Coulomb interaction cannot be neglected in the setup considered here. While pumping through a single quantum dot with a superconducting lead was studied in the limit of zero temperature and infinitely strong Coulomb interaction,[187] in this chapter, we are interested in systems in which Coulomb interaction can be arbitrary and where coupling to the leads is weak. To this purpose we use the adiabatic extension of a generalized master equation approach which has been introduced in Sec. 4.2. In the stationary limit the generalized master equation approach has been applied to hybrid quantum dot systems before.[138,139,145,150]

The motivation of this chapter is to identify and understand CAR in adiabatic pumping. To this purpose we investigate the setup depicted in Fig. 6.1. In the following we will refer to it as NDSDN. Pumping is realized by applying time-dependent potentials, namely one to each of the quantum dots, via gates with a phase-difference in the driving. This gives us the possibility to identify unique features of crossed Andreev

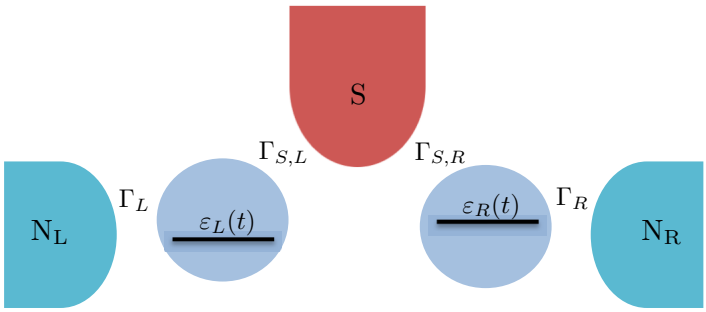

Figure 6.1: NDSDN setup: Two quantum dots are coupled to the same superconductor and each dot is coupled to a normal conductor.

reflection in adiabatic pumping which rely on the *nonlocality* of the effect and can - as we show by a comparison with a setup with the superconductor replaced by a normal lead (NDNDN) - not be reproduced by other parasitic nonlocal effects mediated by quasiparticles.
However, the complexity of this setup makes it difficult to obtain compact analytic formulae. Therefore, we additionally consider a quantum dot with Zeeman-split levels, tunnel coupled to a ferromagnetic and a superconducting lead (FDS). In hybrid systems containing ferromagnets, superconductors, and quantum dots the influence of spin asymmetry on Andreev reflections has been investigated before.[141–145,188] In the present work our motivation of considering the FDS setup is to get a better understanding of the transport processes in the NDSDN system because we can relate the CAR in the NDSDN setup to AR in the FDS setup. The Zeeman splitting and the polarization in the FDS setup corresponds to a difference of the two dot levels and an asymmetry of the coupling to the two normal conductors of the NDSDN system, respectively. From a theoretical point of view the main difference between the two setups is the existence of triplet states in the NDSDN system. Experimentally, although hybrid systems containing ferromagnets and superconductors are realizable,[188] the time dependence of the transport channels through the dot are easier to control in the NDSDN setup.

Most parts of this chapter have already been published in Ref. 112.

6.1 Model

The systems we consider are generally described by a Hamiltonian for a hybrid system composed by multiple quantum dots tunnel coupled to both normal and superconducting leads. Each individual dot, labeled by the index j, is described by the Anderson-impurity model with an onsite interaction U_{intra} and the level energy $\varepsilon_{j\sigma}$.

The quantum dots are described by the Hamiltonian

$$H_{\text{dot}} = \sum_{j\sigma} \varepsilon_{j\sigma}(t) n_{j\sigma} + U_{\text{intra}} \sum_{j} n_{j\uparrow} n_{j\downarrow} + \frac{1}{2} U_{\text{inter}} \sum_{j \neq j' \sigma\sigma'} n_{j\sigma} n_{j'\sigma'} \,, \tag{6.1}$$

which differs from Eq. (2.6) by the existence of the inter-dot repulsion U_{inter}. Here, we explicitly introduce the time-dependence of the dot levels, which is used to realize the pumping cycles. The leads are described by the mean field BCS Hamiltonian

$$H_r = \sum_{k\sigma} \varepsilon_{rk\sigma} c^\dagger_{rk\sigma} c_{rk\sigma} - \delta_{rS} \sum_{k} \left(\Delta c_{r-k\downarrow} c_{rk\uparrow} + \text{h.c.} \right)$$

which has been introduced in Sec. 2.3.3. The second term is only present for the superconducting leads and it is simply the attractive potential of the mean-field BCS Hamiltonian. We are using a gauge, where the superconductor has a vanishing chemical potential and, therefore, Cooper pair operators do not enter Eq. (6.1). Without loss of generality the pair potential Δ can be chosen to be real, because we consider only one superconductor. Finally, the dots are coupled to the different leads by means of the tunneling Hamiltonian

$$H_{\text{tunn}} = \sum_{rjk\sigma} t_{rj} c^\dagger_{rk\sigma} d_{j\sigma} + \text{h.c.} \,. \tag{6.2}$$

which is the same as in Eq. (2.8) with an additional summation over the different dots. Tunnel-coupling strengths are then defined as $\Gamma_{r,j,\sigma} = 2\pi |t_{rj}|^2 \rho_{r,\sigma}$. Notice that no inter-dot tunneling is included in the model. Finally, the total Hamiltonian for this type of hybrid system can be written as $H = H_{\text{dot}} + H_{\text{tunn}} + \sum_r H_r$.

6.1.1 Double-Dot Device

The main focus of this work is on the parallel double-dot device shown in Fig. 6.1, that is ideal for studying Cooper-pair splitting. It is composed of two quantum dots which are tunnel coupled to different normal conductors but the same superconducting lead. We will refer to it as to the NDSDN system, where N indicates a normal lead, S a superconducting lead and D a quantum dot. The Hamiltonian of the NDSDN system is obtained from the general Hamiltonian of the previous subsection by having $j \in \{L, R\}$, $r \in N_L, N_R, S$ and $\Gamma_{N_L} \equiv \Gamma_{N_L,L}$, $\Gamma_{N_R} \equiv \Gamma_{N_R,R}$, $\Gamma_{S,j}$ as spin-independent tunnel-coupling strengths. With this we define $\Gamma_N \equiv \Gamma_{N_L} + \Gamma_{N_R}$. Furthermore, electrons cannot tunnel from the left (right) quantum dot to the right (left) normal conductor, i.e., $t_{N_R,L} = t_{N_L,R} = 0$. For the double-dot system we assume the dots' levels to be spin degenerate, that is $\varepsilon_{j\uparrow} = \varepsilon_{j\downarrow} = \varepsilon_j$, the Coulomb repulsion within one dot to be infinite $U_{\text{intra}} \to \infty$, and a finite inter-dot interaction $U_{\text{inter}} \equiv U$. The limit $U_{\text{intra}} \to \infty$ excludes the possibility of double occupation of the same dot and, therefore, only CAR and no local AR appears. As independent pumping parameters we choose the two spin-degenerate dot levels, $\{\varepsilon_L, \varepsilon_R\}$, which can be varied by means of gate voltages. This system will be contrasted to the system with the lead S in its normal state, which is referred to as NDNDN and in which we take $r \in N_L, N_R, N_c$.

6.1.2 Single-Dot Device

In order to identify the processes relevant for pumping, we consider a single-level quantum dot tunnel coupled to a ferromagnet and a superconductor (FDS), which having a smaller Hilbert space allows for a simpler analysis. The Hamiltonian of the single-dot system is obtained from the general Hamiltonian considering only one dot (we consistently drop the index j) and two leads: $r \in F, S$. The ferromagnet is described by the Stoner model which induces $\Gamma_\uparrow \neq \Gamma_\downarrow$. The nonvanishing tunnel-coupling strengths are: Γ_F and Γ_S. The pumping cycle in this case is realized by varying independently the two spin-split levels $\varepsilon_\uparrow, \varepsilon_\downarrow$. This can be done by means of a time-dependent gate voltage and magnetic field.

6.1.3 Large-Δ Limit

In the $\Delta \to \infty$ limit quasi-particle transport in the superconducting lead is suppressed and an effective description of the dot that takes into account Andreev tunneling can be obtained by integrating out the superconducting degrees of freedom.[141,150,189–192] Here we will discuss the resulting effective Hamiltonian only for the NDSDN system. The one for the FDS system is completely analogous. The effective Hamiltonian in the limit $U_{\text{intra}} \to \infty$ reads[150]

$$H_{\text{eff}} = \sum_{j\sigma} \varepsilon_j n_{j\sigma} + U \sum_{\sigma\sigma'} n_{L\sigma} n_{R\sigma'} + \frac{1}{2}\Gamma_S \left(d^\dagger_{R\uparrow} d^\dagger_{L\downarrow} - d^\dagger_{R\downarrow} d^\dagger_{L\uparrow} + \text{h.c.} \right) \tag{6.3}$$

with $\Gamma_S = \sqrt{\Gamma_{SL}\Gamma_{SR}}$ being the effective coupling. The eigenstates are $|\chi\rangle \in \{|+\rangle, |-\rangle, |\sigma,0\rangle, |0,\sigma\rangle, |T_{-1}\rangle, |T_0\rangle, |T_1\rangle\}$, where $|\sigma,0\rangle$ ($|0,\sigma\rangle$) corresponds to the left (right) dot being singly occupied with spin σ and the right (left) dot being empty. The triplet states are $|T_{-1}\rangle = |\downarrow,\downarrow\rangle$, $|T_0\rangle = (|\downarrow,\uparrow\rangle + |\uparrow,\downarrow\rangle)/\sqrt{2}$ and $|T_1\rangle = |\uparrow,\uparrow\rangle$. The tunnel-coupling to the superconductor leads to eigenstates that are coherent superpositions of the state with both dots empty $|0\rangle$ and the singlet state $|S\rangle = (|\downarrow,\uparrow\rangle - |\uparrow,\downarrow\rangle)/\sqrt{2}$,

$$|\pm\rangle = \frac{1}{\sqrt{2}}\sqrt{1 \mp \frac{\delta}{2\varepsilon_A}}\,|0\rangle \mp \frac{1}{\sqrt{2}}\sqrt{1 \pm \frac{\delta}{2\varepsilon_A}}\,|S\rangle \ , \tag{6.4}$$

where $\delta \equiv \varepsilon_L + \varepsilon_R + U$ is the detuning between the empty state and the singlet and $2\varepsilon_A \equiv \sqrt{\delta^2 + 2\Gamma_S^2}$ is the energy splitting between the $|+\rangle$ and $|-\rangle$ states. The corresponding eigenenergies are $E_\pm = \frac{\delta}{2} \pm \varepsilon_A$, $E_{(\sigma,0)} = \varepsilon_L$, $E_{(0,\sigma)} = \varepsilon_R$, and $E_{T_{-1}} = E_{T_0} = E_{T_1} = \varepsilon_L + \varepsilon_R + U$. In the FDS setup the eigenenergies and eigenstates are the same except that L and R are replaced by $\uparrow$ and $\downarrow$, respectively, the triplet states do not exist, the singlet state $|S\rangle$ is replaced by a double occupation $|d\rangle = d^\dagger_\uparrow d^\dagger_\downarrow |0\rangle$ of the dot, and $2\varepsilon_A \equiv \sqrt{\delta^2 + \Gamma_S^2}$.

6.2 Method

In order to calculate the pumped charge we use the real-time approach to adiabatic pumping, which has been introduced in Sec. 4.2. Here, we briefly review the most

important formulae without going to much into detail. On top of the adiabatic expansion we perform a systematic expansion in the weak tunnel-coupling strengths between normal conductor and leads, $\Gamma_N < k_B T$, of the kernel and the reduced density matrix, taking into account tunneling processes up to first order in Γ_N. Tunneling processes between the dots and the superconductor are taken into account exactly by means of the effective Hamiltonian. Orders in the perturbation expansion in the tunnel coupling are denoted by numbers in the superscript. The instantaneous and the adiabatic contributions to the reduced density matrix are determined by

$$0 = \left(-\mathrm{i}\mathbf{E}(t) + \mathbf{W}_t^{(i,1)}\right) \boldsymbol{\pi}_t^{(i,0)} \tag{6.5}$$

$$\frac{d}{dt}\boldsymbol{\pi}_t^{(i,0)} = \left(-\mathrm{i}\mathbf{E}(t) + \mathbf{W}_t^{(i,1)}\right) \boldsymbol{\pi}_t^{(a,-1)} \tag{6.6}$$

together with the normalization condition $\boldsymbol{n}\boldsymbol{\pi}_t^{(\mathrm{i},0)} = 1$ and $\boldsymbol{n}\boldsymbol{\pi}^{(a,-1)} = 0$. The rates $\mathbf{W}_t^{(i,1)}$ between diagonal elements of the reduced density matrix can be obtained by means of Fermi's Golden Rule. Solely for the ones connecting off-diagonal elements this is not sufficient and one has to resort to a diagrammatic method whose rules are presented in Appendix A. In general, offdiagonal elements of the reduced density matrix, $p_{\chi'}^{\chi}$, enter Eqs. (6.5) and (6.6). However, we assume weak coupling to the normal conductors $\Gamma_N \ll k_B T, \varepsilon_A$, where for the FDS as well as the NDSDN setup the offdiagonal elements of the reduced density matrix are decoupled from the diagonal ones.[193] As we are interested in the diagonal elements, needed for the computation of the current, we can therefore disregard the offdiagonal ones. Solely in the NDNDN setup the dynamics of the offdiagonal elements $p_{(0,\sigma)}^{(\sigma,0)}$ and $p_{(\sigma,0)}^{(0,\sigma)}$ are coupled with the dynamics of the occupation probabilities. In the NDNDN system, where also offdiagonal elements of the reduced density matrix contribute, we assume $\Delta\varepsilon = \varepsilon_L - \varepsilon_R \approx \Gamma_N$ and $\mathbf{E}$ as well as $\mathbf{W}_t^{(i,1)}$ have to be of the same order in the small parameter $\Gamma_N \simeq \Delta\varepsilon$.[194,195]

In a similar way, one can write rate equations for the expectation value of the current into lead r. The instantaneous contribution to the current is

$$I_r^{(i)}(t) = e\mathbf{n}\mathbf{W}_t^{r,(i)}\boldsymbol{\pi}_t^{(i)}\,, \tag{6.7}$$

which we consider in first order in the tunnel coupling, only. From Eq. (6.7), we derive the conductance, which is given by $G = (dI^{(i,1)}/dV)|_{V=0}$, with V being the bias voltage. The instantaneous current vanishes exactly in the absence of an applied bias. The adiabatic correction to the current is then the dominant one and it is given by

$$I_r^{(a,0)}(t) = e\mathbf{n}\mathbf{W}_t^{r,(i,1)}\boldsymbol{\pi}_t^{(a,-1)}\,. \tag{6.8}$$

We are interested in the charge transferred into lead r per cycle of the parameter variation. This is found by integrating the current over one period

$$Q_{X_1,X_2}^r = \int_0^{2\pi/\Omega} dt I_r^{(a,0)}(t). \tag{6.9}$$

In the following we consequently drop the index r if the pumped charge corresponds to the superconductor, $Q_{X_1,X_2} \equiv Q^S_{X_1,X_2}$. Two time-dependent parameters are necessary to create a nonvanishing pumped charge. We indicate the parameter choice in the subscript. The pumping parameters can be written as $X_i(t) = \overline{X}_i + \delta X_i(t)$, where $\overline{X}_i$ is the mean value and $\delta X_i(t)$ the oscillating component. We concentrate on the limit of weak pumping, that is, the oscillating component is small compared to the tunnel coupling $\delta X_i(t) \ll \Gamma_N$. Therefore, we only account for terms up to bilinear order in $\delta X_i(t)$ and the pumped charge is proportional to $\eta_{X_1,X_2} \equiv \int_0^{2\pi/\Omega} dt \delta X_1(t) \frac{d}{dt} \delta X_2(t)$.

6.3 Results

Using the effective Hamiltonian and performing the perturbation expansion as presented in the previous section we calculate the pumped charge in lowest order in Γ_N or Γ_F, respectively. Close to the dot levels being at resonance, the lowest order processes are the dominant ones and cotunneling processes can safely be neglected. Before tackling the more complicated problem of CAR, we will first study the FDS system, in order to understand the features of local AR in adiabatic pumping and to identify the different transport processes occurring in this simple setup. For this setup, we also examine the influence of cotunneling processes on the pumped charge far from resonance (Coulomb-blockade regime), which are important when the interaction U becomes much larger than the temperature. In Sec. 6.3.2, we discuss how adiabatic pumping provides the possibility to study CAR. To this end, we finally compare the NDSDN setup with the NDNDN setup.

6.3.1 Local Andreev Reflection

In this subsection we consider adiabatic pumping through the FDS setup. We choose the dot-level positions for electrons with different spins $\varepsilon_\uparrow(t)$ and $\varepsilon_\downarrow(t)$ to be the pumping parameters. Such a situation can be realized by a time-dependent gate voltage and a time-dependent magnetic field, the latter introducing a time-dependent Zeeman splitting. This choice of pumping parameters is convenient here as it allows for a direct comparison with a double dot in the absence of a magnetic field, in which gate voltages applied to the two dots are independently modulated. Pumping is possible whenever the polarization of the leads or the average level splitting $\overline{\Delta\varepsilon} \equiv \overline{\varepsilon}_\uparrow - \overline{\varepsilon}_\downarrow$ are nonvanishing. To get a better understanding of the transport properties we first focus on two different limits: a vanishing polarization ($p = 0$) and a vanishing average level splitting ($\overline{\varepsilon}_\uparrow = \overline{\varepsilon}_\downarrow$). We start with the case of a vanishing polarization and a finite level splitting.

For the pumped charge we find

$$Q_{\varepsilon_\uparrow,\varepsilon_\downarrow}(p=0) \approx -\frac{e\eta_{\varepsilon_\uparrow,\varepsilon_\downarrow}\Gamma_S^2}{\left[\Gamma_S^2 + (U + \overline{\varepsilon}_\uparrow + \overline{\varepsilon}_\downarrow)^2\right]^{\frac{3}{2}}} \times \frac{f(\overline{E}_- - \overline{\varepsilon}_\uparrow) f'(\overline{E}_- - \overline{\varepsilon}_\downarrow) - f(\overline{E}_- - \overline{\varepsilon}_\downarrow) f'(\overline{E}_- - \overline{\varepsilon}_\uparrow)}{\left[f(\overline{E}_- - \overline{\varepsilon}_\uparrow) + f(\overline{E}_- - \overline{\varepsilon}_\downarrow) - f(\overline{E}_- - \overline{\varepsilon}_\uparrow) f(\overline{E}_- - \overline{\varepsilon}_\downarrow)\right]^2} \tag{6.10}$$

with $f'(x) = \frac{d}{dx}f(x)$ being the derivative of the Fermi function. We made use of the approximation $f(E_+ - \varepsilon_\uparrow) \approx f(E_+ - \varepsilon_\downarrow) \approx 0$ and $f(\varepsilon_\uparrow - E_+) \approx f(\varepsilon_\downarrow - E_+) \approx 1$, which is justified for $\Gamma_S > k_B T$. Equation (6.10) shows that the pumped charge vanishes for an average Zeeman splitting equal to zero, that is $\overline{\varepsilon}_\uparrow = \overline{\varepsilon}_\downarrow$.

In Fig. 6.2a), we show the pumped charge $Q_{\varepsilon_\uparrow \varepsilon_\downarrow}$, without the approximation on the Fermi functions used to write Eq. (6.10), as function of the average value of the mean dot level $\overline{\varepsilon} \equiv (\overline{\varepsilon}_\uparrow + \overline{\varepsilon}_\downarrow)/2$.

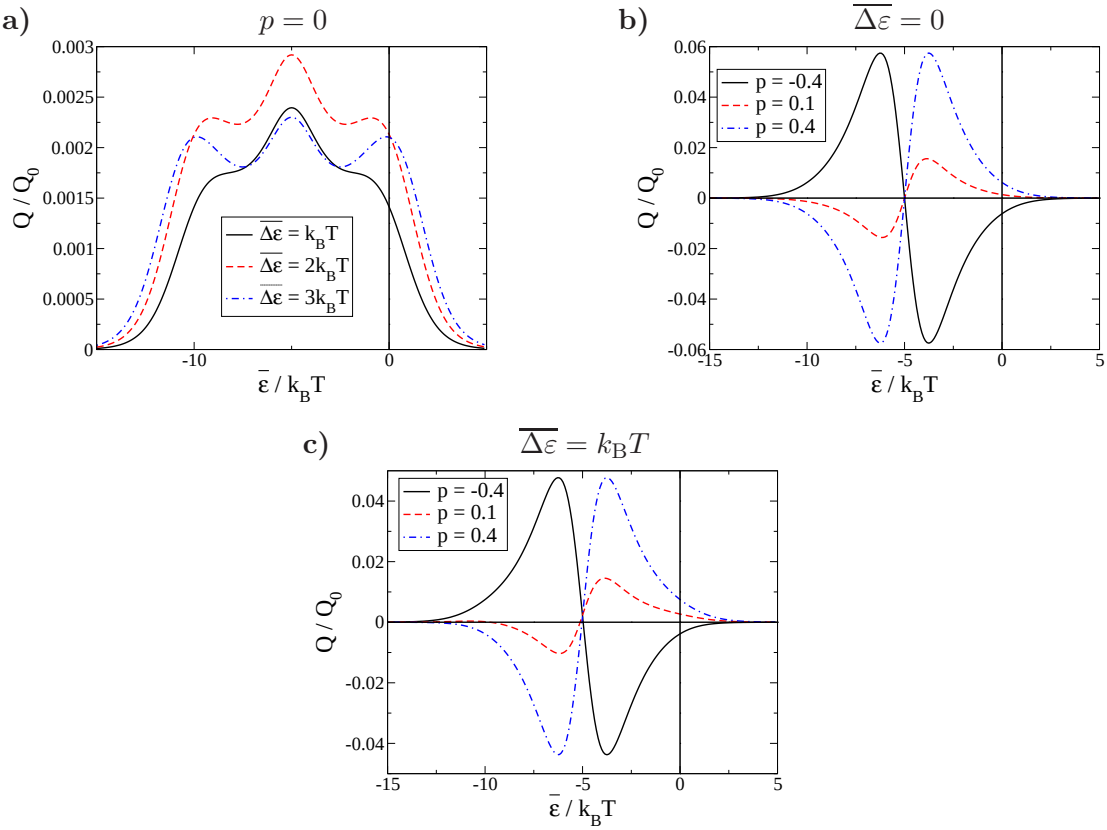

Figure 6.2: FDS setup: Pumped charge $Q \equiv Q_{\varepsilon_\uparrow, \varepsilon_\downarrow}$ in units of $Q_0 = \frac{e\eta_{\varepsilon_\uparrow, \varepsilon_\downarrow}}{(k_B T)^2}$ as a function of the average dot level $\overline{\varepsilon}$. The parameters in all figures are $\Gamma_S = 4k_B T$ and $U = 10k_B T$.

The pumped charge exhibits a three-peak structure. The two external peaks are observed when the dot is in resonance with the normal lead, that is, when the addition energy for a single electron equals the chemical potential. This is realized for $E_- - \varepsilon_\sigma = 0$. Since we consider Zeeman splitting $\Delta\varepsilon$ being larger than $k_B T$ (with $\varepsilon_\downarrow$ being the level with the lower energy), only the resonance $E_- - \varepsilon_\downarrow = 0$ is accessible due to Coulomb blockade. The other Andreev bound state, with energy E_+, is only accessible in the high-bias or high temperature regime. The two resonances associated to the condition $E_- - \varepsilon_\downarrow = 0$ are at the two positions, $\varepsilon_{\max,1\pm} \approx \frac{1}{2}(-U \pm [(U + |\Delta\varepsilon|)^2 - \Gamma_S^2]^{1/2})$.

The central peak appears when the dot is in resonance with the superconductor,

that is, the average dot level is $\overline{\varepsilon}_{\max,2} \approx -U/2$ which is realized for $\delta < \Gamma_N$. In this case the dot undergoes fast oscillations between the empty and doubly-occupied state due to coherent Cooper-pair transfer. In particular these oscillations are much faster than tunneling events of single particles between the normal conductor and the dot. However, transport requires exchange of charge both with the normal and the superconducting leads. Therefore, increasing the Coulomb repulsion U leads to an overall suppression of the pumped charge. The three peaks are not suppressed in the same manner. The side peaks are suppressed by the factor $\left[1+(U+\overline{\varepsilon}_\uparrow+\overline{\varepsilon}_\downarrow)^2/\Gamma_S^2\right]^{-\frac{3}{2}}$, appearing in Eq. (6.10). Instead the central peak is suppressed by the combination of Fermi functions in Eq. (6.10).

We now focus on the limit of a vanishing average level splitting ($\overline{\Delta\varepsilon}=0$) and a finite polarization. The pumped charge is then given by

$$Q_{\varepsilon_\uparrow,\varepsilon_\downarrow}(\overline{\Delta\varepsilon}=0) \approx \frac{4e\eta_{\varepsilon_\uparrow,\varepsilon_\downarrow} p\left(1-p^2\right)\Gamma_S^2\delta}{k_BT\left[\Gamma_S^2+(1-p^2)\delta^2\right]^2}\cdot\frac{1-f(\overline{E}_- -\overline{\varepsilon})}{2-f(\overline{E}_- -\overline{\varepsilon})} \tag{6.11}$$

approximating the Fermi functions as done above. We find that the pumped charge is an odd function of δ, therefore vanishing at the electron-hole symmetric point. The full result for the pumped charge at zero average detuning, $\overline{\Delta\varepsilon}=0$, is shown in Fig. 6.2b). As shown in Eq. (6.11), the pumped charge vanishes at $\overline{\varepsilon}=-U/2$. However, we find a peak-trough structure, that is, the maximum contribution to the pumped charge appears in two peaks, close to $\overline{\varepsilon}\approx -U/2$, with opposite sign. As argued above this relies on fast Cooper-pair oscillation. The amplitude of the pumped charge is much larger than in Fig. 6.2a) and strongly depends on the polarization of the leads: the stronger the polarization the larger the amplitude. Furthermore, the pumped charge, in the vicinity of the electron-hole symmetric point is not suppressed by the strong Coulomb repulsion. We will address this, when discussing the cotunneling regime.

Instead of giving the lengthy expression of the pumped charge for a finite average level splitting, $\overline{\Delta\varepsilon}\neq 0$, and a finite polarization, $p\neq 0$, we show it in Fig. 6.2c) as a function of the average dot level. The shape is a combination of the two structures shown in Figs. 6.2a) and 6.2b). We find that the effect for the finite polarization dominates. Therefore, the peaks around $\overline{\varepsilon}\approx -U/2$ with opposite sign are the main feature to identify the proximization of the dot.

When lowering the temperature, the height of the peak-trough structure increases with inverse temperature, that is, it becomes more and more pronounced. This result can, however, only be trusted as long as temperature is still large enough such that all charge states are thermally occupied. In the Coulomb-blockade regime, $U \gg k_\mathrm{B}T$ and $\delta \equiv \varepsilon_\uparrow+\varepsilon_\downarrow+U \approx k_\mathrm{B}T$, when the sequential tunneling rates to reach an empty or doubly-occupied dot are exponentially small, higher-order processes such as cotunneling need to be taken into account. To compare with the result presented in Eq. (6.11), we analyze the pumped charge in the cotunneling regime. For this, we first of all note that Eq. (6.6) looses its validity in the Coulomb-blockade regime, since the rates $W^{(i,1)}$ get exponentially suppressed, while - in contrast to situations where the magnetic field is constant[80] - the time-derivative of the instantaneous occupation probabilities, $\frac{d}{dt}p_{t,\sigma}^{(i,0)}$, of single occupation with spin σ do not. The time-evolution of the probabilities

of single occupation is then governed by spin-flip processes in second order in the tunneling, $W^{(i,2)}_{t,\downarrow\uparrow}$, entering Eqs. (6.6) and (6.8) together with adiabatic corrections to the probability in minus second order in Γ, $p^{(a,-2)}_{t,\sigma}$. However, since $U \gg k_{\mathrm{B}}T$ and $\delta \approx k_{\mathrm{B}}T$ results in an exponential suppression of $\frac{d}{dt}p^{(i,0)}_{t,\pm}$, also the elements $p^{(a,-2)}_{t,\pm}$ are suppressed and will not enter the current in the Coulomb blockade regime. For the calculation of the cotunneling rates we follow the procedure introduced in Refs. 181,182 for metallic islands and applied for single-level quantum dots, for example, in Ref. 183. In contrast to Eq. (6.8) in the cotunneling regime the current is then

$$I^{(a,0)}_F(t) = e\left[W^{F,(i,2)}_{t,\downarrow\uparrow}p^{(a,-2)}_{t,\uparrow} + W^{F,(i,2)}_{t,\uparrow\downarrow}p^{(a,-2)}_{t,\downarrow}\right], \tag{6.12}$$

which is nonvanishing due to $p^{(a,-2)}_{t,\uparrow} = -p^{(a,-2)}_{t,\downarrow}$ and $W^{F,(i,2)}_{t,\downarrow\uparrow} = -W^{F,(i,2)}_{t,\uparrow\downarrow}$. Due to charge conservation, $Q_{\varepsilon_\uparrow,\varepsilon_\downarrow} = -Q^F_{\varepsilon_\uparrow,\varepsilon_\downarrow}$, the charge pumped into the superconductor is found as

$$Q_{\varepsilon_\uparrow,\varepsilon_\downarrow} \approx -\frac{3e\pi^2 k_B T \eta_{\varepsilon_\uparrow,\varepsilon_\downarrow}\Gamma_S^2 p\left(1-p^2\right)\delta\left(\Gamma_S^2+\delta^2-U^2\right)}{\left[(1+p^2)\pi^2(k_BT)^2\Gamma_S^2 + \frac{3}{32}(1-p^2)\left(\Gamma_S^2+\delta^2-U^2\right)^2\right]^2}, \tag{6.13}$$

where we used $\overline{\Delta\varepsilon}/U \ll 1$. The qualitative behavior of the pumped charge in the cotunneling regime strongly differs from the sequential tunneling regime. For strong Coulomb interaction, in the cotunneling regime transport is suppressed with $1/U^6$. To find a possible explanation for this suppression we focus on the transport processes during one pumping cycle. Consider the following process where a net transport is obtained in the cotunneling as well as in the sequential tunneling regimes: An electron tunnels from the ferromagnet onto a singly occupied dot. The dot is then, for example, in state $|-\rangle$. To obtain a net transport another electron has to tunnel from the ferromagnet onto the quantum dot bringing it back into single occupation which is possible due to Cooper-pair oscillations. A comparison of the system's time scales for the two regimes might shed light on the origin of the suppression of the pumped charge. In the sequential tunneling regime the time between two single-electron transport processes scales with $1/\Gamma_N$. In the cotunneling regime the intermediate state can only be virtually occupied due to energy conservation and hence the time between two tunneling events scales with $1/U$. In the considered limit of large $U \gg k_BT$ and small $\Gamma_N \ll k_BT$, Cooper-pair oscillations are fast compared to the time between two tunneling events in the sequential but slow in the cotunneling regime. This gives an interpretation of the suppression of the pumped charge in the cotunneling regime.

6.3.2 Crossed Andreev Reflection

We now consider a system made out of two quantum dots each coupled to one normal conducting lead. The two QDs are then coupled to each other via a common superconducting lead, see Fig. 6.1. We take the pair potential in the superconducting lead to be the largest energy scale ($\Delta \to \infty$), such that single-particle transport between superconductor and QDs is suppressed. Furthermore, we take the intra-dot Coulomb

repulsion ($U_{\text{intra}} \to \infty$) to be large excluding double occupation of each of the single dots, as discussed in Sec. 6.1.3. In this regime, *only nonlocal* effects enable transport between the superconductor and the dots, that is a Cooper pair has to be split into two electrons occupying different dots or electrons from different dots enter the superconductor to form a Cooper pair.
We now calculate the charge pumped through the system due to the periodic modulation of the dot levels $\varepsilon_{\text{L}}(t)$ and $\varepsilon_{\text{R}}(t)$, which can be achieved by two time-dependent gate voltages. We are interested in the charge, $Q_{\varepsilon_L,\varepsilon_R}$, pumped into the superconducting lead, which due to charge conservation and to the fact that only CAR is allowed is twice the charge pumped out of each normal lead.

In Figs. 6.3a) and 6.3b) we show $Q_{\varepsilon_L,\varepsilon_R}$ as a function of $\overline{\varepsilon}$ for different values of $\overline{\Delta\varepsilon}$ and for different coupling asymmetries with the normal conducting leads, $\lambda = (\Gamma_{N_L} - \Gamma_{N_R})/\Gamma_N$, respectively. Features appear at the resonance condition with the

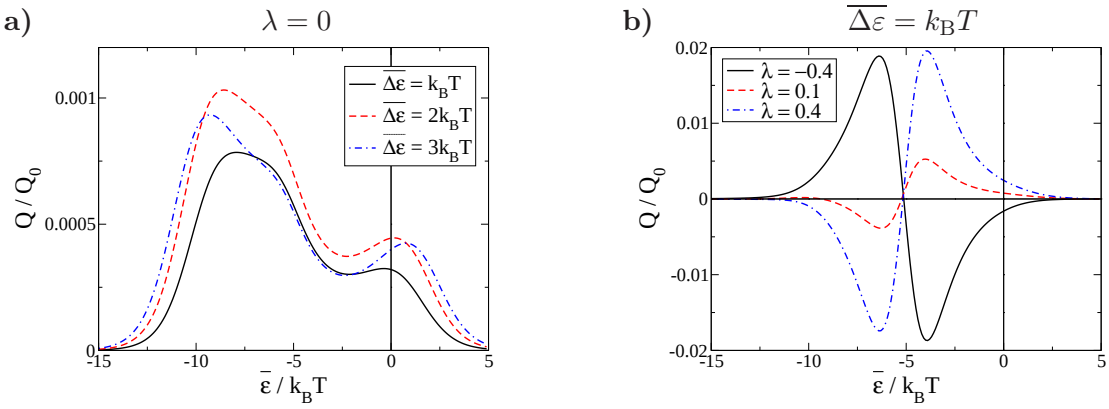

Figure 6.3: NDSDN setup: Pumped charge $Q \equiv Q_{\varepsilon_L,\varepsilon_R}$ in units of $Q_0 = \frac{e\eta_{\varepsilon_L,\varepsilon_R}}{(k_BT)^2}$ as a function of the average dot level $\overline{\varepsilon}$. The parameters are $\Gamma_S = 3k_BT$ and $U = 10k_BT$.

normal and superconducting leads, that are equivalent to the one in the FDS case with Zeeman splitting replaced by the difference of the energy levels of the left and right dots and the polarization p replaced by coupling asymmetry λ. If the couplings to the normal leads are symmetric, $\lambda = 0$, the charge as a function of the average mean dot level position $\overline{\varepsilon}$, shows three peaks similarly to the FDS case. In this respect, CAR exhibits similar features to AR through the single dot. The main difference between the two is the asymmetry in the heights of the external peaks which can be attributed to the triplet blockade discussed in Ref. 150. Since the proximization by the superconductor solely causes a coupling between the empty and the singlet state, Cooper-pair tunneling is blocked whenever the dot is in the triplet state. In the FDS setup the symmetry of the two external peaks can be related to particle-hole symmetry which is broken by this triplet blockade in the NDSDN structure.

As in the FDS with finite polarization, also in the NDSDN the scenario changes completely in the asymmetric-coupling case ($\lambda \neq 0$). In this case the peak at $\overline{\varepsilon} = -U/2$ is replaced by a large peak-trough structure. Interestingly, this feature dominates the

external peaks which are barely visible in Fig. 6.3b). The position of the maxima and minima of this feature are exchanged when reversing the coupling asymmetry ($\lambda \to -\lambda$).

However, in the linear conductance, the coupling asymmetry does not introduce any new feature, as shown in Fig. 6.4, where for different coupling asymmetries only the weight of the three peaks is influenced and not their polarity. Furthermore, the central peak is strongly suppressed. That means that the characteristic features of CAR in adiabatic pumping are not present in the linear conductance. As we will see in the next subsection these features are fundamental to distinguish single-particle transport from CAR.

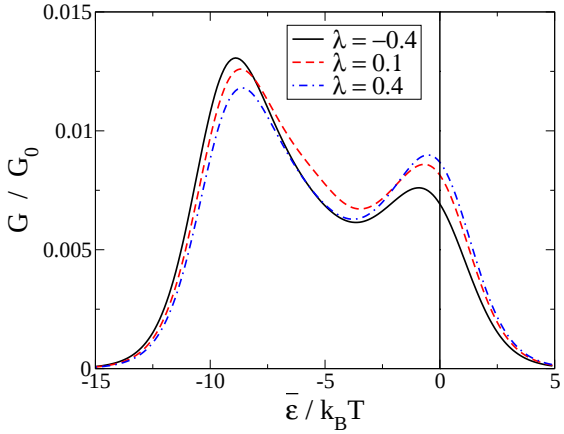

Figure 6.4: NDSDN setup: Linear conductance as a function of the average dot level $\overline{\varepsilon}$ for different coupling asymmetries λ. The parameters are $\Gamma_S = 3k_BT$, $\Gamma_N = k_BT$, $U = 10k_BT$, and $\overline{\Delta\varepsilon} = k_BT$.

6.3.3 Single-Particle Transport

A finite pumped charge can be obtained by varying in time the properties of the two spatially-separated dots exclusively by nonlocal correlations. CAR has such a nonlocal character. However, there may be other nonlocal effects that can produce a finite pumped charge and, thus, mask the signal from CAR. In order to distinguish CAR from other nonlocal transport processes, we investigate single-particle transport in a NDNDN setup, where the superconductor in the NDSDN setup is replaced by a normal conductor. While in the NDSDN setup the nonlocality arises from CAR, in the NDNDN setup pumping is possible due to the formation of a coherent superposition of states with one electron either in the left or the right dot. This superposition is generated by the tunnel coupling to the common normal lead. In contrast to the NDSDN setup, the coherent superposition is strongly suppressed if the difference of the two dot levels is large compared to temperature ($|\Delta\varepsilon| \gg k_BT$).

Furthermore, in the NDSDN setup pumping cannot lead to an average charge transfer from the left into the right normal lead (and vice versa) because transport through

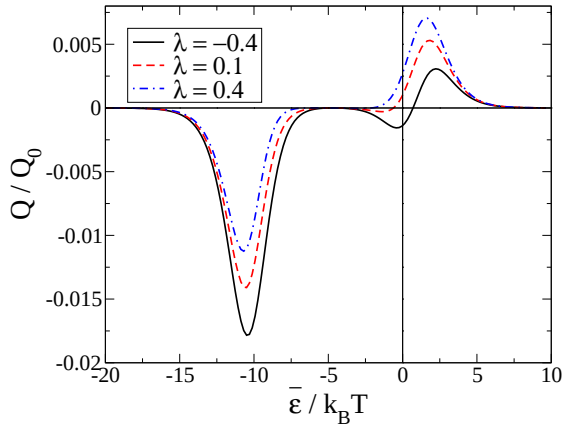

Figure 6.5: NDNDN setup: Pumped charge $Q \equiv Q^{N_c}_{\varepsilon_L,\varepsilon_R}$ in units of $Q_0 = \frac{e\eta_{\varepsilon_L,\varepsilon_R}}{(k_BT)^2}$ as a function of the average dot level $\overline{\varepsilon}$ for different coupling asymmetries λ. The other parameters are $\Gamma_{N_{\mathrm{c,L}}} = 0.4k_BT$, $\Gamma_{N_{\mathrm{c,R}}} = 0.2k_BT$, $\Gamma_N = 0.1k_BT$, $U = 10k_BT$, and $\overline{\Delta\varepsilon} = k_BT$.

the superconductor always involves CAR in the infinite-Δ limit. Instead, in the NDNDN setup, charge can also be transferred from the left lead N_L to the right lead N_R. Therefore an asymmetry of transport into lead N_L and into lead N_R is one possible indication for single-particle transport.

The motivation of this work is the identification of CAR with respect to quasiparticle transport in form of an easily detectable signature in the pumped charge. We find this to be the peak-trough structure at $\overline{\varepsilon} = -U/2$ that appears in the presence of a coupling asymmetry. In single-particle transport, modeled by the NDNDN setup, this feature is completely absent and only the peaks at the normal resonances appear, see Fig. 6.5. These normal resonances also have opposite signs, which cannot be reversed by changing the coupling asymmetry. Also in the very special situation of a symmetric coupling ($\lambda = 0$) CAR can be distinguished from single-particle transport by the presence of the peak at $\overline{\varepsilon} = -U/2$. Therefore, an experimental study of the pumped charge in the double-dot system as a function of λ as well as its behavior around $\overline{\varepsilon} \approx -U/2$ can clearly distinguish CAR from quasiparticle transport.

6.4 Conclusions

We have investigated adiabatic pumping through two quantum dots tunnel coupled to the same superconductor and additionally coupled to different normal conductors. For an infinite intra-dot Coulomb repulsion in this setup pumping relies on CAR. In order to understand the underlying transport processes we mapped the setup to the simpler setup of a quantum dot tunnel coupled to a ferromagnet and a superconductor where only AR appears. We found that most of the features of pumping including CAR are also present in pumping with local AR. The main difference are asymmetries

due to the presence of the triplet state. To distinguish CAR from single-electron tunneling, which does not appear in our model but might be relevant in experiments, we compare transport through the double-dot setup containing a superconductor with a setup where the superconductor is replaced by a normal conductor. The dependence on the average dot-level position and the dependence on the coupling asymmetry λ turn out to be the main distinguishing features.

7 AC Josephson Transport through Interacting Quantum Dots

Josephson junctions are formed in different ways. Two superconductors can be linked by an insulator, a normal conductor, or a constriction in an otherwise continuous superconducting material.[151,152] Advancements in nanofabrication even enabled to contact superconductors with quantum dots (QDs), which can be formed in carbon nanotubes,[97–102] in InAs nanowires,[103–105] in graphene,[106] or by means of self-organization in InAs with Al electrodes.[107–109] There are several motivations to investigate such devices.[110,111] The interplay of strong Coulomb repulsion and superconducting correlations provide a large variety of physical effects. Furthermore, the discrete energy levels of the QD can be tuned by external electrodes creating different transport regimes. In junctions where a quantum dot is contacted to two superconductors (S-QD-S) different transport processes appear. In the absence of any bias voltage the only mechanism leading to transport is the DC Josephson effect. In the noninteracting case it can be studied, e.g., by a scattering approach.[196] But also Coulomb repulsion has been included by many different formalisms as a perturbation expansion in the tunneling Hamiltonian[138,139,153,154] and in the Coulomb repulsion,[197,198] a mean-field approach,[199] quantum Monte-Carlo simulations,[200] a renormalization group technique,[201] or the numerical diagonalization of an effective dot Hamiltonian.[190–192] In the context of the DC Josephson effect it has been theoretically predicted[153,154] and experimentally confirmed[100,103] that the two electrons forming a Cooper pair can tunnel coherently one by one through a strongly interacting quantum dot.

Applying a finite bias voltage complicates the problem. A DC signal is sustained by quasiparticle tunneling and (multiple) Andreev reflection. Furthermore, the AC Josephson effect gives rise to a time dependent signal. The stationary current has been investigated also for a nonvanishing Coulomb repulsion by focusing on single-quasiparticle tunneling,[128–130] within a slave boson mean-field approximation,[99,131] or a perturbation expansion in the Coulomb repulsion.[132] Multiple Andreev reflection processes not only give rise to a stationary current but also lead to higher harmonics contributing to the AC Josephson transport. The first quantitative description including this interplay has been investigated in quantum point contacts by means of a scattering approach.[202,203] In a noninteracting quantum dot the dependence of the bias voltage on the different harmonics has also been studied.[204] The used formalism has been a general Hamiltonian approach applied to this noninteracting system. In a S-QD-S setup where a normal conductor is additionally coupled to the QD dephasing effects have been investigated.[205] It has been observed that for a gradually increasing coupling to the normal conductor the AC signal decreases. To this end, a Keldysh formalism has been applied to a noninteracting system. Further works deal with the

time evolution of the current after switching on a finite bias voltage.[206,207]

Since Coulomb repulsion plays an important role in transport through quantum dots the motivation of this work is to investigate the AC Josephson effect through quantum dots where the Coulomb repulsion is taken into account in a nonperturbative way. To this end, we introduce a real-time diagrammatic approach, where a perturbation expansion in tunnel coupling is performed. It can be understood as extension to the DC formalism presented in Ref. 139. We apply this formalism to a three-terminal geometry consisting of a strongly interacting quantum dot, which is tunnel coupled to two superconductors and one normal conductor, see Fig. 7.1 To sustain (DC and AC)

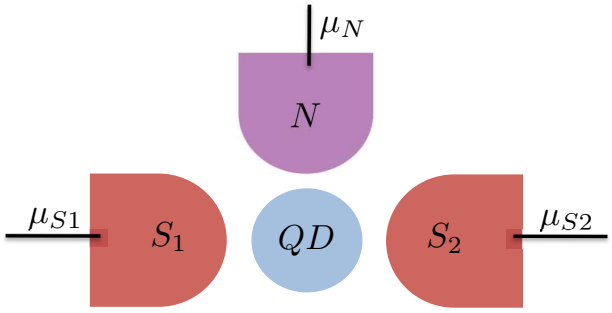

Figure 7.1: A normal conductor additionally coupled to the S-QD-S setup.

Josephson transport through the QD in first order in the tunnel-coupling strengths, superconducting correlations must be induced on the QD by the proximity of the superconducting leads. We find that a large AC signal between QD and one superconducting lead requires a large proximization of the QD by the other superconducting lead which can be achieved by tuning the gate voltage accordingly. Another possibility to tune the AC Josephson effect is to apply a finite bias voltage to the normal lead. We discuss the amplitude of the AC components of the current between the superconductors as a function of the gate and bias voltages.

7.1 Model

The system under consideration is decomposed by a quantum dot tunnel coupled to two superconducting and one normal conducting leads. The different building blocks have been introduced in previous chapters in detail. Here, we briefly review the most important parts. The quantum dot is assumed to accommodate one spin-degenerate level ε. It is described by the Anderson impurity model,

$$H_{\mathrm{dot}} = \varepsilon \sum_{\sigma} d_{\sigma}^{\dagger} d_{\sigma} + U n_{\uparrow} n_{\downarrow} \,,$$

which has already been presented in Eq. (2.6).

The superconductors are modeled by the mean-field BCS Hamiltonian, which has

been introduced in Sec. 2.3.3. It is given by

$$H_r^{\text{mf-BCS}} = \sum_{k,\sigma} \varepsilon_k c_{rk\sigma}^\dagger c_{rk\sigma} - \Delta_r^* \sum_k S_r^\dagger c_{r-k\downarrow} c_{rk\uparrow} - \Delta_r \sum_k S_r c_{r-k\uparrow}^\dagger c_{rk\downarrow}^\dagger \,.$$

In order to diagonalize this Hamiltonian, we perform a Bogoliubov transformation, see Sec. 2.3.3. The normal conductor's Hamiltonian is described by the first term of the mean-field BCS Hamiltonian, see Eq. (2.7). As presented in Eq. (2.8) the tunneling Hamiltonian reads

$$H_{\text{tun}} = \sum_{rk\sigma} t_r c_{rk\sigma}^\dagger d_\sigma + H.c.\,.$$

Finally, the total Hamiltonian is given by $H = H_{\text{dot}} + H_{\text{tun}} + \sum_r H_r$.

7.2 Method

In Ref. 139 a real-time diagrammatic approach to the stationary transport through heterostructures, where a quantum dot is tunnel coupled to normal conductors and superconductors, is introduced. Here, we give a brief review of this formalism and present an extension also allowing for the AC Josephson transport. For simplicity we focus on a setup containing two superconductors. The system under consideration can be divided into three subsystems, the dot, the fermionic states of the leads, and the Cooper pair condensates in the superconductors. Since we are not interested in the fermionic dynamics of the leads, we can trace out their degrees of freedom and arrive at a reduced density matrix for the remaining part, i.e., the dot's degrees of freedom and the Cooper pair condensates. Its elements are given by $P_{\xi_2}^{\xi_1} \equiv \langle \xi_1 | \rho_{\text{red}} | \xi_2 \rangle$, where $|\xi\rangle \equiv |\chi, \{n_{S1}, n_{S2}\}\rangle$ includes the dot state $\chi = 0, \uparrow, \downarrow, d$ as well as the number of Cooper pairs in the two superconductors, n_{S1} and n_{S2}, measured relative to an arbitrary but fixed reference. The diagonal elements $P_\xi \equiv P_\xi^\xi$ give the probability to be in state ξ. The states ξ_1 and ξ_2 in $P_{\xi_2}^{\xi_1}$ provide more information than is needed to study the electric transport. In fact, only the differences of the Cooper pair numbers of the states $|\xi_1\rangle$ and $|\xi_2\rangle$ are important. Moreover, particle number conservation sets a constraint that the total number of electrons in $|\xi_1\rangle$ has to be the same is in $|\xi_2\rangle$. For convenience, we define

$$P_{\chi_2}^{\chi_1}(\{n_{S1}, n_{S2}\}) \equiv \sum_{m_{S1}, m_{S2}} P_{(\chi_2, \{m_{S1}, m_{S2}\})}^{(\chi_1, \{m_{S1}+n_{S1}, m_{S2}+n_{S2}\})} \,. \tag{7.1}$$

As a consequence of particle conservation, n_{S2} is a unique function of χ_1, χ_2, and n_{S1}. It is, therefore, enough to keep track of the Cooper pair number n of one lead only. We choose here lead $S1$, i.e., $n = n_{S1}$, and introduce the definitions $P_\chi(n) \equiv P_\chi^\chi(\{n, -n\})$, $P_0^d(n) \equiv P_0^d(\{n, -n-1\})$, and $P_d^0(n) \equiv P_d^0(\{n, -n+1\})$.

Finally, we collect all the nonvanishing elements of the reduced density matrix in the vector $\boldsymbol{\pi}(n) \equiv (P_0(n), P_\uparrow(n), P_\downarrow(n), P_d(n), P_0^d(n), P_d^0(n))^T$. Its dynamics are governed by the generalized master equation

$$\frac{\mathrm{d}}{\mathrm{d}t}\boldsymbol{\pi}(n)(t) + \mathrm{i}\mathbf{E}_n \boldsymbol{\pi}(n)(t) = \sum_{n'} \int_{-\infty}^{t} \mathrm{d}t' \mathbf{W}(n, n')(t, t') \boldsymbol{\pi}(n')(t') \,, \tag{7.2}$$

where the matrix elements of the kernel $W^{\chi_1\chi_1'}_{\chi_2\chi_2'}(n,n')(t,t')$ are the transition rates from an initial state at time t' described by $P^{\chi_1'}_{\chi_2'}(n')(t')$ to a final state at time t described by $P^{\chi_1}_{\chi_2}(n)(t)$. For the kernel we have introduced a notation analogous to the one adopted for the reduced density matrix:
$W^{\chi_1\chi_1'}_{\chi_2\chi_2'}(n_{S1},n'_{S1})(t,t') \equiv W^{\chi_1\chi_1'}_{\chi_2\chi_2'}(\{n_{S1},n_{S2}\},\{n'_{S1},n'_{S2}\})(t,t')$, where the excess number of Cooper pairs in the superconductor S2 is fixed by particle conservation. We get $n_{S1}+n_{S2}$ to be equal to 0 for $\chi_1=\chi_2$, equal to -1 for $[\chi_1=d,\chi_2=0]$, and equal to $+1$ for $[\chi_1=0,\chi_2=d]$. In a similar way, n'_{S2} is determined in terms of n'_{S1}, χ_1', and χ_2'. The only nonvanishing matrix elements of the matrix $\mathbf{E}_n$ are $E_{n\,\chi\chi}^{\chi\chi} = 2n(\mu_{S1}-\mu_{S2})$, $E_{n\,00}^{dd} = 2\varepsilon+U+2n(\mu_{S1}-\mu_{S2})-2\mu_{S2}$, and $E_{n\,dd}^{00} = -E_{-n\,00}^{dd}$.

The current between the dot and lead r is given by

$$I_r(t) = -e\sum_{n'}\int_{-\infty}^{t} \mathrm{d}t' \mathbf{e}^T \mathbf{W}^r(0,n')(t,t')\boldsymbol{\pi}(n')(t')\,, \tag{7.3}$$

where $\mathbf{e}^T=(1,1,1,1,0,0)$ and $n=0$ in $\mathbf{W}^r(0,n')(t,t')$ ensure that the final state on the right hand side is diagonal in the dot state and the Cooper pair numbers, respectively. The current rates $\mathbf{W}^r(n,n')(t,t')$ are similar to the general rates $\mathbf{W}(n,n')(t,t')$ but take into account the electrons transferred into lead r.

The frequency of the AC Josephson signal is given by the energy difference of a Cooper pair being in superconductor $S1$ or $S2$, i.e., by $2(\mu_{S1}-\mu_{S2})=2eV$. Therefore, we perform a Fourier expansion by making use of $A(t)=\sum_{n=-\infty}^{\infty}A^n e^{2\mathrm{i}neVt}$ and $A^n = \int_0^T \mathrm{d}t A(t) e^{-2\mathrm{i}neVt}$ with $T=2\pi/(2eV)$. Within the diagrammatic representation, see Chapter 3, the factor $\exp(-2\mathrm{i}neVt)$ appearing in the n-th Fourier component of the current simply adds a term $2neV$ to the energy difference of the states on the upper and lower Keldysh contour. This terms can easily be incorporated into the energy difference arising from different Cooper pair numbers by shifting $\mathbf{W}^r(0,n')(t,t')$ and $\boldsymbol{\pi}(n')(t')$ in Eq. (7.3) to $\mathbf{W}^r(n,n'+n)(t,t')$ and $\boldsymbol{\pi}(n'+n)(t')$, respectively, i.e., only the 0-th Fourier components of $\mathbf{W}^r$ and $\boldsymbol{\pi}$ are needed. Performing the remaining time integral, we get for the n-th Fourier component of the current

$$I_r^n = -e\sum_{n'} \mathbf{e}^T \mathbf{W}^r(n,n')\boldsymbol{\pi}(n')\,, \tag{7.4}$$

with $\mathbf{W}=\int_{-\infty}^{t}\mathrm{d}t'\mathbf{W}(t,t')e^{\mathrm{i}0^+t'}$ being the zero frequency Laplace transformed rate, that does not depend on the final time t. The 0-th Fourier components $\boldsymbol{\pi}(n')$ are readily obtained from the 0-th Fourier component of Eq. (7.2),

$$\mathrm{i}\mathbf{E}_n\boldsymbol{\pi}(n) = \sum_{n'}\mathbf{W}(n,n')\boldsymbol{\pi}(n') \tag{7.5}$$

together with the normalization condition $\mathbf{e}^T\boldsymbol{\pi}(n)=\delta_{n,0}$. In summary, the n-th Fourier component of the current can be evaluated within the diagrammatic technique in exactly the same way as the DC transport (see Ref. 139) but allowing for off-diagonal final Cooper pair states ($n\neq 0$) in $\mathbf{W}^r(n,n')$ on the right hand side of Eq. (7.4). The diagrammatic rules to calculate the kernels $\mathbf{W}$ and $\mathbf{W}^r$ are given in Appendix A.

7.3 Results

In the following, we perform a systematic perturbation expansion of $\boldsymbol{\pi}(n)$, $\boldsymbol{W}(n,n')$, $\boldsymbol{W}^r(n,n')$ and I_r^n in the tunnel-coupling strengths, $\Gamma \equiv \max\{\Gamma_{S1},\Gamma_{S2},\Gamma_N\}$. Since we assume the tunnel couplings to be weak, we restrict ourselves to lowest (first) order for the kernels $\boldsymbol{W}(n,n')$ and $\boldsymbol{W}^r(n,n')$. In addition, we concentrate on the limit of an infinite superconducting gap in the leads, $\Delta \to \infty$, i.e., quasi-particle tunneling between dot and the superconductors is suppressed. As a consequence, the current into the superconductors is exclusively sustained by Cooper pairs. The normal lead affects the occupation of the quantum dot, which, in turn, affects Cooper pair transport. Even a weakly tunnel coupled normal conductor influences the AC Josephson transport between the two superconductors. All rates required for our calculations are presented in Appendix D. Inserting the current rates in Eq. (7.4) results in

$$I_{S1}^n = \mathrm{i}e\Gamma_{S1}\left[P_0^d(n-1) - P_d^0(n+1)\right] \tag{7.6a}$$

$$I_{S2}^n = \mathrm{i}e\Gamma_{S2}\left[P_0^d(n) - P_d^0(n)\right], \tag{7.6b}$$

i.e., the current into the superconductors is fully determined by the density matrix elements $P_0^d(n)$ and $P_d^0(n) = \left[P_0^d(-n)\right]^*$.

The Cooper pair degree of freedom n in $\boldsymbol{\pi}(n)$ introduces an apparently infinitely large number of density matrix elements that are all coupled to each other via Eq. (7.5). However, in the limit of a large bias voltage compared to the tunnel-coupling strength, $eV \gg \Gamma$, only very few of them need to be taken into account. This is a consequence of $\mathbf{E}_n$ appearing on the left hand side of Eq. (7.5). Most of its matrix elements are of order eV, while $\mathbf{W}(n,n')$ on the right hand side scales with Γ. This mismatch defines a hierarchy in powers of $\Gamma/(eV)$ for the density matrix elements. The lowest order contains all matrix elements of $\boldsymbol{\pi}(n)$ for which the corresponding $\mathbf{E}_n$ is zero or of the order of Γ. This includes all diagonal matrix elements $P_\chi^\chi(0)$ (and excludes all elements $P_\chi^\chi(n)$ with $n \neq 0$). The next order contains all matrix elements of $\boldsymbol{\pi}(n)$, that can be connected to lowest order ones by the kernel $\mathbf{W}(n,n')$. The only off-diagonal matrix elements that can be reached from the diagonal ones for $\Delta \to \infty$ and to first order in Γ are $P_0^d(-1)$, $P_d^0(1)$, $P_0^d(0)$, $P_d^0(0)$. If the gate voltage is tuned such that the quantum dot is in resonance with superconductor r, namely $|2\varepsilon + U - 2\mu_r| \lesssim \Gamma$, then $P_0^d(-1)$ and $P_d^0(1)$ (for $r = S1$) or $P_0^d(0)$ and $P_d^0(0)$ (for $r = S2$) already belong to the lowest order in the hierarchy. But in any case, all off-diagonal matrix elements except $P_0^d(-1)$, $P_d^0(1)$, $P_0^d(0)$, $P_d^0(0)$ can be dropped for describing the current into the superconductors. As a result, the set of kinetic equations that we need to solve includes those with diagonal final states,

$$\begin{aligned} 0 = &\sum_{\chi'} W_{\chi\chi'}^{\chi\chi'}(0,0)P_{\chi'}(0) + W_{\chi 0}^{\chi d}(0,-1)P_0^d(-1) + W_{\chi d}^{\chi 0}(0,1)P_d^0(1)\,, \\ &+ W_{\chi 0}^{\chi d}(0,0)P_0^d(0) + W_{\chi d}^{\chi 0}(0,0)P_d^0(0)\,. \end{aligned} \tag{7.7}$$

The rates with diagonal initial and finite state are related to single-electron tunneling between dot and normal conductor, $W_{\chi\chi'}^{\chi\chi'}(0,0) \propto \Gamma_N$, and can simply be calculated

by means of Fermi's golden rule. In contrast, the rates connecting superpositions between a doubly-occupied and an empty dot to a diagonal state require tunneling of one Cooper pair.

In addition, there are the kinetic equations with off-diagonal final states:

$$\begin{aligned}&\mathrm{i}(2\varepsilon+U-2\mu_{S1})P_0^d(-1)\\&=W_{00}^{dd}(-1,-1)P_0^d(-1)+W_{00}^{d0}(-1,0)P_0(0)+W_{0d}^{dd}(-1,0)P_d(0)\,,\end{aligned}\tag{7.8a}$$

$$\begin{aligned}&\mathrm{i}(2\varepsilon+U-2\mu_{S2})P_0^d(0)\\&=W_{00}^{dd}(0,0)P_0^d(0)+W_{00}^{d0}(0,0)P_0(0)+W_{0d}^{dd}(0,0)P_d(0)\,,\end{aligned}\tag{7.8b}$$

and complex conjugated.

The off-diagonal density matrix elements are, thus, related to the diagonal ones via

$$P_0^d(-1) = \frac{\Gamma_{S1}}{2}\frac{P_0(0)-P_d(0)}{2\varepsilon+U-2\mu_{S1}+\mathrm{i}W_{00}^{dd}(-1,-1)}\,,\tag{7.9a}$$

$$P_0^d(0) = \frac{\Gamma_{S2}}{2}\frac{P_0(0)-P_d(0)}{2\varepsilon+U-2\mu_{S2}+\mathrm{i}W_{00}^{dd}(0,0)}\,,\tag{7.9b}$$

and complex conjugated. After having determined $P_0(0)-P_d(0)$, the final result is,

$$\begin{aligned}P_0^d(-1) &= \frac{\Gamma_{S1}}{2}\frac{1-f(\varepsilon)-f(\varepsilon+U)}{1+f(\varepsilon)-f(\varepsilon+U)}\frac{2\varepsilon+U-2\mu_{S1}+\sigma}{A_{S1}}\\&- \frac{\mathrm{i}}{2}\Gamma_N\Gamma_{S1}\frac{1-f(\varepsilon)-f(\varepsilon+U)}{A_{S1}}\,,\end{aligned}\tag{7.10a}$$

$$\begin{aligned}P_0^d(0) &= \frac{\Gamma_{S2}}{2}\frac{1-f(\varepsilon)-f(\varepsilon+U)}{1+f(\varepsilon)-f(\varepsilon+U)}\frac{2\varepsilon+U-2\mu_{S2}+\sigma}{A_{S2}}\\&- \frac{\mathrm{i}}{2}\Gamma_N\Gamma_{S2}\frac{1-f(\varepsilon)-f(\varepsilon+U)}{A_{S2}}\end{aligned}\tag{7.10b}$$

with $f(x)\equiv 1/(1+\exp[x-\mu_N])$ being the Fermi function of the normal conductor. Here, we used that the bias voltage is large $|eV|\gg\Gamma$. Please note that for the order in the hierarchy of the different terms of the density matrix it is crucial whether a superconductor is in resonance with the dot, $|2\varepsilon+U-2\mu_r|\lesssim\Gamma$, or not, $|2\varepsilon+U-2\mu_r|\gg\Gamma$. Furthermore, we have introduced the quantity

$$A_r\equiv\Gamma_r^2+(2\varepsilon+U-2\mu_r+\sigma)^2+\Gamma_N^2(1+f(\varepsilon)-f(\varepsilon+U))^2\,.\tag{7.11}$$

The symbol σ in Eqs. (7.10) denotes the renormalization of the dot's energy level due to the tunnel coupling to the normal lead and it reads

$$\sigma\equiv\frac{\Gamma_N}{\pi}\mathrm{Re}\left[\Psi\left(\frac{1}{2}+\mathrm{i}\frac{\varepsilon+U-\mu_N}{2\pi k_BT}\right)-\Psi\left(\frac{1}{2}+\mathrm{i}\frac{\varepsilon-\mu_N}{2\pi k_BT}\right)\right]\,,\tag{7.12}$$

where Ψ is the digamma function.

We can now compute the current flowing in the different superconducting leads by inserting the off-diagonal density matrix elements Eqs. (7.10) into the expressions for

the currents Eqs. (7.6). Without loss of generality, we show results for the current flowing in lead $S1$. We start with the DC component:

$$I_{S1}^{DC} = e\Gamma_N \Gamma_{S1}^2 \frac{1 - f(\varepsilon) - f(\varepsilon + U)}{A_{S1}}. \tag{7.13}$$

If the lead $S1$ is out of resonance with the quantum dot, i.e. if $|2\varepsilon + U - 2\mu_{S1}| \gg \Gamma$, then $A_{S1} \approx (2\varepsilon + U - 2\mu_{S1})^2$ and the current I_{S1}^{DC} is zero in the order of perturbation theory considered here. However, when the lead $S1$ is in resonance with the dot, i.e. if $|2\varepsilon + U - 2\mu_{S1}| \lesssim \Gamma$, then A_{S1} is of order Γ^2 and the DC transport is finite and first order in Γ. In this latter case, the DC transport in lead $S1$ is due to direct transport between $S1$ and the normal lead through the quantum dot and it can be explicitly shown that $I_{S1}^{DC} = -I_N^{DC}$.

Far more interesting is the AC signal in lead $S1$. We notice that in this order of perturbation expansion, the current will only contain the first harmonic of the Josephson frequency $\omega_J = |2eV|$. The higher harmonics arise in higher orders and are suppressed in the weak coupling limit. In fact, the higher Fourier components of the current are due to the presence of multiple Andreev reflection, which can be present in the system under investigation even in the limit of an infinite superconducting gap, since quasiparticles are provided by the normal lead. The AC transport in lead $S1$ reads

$$\begin{aligned} I_{S1}^{AC}(t) = {} & e\Gamma_N \Gamma_{S1} \Gamma_{S2} \tfrac{1-f(\varepsilon)-f(\varepsilon+U)}{A_{S2}} \cos[2eVt] \\ & - e\Gamma_{S1}\Gamma_{S2} \tfrac{1-f(\varepsilon)-f(\varepsilon+U)}{1+f(\varepsilon)-f(\varepsilon+U)} \tfrac{2\varepsilon+U-2\mu_{S2}+\sigma}{A_{S2}} \sin[2eVt]. \end{aligned} \tag{7.14}$$

The expression for $I_{S1}^{AC}(t)$ describes very different physical scenarios depending whether or not the other superconductor, in this case $S2$, is in resonance or not with the dot. First, we discuss the resonant case, $|2\varepsilon + U - 2\mu_{S2}| \ll \Gamma$, then $A_{S2} \propto \Gamma^2$ and both the sine and cosine terms in Eq. (7.14) are first-order in Γ. From Eq. (7.14), it is clear that the amplitude of the AC signal in leads $S1$ depends on the chemical potential μ_{S2} of the other superconductor and not only on the voltage difference V. This can be understood in the following way: stochastic Cooper pair fluctuations lead to a proximization of the dot by the two superconductors. Since the AC Josephson effect requires the presence of two different superconductors exclusively the proximization by $S2$ is responsible for the AC signal between dot and $S1$. This proximization depends on μ_{S2} and hence the amplitude of the current I_{S1} does. The chemical potential μ_{S1} only influences the frequency. Another interesting feature of the expression for the AC signal, Eq. (7.14), is the behavior for $V \to 0$. The amplitude of the sine first harmonic exactly reproduces the DC Josephson transport which is discussed in Ref. 138. This crossover has been discussed before in quantum point contacts[203,205] as well as in the three-terminal setup under consideration in this paper in the noninteracting limit.[205]

We also notice that the cosine term in $I_{S1}^{AC}(t)$ vanishes for $\Gamma_N \to 0$ while the sine term remains finite. We focus on the limit of weak coupling Γ_N, as a strong coupling to the normal conductor leads to dephasing and suppresses the Josephson current.[205] In this limit the sine term is the dominant one and we neglect the cosine one in the following.

Now we consider Eq. (7.14) in the case when the superconductor is not resonant with the dot, $|2\varepsilon + U - 2\mu_{S2}| \gg \Gamma$, then $A_{S2} \approx (2\varepsilon + U - 2\mu_{S2})^2$ and the cosine term vanishes in this oder of the perturbation expansion. In this limit the AC signal in $S1$ is second order in Γ and reads:

$$I_{S1}^{AC}(t) = -e\frac{\Gamma_{S1}\Gamma_{S2}\sin[2eVt]}{2\varepsilon + U - 2\mu_{S2}}\frac{1 - f(\varepsilon) - f(\varepsilon + U)}{1 + f(\varepsilon) - f(\varepsilon + U)}\,. \tag{7.15}$$

We are now in the position to make some general comments on the lowest-order processes contributing to the AC Josephson transport through a quantum dot: either we need second order processes in Γ as in Eq. (7.15), or first order processes in combination with the dot being in resonance with other superconductor.

Finally the current in $S2$ can be obtained from I_{S1} simply by exchanging the labels $S1$ and $S2$ and sending $2eV$ into $-2eV$.

In Fig. 7.2, we plot the amplitudes of the currents I_{S1}^{AC} and I_{S2}^{AC} as a function of the dot level position ε for the case of symmetric bias between the superconductors, $\mu_{S1} = -\mu_{S2}$, and unbiased normal lead, $\mu_N = 0$. The current is exponentially suppressed

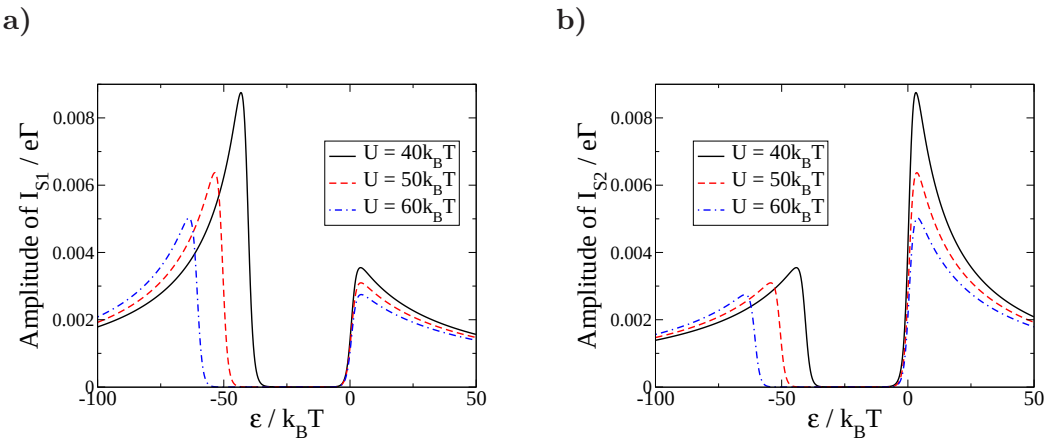

Figure 7.2: Amplitude of the current between quantum dot and **a)** superconductor $S1$ and **b)** superconductor $S2$ as a function of the dot level position ε for different values of the Coulomb repulsion U. The other parameters are $\mu_N = 0$, $\Gamma_{S1} = 0.5k_BT$, $\Gamma_{S2} = 0.5k_BT$, $\mu_{S1} = 10k_BT$, and $\mu_{S2} = -10k_BT$.

in the range $-U \gg \varepsilon \gg 0$. The reason is that in this range the dot is mainly singly occupied and, therefore, Cooper pair transport is blocked. Peaks appear at $\varepsilon \approx -U$ and $\varepsilon \approx 0$, where the dot is mainly occupied with an even number of electrons enabling Cooper pair tunneling. However, for too small or too large values of ε Cooper pair tunneling is algebraically suppressed, because changing the dot occupation becomes energetically more unfavorable. These considerations also apply to the DC Josephson transport through quantum dots and the same dependence of the current on the dot level ε has been observed experimentally[100,103] as well as theoretically.[139]

By now we always considered the current between the dot and each of the two superconductors. However, in an experiment the practical quantity to be measured is

the current between the two superconductors, which is given by $I \equiv I_{S1} - I_{S2}$. It reads

$$\begin{aligned} I(t) &= e\Gamma_{S1}\Gamma_{S2}\frac{1-f(\varepsilon)-f(\varepsilon+U)}{1+f(\varepsilon)-f(\varepsilon+U)}\sin[2eVt] \\ &\times \frac{(2\varepsilon+U-2\mu_{S1}+\sigma)A_{S2}+(2\varepsilon+U-2\mu_{S2}+\sigma)A_{S1}}{A_{S1}A_{S2}}\,. \end{aligned} \tag{7.16}$$

The amplitude is the sum of the amplitudes of I_{S1} and I_{S2}, see Fig. 7.3. Moreover,

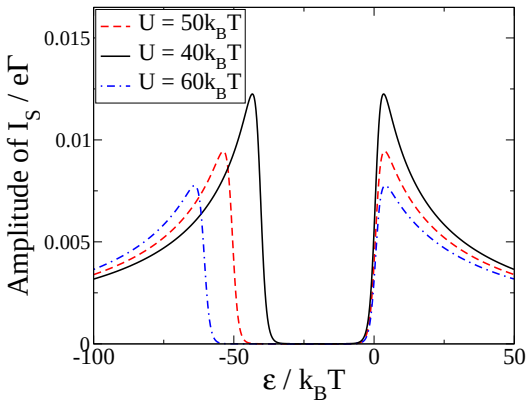

Figure 7.3: Amplitude of the current I between the two superconductors as a function of the dot level position ε for different values of the Coulomb repulsion U. The other parameters are $\mu_N = 0$, $\Gamma_{S1} = 0.5k_BT$, $\Gamma_{S2} = 0.5k_BT$, $\mu_{S1} = 10k_BT$, and $\mu_{S2} = -10k_BT$.

for the chemical potential of the normal conductor being zero, $\mu_N = 0$, the current is an even function of $\varepsilon + U/2$. This a a consequence of the particle-hole symmetry.

Now, we break the particle-hole symmetry by a finite chemical potential of the normal conductor, see Fig. 7.4. As a consequence, the positions of the peaks are shifted to $\varepsilon \approx \mu_N$ and $\varepsilon \approx -U + \mu_N$. But also the maximal value is changed. This behavior gives rise to a very interesting property. In conventional Josephson junctions only the frequency can be controlled by an applied bias voltage and the amplitude is governed by the critical current. In quantum-dot Josephson junctions coupled to an additional normal conductor the frequency is still governed by the voltage applied between the two superconductors, but also the amplitude can be controlled by the gate voltage and the bias voltage applied between the normal conductor and the superconductors. This means the AC signal between the two superconductors can completely be tuned by external DC voltages.

7.4 Conclusions

We have presented a real-time perturbation theory on the AC Josephson transport through quantum dots. By means of this formalism we have calculated the current

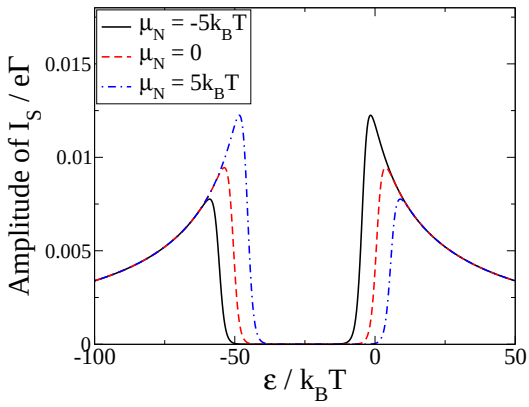

Figure 7.4: Amplitude of the current I between the two superconductors as a function of the dot level position ε for different values of the chemical potential μ_N of the normal conductor. The other parameters are $U = 50k_BT$, $\Gamma_{S1} = 0.5k_BT$, $\Gamma_{S2} = 0.5k_BT$, $\mu_{S1} = 10k_BT$, and $\mu_{S2} = -10k_BT$.

through a quantum dot tunnel coupled to two superconductors and additionally coupled to a normal conductor. It has turned out, that the sine first harmonic clearly dominates the cosine first harmonic. Its amplitude has the same dependence on the dot level as the DC Josephson transport. Moreover, the current between the dot and superconductor $S1$ is strongly affected by the chemical potential of superconductor $S2$. The reason is that in lowest order of the perturbation expansion a finite AC signal between the dot and one of the superconductors requires the proximization of the dot by the other superconductor. Finally, we have found that the amplitude of the AC Josephson current between the two superconductors strongly depends on the gate voltage and the chemical potential of the normal conductor. Therefore, in the considered setup an AC signal can be generated, whose frequency as well as amplitude can be controlled by external DC voltages.

A Diagrammatic Rules

In this thesis most $W^{\chi_1\chi_1'}_{\chi_2\chi_2'}$ have been calculated by means of a diagrammatic perturbation expansion in tunnel coupling. Here, we give the corresponding rules. First, we present the rules for the simple case of a single-level quantum dot tunnel coupled to normal conductors (NDN).[157] The formulations are oriented on Ref. 139. Examples of diagrams are the yellow blocks in Fig. 3.1. The rules for evaluating the generalized rates $W^{\chi_1\chi_1'}_{\chi_2\chi_2'}$ are as follows:

(1) Draw all topologically different diagrams with fixed ordering of the vertices in the real axis. The vertices are connected in pairs by tunneling lines carrying energy ω_i.

(2) For each vertical cut between two vertices assign a factor $1/(\Delta E + \mathrm{i}0^+)$, where ΔE is the difference between the left-going and the right-going energies, including the energies of the dot states E_χ and the tunneling lines ω_i

(3) For each tunneling line assign a factor $\frac{1}{2\pi}\Gamma_r f_r^{\pm}(\omega_i)$, where $f_r^+(\omega_i) = f_r(\omega_i) = [1+\exp(\omega_i-\mu_r)/(k_\mathrm{B}T)]^{-1}$ and $f_r^-(\omega_i) = 1 - f_r(\omega_i)$. The upper (lower) sign applies for lines going backward (forward) with respect to the Keldysh contour.

(4) Assign an overall prefactor $-\mathrm{i}$.

Furthermore, assign a factor -1 for each

a) vertex on the lower propagator;

b) crossing of tunneling lines;

c) vertex that connects the doubly-occupied dot state, $|\mathrm{D}\rangle = d^\dagger_\uparrow d^\dagger_\downarrow|0\rangle$, to spin up, $|\uparrow\rangle$

(5) For each diagram, integrate over all energies ω_i. Sum over all diagrams.

The generalized current rates $W^{\chi_1\chi_1',r}_{\chi_2\chi_2'}$ are evaluated in the following way:

(6) Multiply the value of the corresponding generalized rate $W^{\chi\chi_1'}_{\chi\chi_2'}$ with a factor given by adding up the following number for each tunneling line that is associated with lead r:

1 if the line is going from the lower to the upper, -1 if it is going from the upper to the lower propagator, and 0 otherwise.

Double-Dot Aharonov-Bohm Interferometer

Now, we present the modifications of the rules for each setup under consideration. We start with adiabatic pumping through a double-dot Aharonov-Bohm interferometer with an infinite intra-dot Coulomb repulsion, see Chapter 4. Since the adiabatic corrections[80] of the rates $W^{\chi_1\chi_1'(a)}_{\chi_2\chi_2'}$ do not contribute to our results we do not present the corresponding rates. The difference to the NDN case is that off-diagonal elements

arise due to tunneling between the two dots through the leads.[29] This is reflected in the following additional rules:

(A1) Also take into account tunneling lines where electrons tunnel from one dot to the other. Assign a factor $e^{-\mathrm{i}\varphi/2}$ for each tunneling line associated to the left (right) lead, where an electron tunnels from QD 1 to QD 2 (from QD 2 to QD 1). Assign a factor $e^{\mathrm{i}\varphi/2}$ for each tunneling line associated to the right (left) lead, where an electron tunnels from QD 1 to QD 2 (from QD 2 to QD 1).

(A2) Assign an overall prefactor -1 for each vertex that connects the state where both dots are occupied, $|1\sigma 2\sigma'\rangle$, to only QD 1 being occupied, $|1\sigma\rangle$.

Single-Dot Aharonov-Bohm Interferometer

Due to the reference arm tunneling events that do not change the dot occupation are possible. This is reflected by the presence of *double vertices*[29] , see Fig. A.1. They give rise to the following rules:

(B1) Additionally include double vertices, where two lines associated to different leads come together. One line comes into the double vertex and the other one goes out of the vertex. The Fermi functions are included as in rule (3) but the prefactor is $e^{\pm\mathrm{i}\varphi}|t_\sigma^{\mathrm{ref}}|\sqrt{\Gamma_{\mathrm{L}}\Gamma_{\mathrm{R}}}/(4\pi^2)$ for each double vertex. The upper (lower) sign applies whenever the incoming line stems from the left (right) lead. [Please note that in Chapter 5 the left lead is the ferromagnet, $F\widehat{=}L$.]

(B2) The line coming into the double vertex always comes first with respect to the Keldysh contour. Associated to rule (4b) this may give rise to a minus sign.

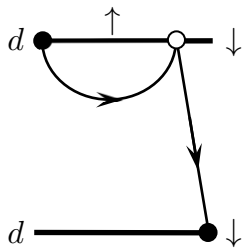

Figure A.1: Example of a double-vertex.

Double-Dot Beam Splitter

In this subsection we discuss the rates of the setups presented in Chapter 6. For the NDSDN as well as the FDS setup no offdiagonal elements of the reduced density matrix contribute. Therefore, in these systems all rates can be calculated by means of Fermi's Golden Rule. Exclusively in the NDNDN setup the rates are calculated in a diagrammatic way. Similar to the double-dot ABI off-diagonal elements arise due to tunneling between the two dots through the central lead. The corresponding rules are:

(A1) Also take into account tunneling lines where electrons tunnel from one dot to the other. For such lines the prefactor Γ_r of rule (3) is replaced by $\sqrt{\Gamma_{N_c,L}\Gamma_{N_c,R}}$.

(A2) Assign an overall prefactor -1 for each vertex that connects a singlet or triplet state, $|S\rangle$,$|T_{-1}\rangle$,$|T_0\rangle$, or$|T_1\rangle$, to only the left QD being occupied, $|\sigma, 0\rangle$.

AC Josephson Transport through Quantum Dots

For setups containing two superconductors the number of Cooper pairs are taken into account explicitly, see Chapter 7. Furthermore, Cooper pair tunneling has the consequence that so called *anomalous* tunneling lines arise. These lines are divided into outgoing lines, where at each end of the line a dot electron is annihilated, and the incoming lines, where at each end of the line an electron is created, see Fig. A.2. In contrast to the three systems presented above, these properties affect nearly all six points of the original rules presented above. Instead of discussing all changes we, therefore, give again the complete rules for the generalized rates $W^{\chi\chi_1'}_{\chi\chi_2'}(\{n_1, n_2\}, \{n_1', n_2'\})$ but now including also the superconducting properties:[139]

(D1) Draw all topologically different diagrams with fixed ordering of the vertices in the real axis. The vertices are connected in pairs by tunneling lines carrying energy ω_i. The tunneling lines can be normal or anomalous. For each anomalous line choose the direction (forward or backward with respect to the Keldysh contour) arbitrarily.

(D2) For each vertical cut between two vertices assign a factor $1/(\Delta E + i0^+)$, where ΔE is the difference between the left-going and the right-going energies, including the energy of the dot states E_χ, the tunneling lines ω_i, and the energy difference in Cooper-pair condensates $E_{\mathbf{n}}$. The latter is increased (decreased) at each vertex of an outgoing (incoming) anomalous line at which the arrow is opposite to the arbitrarily chosen line direction.

(D3) For each tunneling line assign a factor $\frac{1}{2\pi}\Gamma_r D_r(\omega_i) f_r^{\pm}(\omega_i)$, where $f_r^+(\omega_i) = f_r(\omega_i) = [1 + \exp(\omega_i - \mu_r)/(k_{\rm B}T)]^{-1}$ and $f_r^-(\omega_i) = 1 - f_r(\omega_i)$, and $D_r(\omega_i) = \frac{|\omega_i - \mu_r|}{\sqrt{(\omega_i - \mu_r)^2 - |\Delta_r|^2}}\theta(|\omega - \mu_r| - |\Delta_r|)$. The upper (lower) sign applies for lines going backward (forward) with respect to the Keldysh contour. For anomalous lines multiply an additional factor $\pm\mathrm{sign}(\omega_i - \mu_r)\frac{|\Delta_r|}{|\omega_i - \mu_r|}$. Moreover, assign a factor $e^{-\mathrm{i}\Phi_r}$ for an outgoing and $e^{\mathrm{i}\Phi_r}$ for an incoming anomalous line. [For normal leads, only normal lines with $D_r(\omega_{\rm i}) \equiv 1$ appear.]

(D4) Assign an overall prefactor $-\mathrm{i}$.
Furthermore, assign a factor -1 for each
a) vertex on the lower propagator;
b) crossing of tunneling lines;
c) vertex that connects the doubly-occupied dot state, $|\mathrm{D}\rangle = d_\uparrow^\dagger d_\downarrow^\dagger|0\rangle$, to spin up, $|\uparrow\rangle$;
d) outgoing (incoming) anomalous tunneling line in which the earlier (later) tunnel vertex with respect to the Keldysh contour involves a spin-up dot electron.

(D5) For each diagram, integrate over all energies ω_i. Sum over all diagrams.

The generalized current rates $W^{\chi\chi_1{}^r}_{\chi\chi_2'}(\{n_1, n_2\}, \{n_1', n_2'\})$ are evaluated in the following way:

(D6) Multiply the value of the corresponding generalized rate $W^{\chi\chi_1'}_{\chi\chi_2'}(\{n_1, n_2\}, \{n_1', n_2'\})$ with a factor given by adding up the following numbers for each tunneling line that is associated with lead r:
a) for normal lines: 1 if the line is going from the lower to the upper, -1 if it is going from the upper to the lower propagator, and 0 otherwise;
b) for anomalous lines: 1 for incoming lines within the upper propagator and outgoing lines within the lower propagator, -1 for outgoing lines within the upper propagator and incoming lines within the lower propagator, and 0 otherwise.

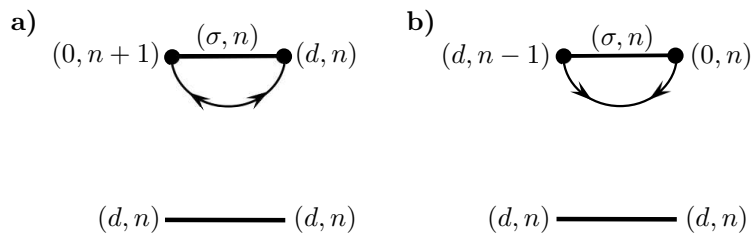

Figure A.2: a) Example of an incoming line of the diagram representing the rate $W^{d0}_{dd}(0, 1)$. b) Example of an outgoing line of the diagram representing the rate $W^{0d}_{dd}(0, -1)$.

B Sequential Tunneling vs. Cotunneling

In Chapter 5 we introduced two different schemes for the calculation of the lowest order density matrix elements $P_\chi^{(0,0)}$, whose validity depends on the average dot level position. As long as the dot level energy is sufficiently small, $|\varepsilon| \lesssim \max\{k_\mathrm{B}T, |eV/2|\}$, scheme 1 applies. Then, the density matrix can be obtained by means of the following master equation

$$\begin{pmatrix} W_{00}^{(1,0)} & W_{0\uparrow}^{(1,0)} & W_{0\downarrow}^{(1,0)} & 0 \\ W_{\uparrow 0}^{(1,0)} & W_{\uparrow\uparrow}^{(1,0)} & W_{\uparrow\downarrow}^{(1,0)} & W_{\uparrow d}^{(1,0)} \\ W_{\downarrow 0}^{(1,0)} & W_{\downarrow\uparrow}^{(2,0)} & W_{\downarrow\downarrow}^{(1,0)} & W_{\downarrow d}^{(1,0)} \\ 0 & W_{d\uparrow}^{(1,0)} & W_{d\downarrow}^{(1,0)} & W_{dd}^{(1,0)} \end{pmatrix} \begin{pmatrix} p_0^{(0,0)} \\ p_\uparrow^{(0,0)} \\ p_\downarrow^{(0,0)} \\ p_d^{(0,0)} \end{pmatrix} = 0\,. \tag{B.1}$$

Here, all rates have been calculated using the diagrammatic rules presented in Appendix A. However, in the limit of a large dot level energy, $|\varepsilon| \gg \max\{k_\mathrm{B}T, |eV/2|\}$ some of the rates are exponentially suppressed. In this case Eq. (B.1) reads

$$\begin{pmatrix} W_{00}^{(1,0)} & 0 & 0 & 0 \\ W_{\uparrow 0}^{(1,0)} & 0 & 0 & W_{\uparrow d}^{(1,0)} \\ W_{\downarrow 0}^{(1,0)} & 0 & 0 & W_{\downarrow d}^{(1,0)} \\ 0 & 0 & 0 & W_{dd}^{(1,0)} \end{pmatrix} \begin{pmatrix} p_0^{(0,0)} \\ p_\uparrow^{(0,0)} \\ p_\downarrow^{(0,0)} \\ p_d^{(0,0)} \end{pmatrix} = 0\,, \tag{B.2}$$

where all exponentially suppressed rates have been set to zero. Obviously, in this regime the elements $p_\uparrow^{(0,0)}$ and $p_\downarrow^{(0,0)}$ cannot be calculated using exclusively lowest order rates. Here, scheme 2 applies. Analogously to Ref. 180 first and second order rates enter the master equation,

$$\begin{pmatrix} W_{00}^{(1,0)} & W_{0\uparrow}^{(2,0)} & W_{0\downarrow}^{(2,0)} & 0 \\ W_{\uparrow 0}^{(1,0)} & W_{\uparrow\uparrow}^{(2,0)} & W_{\uparrow\downarrow}^{(2,0)} & W_{\uparrow d}^{(1,0)} \\ W_{\downarrow 0}^{(1,0)} & W_{\downarrow\uparrow}^{(2,0)} & W_{\downarrow\downarrow}^{(2,0)} & W_{\downarrow d}^{(1,0)} \\ 0 & W_{d\uparrow}^{(2,0)} & W_{d\downarrow}^{(2,0)} & W_{dd}^{(1,0)} \end{pmatrix} \begin{pmatrix} p_0^{(1,0)} \\ p_\uparrow^{(0,0)} \\ p_\downarrow^{(0,0)} \\ p_d^{(1,0)} \end{pmatrix} = 0\,. \tag{B.3}$$

The corresponding cotunneling rates are presented in Chapter 5. In scheme 2 the lowest order density matrix elements $P_\chi^{(0,0)}$ can be obtained by means of Eq. (B.1) and Eq. (B.3).

C Calculation of a Cotunneling Rate

In this appendix we give an example of how to calculate the cotunneling rates used in Chapter 5. For this, we choose the rate $\gamma_{rr'}^{\bar{\sigma}\sigma(2,0)}$, where an electron is transferred from lead r' to lead r accompanied by a change of the dot state from σ to $\bar{\sigma}$. We start with

$$\gamma_{rr'}^{\bar{\sigma}\sigma(2,0)} = \frac{1}{2\pi} \int_{-\infty}^{\infty} d\omega f(\omega - \mu_{r'}) \left(1 - f(\omega - \mu_r)\right) \times \mathrm{Re}\left[\frac{\sqrt{\Gamma_{r'}^{\bar{\sigma}}\Gamma_r^{\sigma}}}{\varepsilon - \omega + i0^+} + \frac{\sqrt{\Gamma_{r'}^{\bar{\sigma}}\Gamma_r^{\sigma}}}{\varepsilon + U - \omega + i0^+}\right]^2 . \tag{C.1}$$

The regularization $+\mathrm{i}0^+$ in the resolvents is added here by hand. However, it appears naturally when employing the real-time diagrams. In the present case, there are two possible intermediate states, the dot being empty or doubly occupied. Both corresponding cotunneling processes have the same initial and the same final state also concerning the lead electrons. Therefore, the energy differences to the final state, that appear in the denominator of the resolvents, have to be added before performing the square. The Fermi functions guarantee that the lead state of the electron that enters the dot is occupied and that the lead state into which the dot electron leaves is unoccupied. The integral sums over all possible energies of the incoming electron. For an infinite Coulomb repulsion $U = \infty$ and $|\varepsilon| \gg \max\{k_\mathrm{B}T, \mu_r\}$ the rate simplifies to

$$\begin{aligned}\gamma_{rr'}^{\bar{\sigma}\sigma(2,0)} &= \frac{1}{2\pi\varepsilon^2}\Gamma_{r'}^{\bar{\sigma}}\Gamma_r^{\sigma} \int_{-\infty}^{\infty} d\omega f(\omega - \mu_{r'}) \left(1 - f(\omega - \mu_r)\right) \\ &= \frac{1}{2\pi\varepsilon^2}\Gamma_{r'}^{\bar{\sigma}}\Gamma_r^{\sigma} \frac{\mu_r - \mu_{r'}}{e^{\beta(\mu_r - \mu_{r'})} - 1} .\end{aligned} \tag{C.2}$$

The calculation of the current rate is similar. The only difference is that one has to multiply the rates with the charge that is being transferred through the dot during the cotunneling process.

D Rates for the AC Josephson Transport

In this appendix we present all rates required in Chapter 7.

Rates Involving the Superconductors

$$
\begin{aligned}
W_{00}^{0d}(n,n-1) &= W_{dd}^{d0}(n,n+1) = \mathrm{i}\Gamma_{S1}/2 \\
W_{d0}^{dd}(n,n-1) &= W_{0d}^{00}(n,n+1) = -\mathrm{i}\Gamma_{S1}/2 \\
W_{00}^{d0}(n,n+1) &= W_{dd}^{0d}(n,n-1) = \mathrm{i}\Gamma_{S1}/2 \\
W_{0d}^{dd}(n,n+1) &= W_{d0}^{00}(n,n-1) = -\mathrm{i}\Gamma_{S1}/2 \\
W_{00}^{0d}(n,n) &= W_{dd}^{d0}(n,n) = \mathrm{i}\Gamma_{S2}/2 \\
W_{d0}^{dd}(n,n) &= W_{0d}^{00}(n,n) = -\mathrm{i}\Gamma_{S2}/2 \\
W_{00}^{d0}(n,n) &= W_{dd}^{0d}(n,n) = \mathrm{i}\Gamma_{S2}/2 \\
W_{0d}^{dd}(n,n) &= W_{d0}^{00}(n,n) = -\mathrm{i}\Gamma_{S2}/2\,.
\end{aligned}
$$

$$
\begin{aligned}
W_{00}^{0d,S1}(n,n-1) &= W_{d0}^{dd,S1}(n,n-1) = -\mathrm{i}\Gamma_{S1}/2 \\
W_{0d}^{00,S1}(n,n+1) &= W_{dd}^{d0,S1}(n,n+1) = \mathrm{i}\Gamma_{S1}/2 \\
W_{00}^{0d,S2}(n,n) &= W_{d0}^{dd,S2}(n,n) = -\mathrm{i}\Gamma_{S2}/2 \\
W_{0d}^{00,S2}(n,n) &= W_{dd}^{d0,S2}(n,n) = \mathrm{i}\Gamma_{S2}/2\,.
\end{aligned}
$$

Rates Involving the Normal Conductor

$$
\begin{aligned}
W_{00}^{dd}(n,n) &= -\Gamma_N - \Gamma_N f(-\varepsilon - U - 2neV + 2\mu_{S2}) + \Gamma_N f(-\varepsilon - 2neV + 2\mu_{S2}) \\
&+ \frac{\mathrm{i}\Gamma_N}{\pi}\mathrm{Re}\left[\Psi\left(\frac{1}{2} + \mathrm{i}\frac{-\varepsilon - U - 2neV + 2\mu_{S2} - \mu_N}{2\pi k_B T}\right)\right] \\
&- \frac{\mathrm{i}\Gamma_N}{\pi}\mathrm{Re}\left[\Psi\left(\frac{1}{2} + \mathrm{i}\frac{-\varepsilon - 2neV + 2\mu_{S2} - \mu_N}{2\pi k_B T}\right)\right]
\end{aligned}
\tag{D.1}
$$

$$
[W_{dd}^{00}(n,n)]^* = W_{00}^{dd}(n,n) \tag{D.2}
$$

$$
\begin{aligned}
W_{\sigma 0}(0,0) &= \Gamma_N f(\varepsilon) \\
W_{0\sigma}(0,0) &= \Gamma_N (1 - f(\varepsilon)) \\
W_{d\sigma}(0,0) &= \Gamma_N f(\varepsilon + U) \\
W_{\sigma d}(0,0) &= \Gamma_N (1 - f(\varepsilon + U)) \\
W_{00}(0,0) &= -2\Gamma_N f(\varepsilon) \\
W_{\sigma\sigma}(0,0) &= -\Gamma_N (1 - f(\varepsilon) + f(\varepsilon + U)) \\
W_{dd}(0,0) &= -2\Gamma_N (1 - f(\varepsilon + U))
\end{aligned}
$$

with $W_{\chi\chi'}(0,0) \equiv W^{\chi\chi'}_{\chi\chi'}(0,0)$.

$$
\begin{aligned}
W^N_{\sigma 0}(0,0) &= \Gamma_N f(\varepsilon) \\
W^N_{0\sigma}(0,0) &= -\Gamma_N (1 - f(\varepsilon)) \\
W^N_{d\sigma}(0,0) &= \Gamma_N f(\varepsilon + U) \\
W^N_{\sigma d}(0,0) &= -\Gamma_N (1 - f(\varepsilon + U))
\end{aligned}
$$

with $W^N_{\chi\chi'}(0,0) \equiv W^{\chi\chi',N}_{\chi\chi'}(0,0)$.

Bibliography

[1] A. T. Johnson, L. P. Kouwenhoven, W. de Jong, N. C. van der Vaart, C. J. P. M. Harmans, and C. T. Foxon, Phys. Rev. Lett. **69**, 1592 (1992).

[2] T. Heinzel, D. A. Wharam, J. P. Kotthaus, G. Böhm, W. Klein, G. Tränke, and G. Weimann, Phys. Rev. B **50**, 15113 (1994).

[3] D. Goldhaber-Gordon, H. Shtrikman, D. Mahalu, D. Abusch-Magder, U. Meirav, and M. A. Kastner, Nature **391**, 156 (1998).

[4] T. S. Jesperson, M. Aagesen, C. Sørensen, P. E. Lindelof, and J. Nygård, Phys. Rev. B **74**, 233303 (2006).

[5] C. Fasth, A. Fuhrer, L. Samuelson, V. N. Golovach, and D. Loss, Phys. Rev. Lett. **98**, 266801 (2007).

[6] G. Sallen, A. Tribu, T. Aichele, R. André, L. Besombes, C. Bougerol, S. Tatarenko, K. Kheng, and J. P. Poizat, Phys. Rev. B **80**, 085310 (2009).

[7] P. Jarillo-Herrero, S. Sapmaz, C. Dekker, L. P. Kouwenhoven, and H. S. J. van der Zant, Nature **429**, 389 (2004).

[8] M. R. Buitelaar, A. Bachtold, T. Nussbaumer, M. Iqbal, and C. Schönenberger, Phys. Rev. Lett. **88**, 156801 (2002).

[9] S. Moriyama, T. Fuse, M. Suzuki, Y. Aoyagi, and K. Ishibashi, Phys. Rev. Lett. **94**, 186806 (2005).

[10] B. Hiltscher, M. Governale, and J. König, Phys. Rev. B **82**, 165452 (2010).

[11] D. V. Averin, A. N. Korotkov und K. K. Likharev, Phys. Rev. B **44**, 6199 (1991).

[12] C. W. Beenakker, Phys. Rev. B **44**, 1646 (1991).

[13] *Single Charge Tunneling*, NATO ASI Series, Vol. B **294**, edited by H. Grabert and M. H. Devoret (Plenum Press, New York, 1992).

[14] L. I. Glazman and M. E. Raikh, JETP Lett. **47**, 452 (1988).

[15] Y. Aharonov and D. Bohm, Phys. Rev. **115**, 485 (1959).

[16] H. Aikawa, K. Kobayashi, A. Sano, S. Katsumoto, and Y. Iye, Phys. Rev. Lett. **92**, 176802 (2004).

[17] T. Ihn, M. Sigrist, K. Ensslin, W. Wegscheider, and M. Reinwald, New J. Phys. **9**, 111 (2007).

[18] A. Yacoby, M. Heiblum, D. Mahalu, and H. Shtrikman, Phys. Rev. Lett. **74**, 4047 (1995).

[19] R. Schuster, E. Buks, M. Heiblum, D. Mahalu, V. Umansky, and H. Shtrikman, Nature **385**, 417 (1997).

[20] Y. Ji, M. Heiblum, D. Sprinzak, D. Mahalu, and H. Shtrikman, Science **290**, 779 (2000).

[21] W. G. van der Wiel *et al.*, Science **289**, 2105 (2000).

[22] A. W. Holleitner, C. R. Decker, H. Qin, K. Eberl, and R. H. Blick, Phys. Rev. Lett. **87**, 256802 (2001).

[23] M. Sigrist, T. Ihn, K. Ensslin, D. Loss, M. Reinwald, and W. Wegscheider , Phys. Rev. Lett. **96**, 036804 (2006).

[24] S. Gustavsson, R. Leturcq, M. Studer, T. Ihn, K. Ensslin, D. C. Driscoll, A. C. Gossard, Nano Lett. **8**, 2547 (2008).

[25] I. L. Aleiner, N. S. Wingreen, and Y. Meir, Phys. Rev. Lett. **79**, 3740 (1997).

[26] G. L. Khym and K. Kang, Phys. Rev. B **74**, 153309 (2006).

[27] V. Moldoveanu, M. Tolea, and B. Tanatar, Phys. Rev. B **75**, 045309 (2007).

[28] J. König and Y. Gefen, Phys. Rev. Lett. **86**, 3855 (2001).

[29] J. König and Y. Gefen, Phys. Rev. B **65**, 045316 (2002).

[30] W. Hofstetter, J. König, and H. Schoeller Phys. Rev. Lett. **87**, 156803 (2001).

[31] H. Akera , Phys. Rev. B **47**, 6835 (1993).

[32] A. Levy Yeyati and M. Büttiker, Phys. Rev. B **52**, R14360 (1995).

[33] C. Bruder, R. Fazio, and H. Schoeller, Phys. Rev. Lett. **76**, 114 (1996).

[34] G. Hackenbroich and H. A. Weidenmüller, Phys. Rev. Lett. **76**, 110 (1996).

[35] G. Hackenbroich and H. A. Weidenmüller, Phys. Rev. B **53**, 16379 (1996).

[36] J. Wu, B.-L. Gu, H. Chen, W. Duan, and Y. Kawazoe, Phys. Rev. Lett. **80**, 1952 (1998).

[37] K. Kang, Phys. Rev. B **59**, 4608 (1999).

[38] P. G. Silvestrov and Y. Imry, Phys. Rev. Lett. **85**, 2565 (2000).

[39] U. Gerland, J. von Delft, T. A. Costi, and Y. Oreg, Phys. Rev. Lett. **84**, 3710 (2000).

[40] K. Kang and S. C. Shin, Phys. Rev. Lett. **85**, 5619 (2000).

[41] D. Boese, W. Hofstetter, and H. Schoeller, Phys. Rev. B **64**, 125309 (2001).

[42] P. G. Silvestrov and Y. Imry, Phys. Rev. Lett. **90**, 106602 (2003).

[43] R. López, D. Sánchez, M. Lee, M.-S. Choi, P. Simon, and K. Le Hur, Phys. Rev. B **71**, 115312 (2005).

[44] D. Urban, J. König, and R. Fazio, Phys. Rev. B **78**, 075318 (2008).

[45] L. G. G. V. Dias da Silva, N. Sandler, P. Simon, K. Ingersent, and S. E. Ulloa, Phys. Rev. Lett. **102**, 166806 (2009).

[46] L. D. Landau, E. M. Lifshitz, *Lehrbuch der theoretischen Physik Bd. 3: "Quantenmechanik"*, Akademie-Verlag Berlin, 9th edition (1986).

[47] P. W. Anderson, Phys. Rev. **124**, 41 (1961).

[48] H. Pothier, P. Lafarge, C. Urbina, D. Esteve, and M. H. Devoret, Europhys. Lett. **17**, 249 (1992).

[49] J. M. Martinis, M. Nahum, and H. D. Jensen, Phys. Rev. Lett. **72**, 904 (1994).

[50] M.W. Keller, J. M. Martinis, N. M. Zimmerman, and A. H. Steinbach, Appl. Phys. Lett. **69**, 1804 (1996).

[51] R. L. Kautz, M. W. Keller, and J. M. Martinis, Phys. Rev. B **60**, 8199 (1999).

[52] M. Switkes, C. M. Marcus, K. Campman, and A. C. Gossard, Science **283**, 1905 (1999).

[53] S. K. Watson, R. M. Potok, C. M. Marcus, and V. Umansky, Phys. Rev. B **9**, 258301 (2003).

[54] M. D. Blumenthal, B. Kaestner, L. Li, S. Giblin, T. J. B. M. Janssen, M. Pepper, D. Anderson, G. Jones, and D. A. Ritchie, Nature Phys. **3**, 343 (2007).

[55] M. R. Buitelaar, V. Kashcheyevs, P. J. Leek, V. I. Talyanskii, C. G. Smith, D. Anderson, G. A. C. Jones, J. Wei, and D. H. Cobden, Phys. Rev. Lett. **101**, 126803 (2008).

[56] V. F. Maisi, Yu. A. Pashkin, S. Kafanov, J.-S. Tsai, and J. P. Pekola, New J. Phys. **11**, 113057 (2009).

[57] P. Mirovsky, B. Kaestner, C. Leicht, A. C. Welker, T. Weimann, K. Pierz, and H. W. Schumacher, Appl. Phys. Lett. **97**, 252104 (2010).

[58] F. Giazotto, P. Spathis, S. Roddaro, S. Biswas, F. Taddei, M. Governale, and L. Sorba, Nature Phys. **7**, 857 (2011).

[59] B. Hiltscher, M. Governale, and J. König, Phys. Rev. B **81**, 085302 (2010).

[60] D. J. Thouless, Phys. Rev. B **27**, 6083 (1983).

[61] Q. Niu, Phys. Rev. Lett **64**, 1812 (1990).

[62] F. Hekking and Yu. V. Nazarov, Phys. Rev. B **44**, 9110 (1991).

[63] P. W. Brouwer, Phys. Rev. B **63**, 121303 (2001).

[64] M. Büttiker , H. Thomas, and A. Pretré, Z. Phys. B: Condens. Matter **94**, 133 (1994).

[65] P. W. Brouwer, Phys. Rev. B **58**, R10135 (1998).

[66] F. Zhou, B. Spivak, and B. Altshuler, Phys. Rev. Lett. **82**, 608 (1999).

[67] M. Moskalets and M. Büttiker, Phys. Rev. B **64**, 201305(R) (2001).

[68] Y. Makhlin and A.D. Mirlin, Phys. Rev. Lett. **87**, 276803 (2001).

[69] M. Moskalets and M. Büttiker, Phys. Rev. B **66**, 035306 (2002).

[70] O. Entin-Wohlman, A. Aharony, and Y. Levinson, Phys. Rev. B **65**, 195411 (2002).

[71] M. Moskalets and M. Büttiker, Phys. Rev. B **66**, 205320 (2002).

[72] Luis E. F. Foa Torres, Phys. Rev. B **72**, 245339 (2005).

[73] L. Arrachea and M. Moskalets, Phys. Rev. B **74**, 245322 (2006).

[74] M. Moskalets and M. Büttiker, Phys. Rev. B **78**, 035301 (2008).

[75] R. Landauer, IBM J. Res. Dev. **1**, 233 (1957).

[76] M. Büttiker, Phys. Rev. Lett. **57**, 1761 (1986).

[77] T. Aono, Phys. Rev. Lett. **93**, 116601 (2004).

[78] E. Sela and Y. Oreg, Phys. Rev. Lett. **96**, 166802 (2006).

[79] D. Fioretto and A. Silva, Phys. Rev. Lett. **100**, 236803 (2008).

[80] J. Splettstoesser, M. Governale, J. König, and R. Fazio, Phys. Rev. B **74**, 085305 (2006).

[81] I. L. Aleiner and A. V. Andreev, Phys. Rev. Lett. **81**, 1286 (1998).

[82] R. Citro, N. Andrei, and Q. Niu, Phys. Rev. B **68**, 165312 (2003).

[83] E. Cota, R. Aguado, and G. Platero, Phys. Rev. Lett. **94**, 107202 (2005); Phys. Rev. Lett. **94**, 229901(E) (2005).

[84] P. W. Brouwer, A. Lamacraft, and K. Flensberg, Phys. Rev. B **72**, 075316 (2005).

[85] J. Splettstoesser, M. Governale, J. König, and R. Fazio, Phys. Rev. Lett. **95**, 246803 (2005).

[86] R. Sánchez, E. Cota, R. Aguado, and G. Platero, Phys. Rev. B **74**, 035326 (2006).

[87] M. Braun and G. Burkard, Phys. Rev. Lett. **101**, 036802 (2008).

[88] L. Arrachea, A. Levy Yeyati, and A. Martin-Rodero, Phys. Rev. B **77**, 165326 (2008).

[89] J. Splettstoesser, M. Governale, and J. König, Phys. Rev. B **77**, 195320 (2008).

[90] F. Cavaliere, M. Governale, and J. König, Phys. Rev. Lett. **103**, 136801 (2009).

[91] A. R. Hernández, F. A. Pinheiro, C. H. Lewenkopf, and E. R. Mucciolo, Phys. Rev. B **80**, 115311 (2009).

[92] F. Reckermann, J. Splettstoesser, and M. R. Wegewijs, Phys. Rev. Lett. **104**, 226803 (2010).

[93] B. L. Altshuler and L. I. Glazman, Science **283**, 1864 (1999).

[94] Physik Journal, june 2011, pp. 20-28.

[95] G. Czycholl, *Theoretische Festkörperphysik*, 3rd edition, Springer (2007).

[96] J. Bardeen, L. N. Cooper, and J. R. Schrieffer, Phys. Rev. **108**, 1175 (1957).

[97] M. R. Buitelaar, T. Nussbaumer, and C. Schönenberger, Phys. Rev. Lett. **89**, 256801 (2002).

[98] J.-P. Cleuziou, W. Wernsdorfer, V. Bouchiat, T. Ondarçuhu, and M. Monthioux, Nat. Nanotech. **1**, 53 (2006).

[99] A. Eichler, M. Weiss, S. Oberholzer, C. Schönenberger, A. Levy Yeyati, J. C. Cuevas, and A. Martín-Rodero, Phys. Rev. Lett. **99**, 126602 (2007).

[100] H. I. Jørgensen, T. Novotný, K. Grove-Rasmussen, K. Flensberg, and P. E. Lindelof, Nano Lett. **7**, 2441 (2007).

[101] J-D. Pillet, C. H. L. Quay, P. Morfin, C. Bena, A. Levy Yeyati, and P. Joyez, Nature Phys. **6**, 965 (2010).

[102] L. G. Herrmann, F. Portier, P. Roche, A. Levy Yeyati, T. Kontos, and C. Strunk, Phys. Rev. Lett. **104**, 026801 (2010).

[103] J. A van Dam, Yu. V. Nazarov, E. P. A. M. Bakkers, S. De Franceschi, and L. P. Kouwenhoven, Nature **442**, 667 (2006).

[104] T. Sand-Jespersen, J. Paaske, B. M. Andersen, K. Grove-Rasmussen, H. I. Jørgensen, M. Aagesen, C. B. Sørensen, P. E. Lindelof, K. Flensberg, and J. Nygård, Phys. Rev. Lett. **99**, 126603 (2007).

[105] L. Hofstetter, S. Csonka, J. Nygård, and C. Schönenberger, Nature **461**, 960 (2009).

[106] T. Dirks, T. L. Hughes, S. Lal, B. Uchoa, Y-F. Chen, C. Chiavlo, P. M. Goldbart, and N. Mason, Nat. Phys. **7**, 386 (2011).

[107] C. Buizert, A. Oiwa, K. Shibata, K. Hirakawa, and S. Tarucha, Phys. Rev. Lett. **99**, 136806 (2007).

[108] R. S. Deacon, Y. Tanaka, A. Oiwa, R. Sakano, K. Yoshida, K. Shibata, K. Hirakawa, and S. Tarucha, Phys. Rev. Lett. **104**, 076805 (2010).

[109] Y. Kanai, R. S. Deacon, A. Oiwa, K. Yoshida, K. Shibata, K. Hirakawa, and S. Tarucha, Phys. Rev. B **82**, 054512 (2010).

[110] S. De Franceschi, L. Kouwenhoven, C. Schönenberger, and W. Wernsdorfer, Nat. Nanotech. **1**, 703 (2010).

[111] A. Martín-Rodero and A. Levy Yeyati, Adv. Phys. **60**, 899 (2011).

[112] B. Hiltscher, M. Governale, and J. König, Phys. Rev. B, **84**, 155403 (2011).

[113] A. F. Andreev, Sov. Phys. JETP **19**, 1228 (1964).

[114] C. W. J. Beenakker, "Mesoscopic Quantum Physics", edited by E. Akkermans, G. Montambaux, J.-L. Pichard, and J. Zinn-Justin (North-Holland, Amsterdam, 1995).

[115] J. M. Byers and M. E. Flatté, Phys. Rev. Lett. **74**, 306 (1995).

[116] G. Deutscher and D. Feinberg, Appl. Phys. Lett. **76**, 487 (2000).

[117] G. Falci, D. Feinberg, and F. W. J. Hekking, Europhys. Lett. **54**, 255 (2001).

[118] D. Sánchez, R. López, P. Samuelsson, and M. Büttiker, Phys. Rev. B **68**, 214501 (2003).

[119] T. Yamashita, S. Takahashi, and S. Maekawa, Phys. Rev. B **68**, 174504 (2003).

[120] J. P. Morten, A. Brataas, and W. Belzig, Phys. Rev. B **74**, 214510 (2006).

[121] M. S. Kalenkov and A. D. Zaikin, Phys. Rev. B **75**, 172503 (2007).

[122] M. Veldhorst and A. Brinkman, Phys. Rev. Lett. **105**, 107002 (2010).

[123] G. Metalidis, M. Eschrig, R. Grein, and G. Schön, Phys. Rev. B **82**, 180503(R) (2010).

[124] D. Beckmann, H. B. Weber, and H. v. Löhneysen, Phys. Rev. Lett. **93**, 197003 (2004).

[125] S. Russo, M. Kroug, T. M. Klapwijk, and A. F. Morpurgo, Phys. Rev. Lett. **95**, 027002 (2005).

[126] P. Cadden-Zimansky and V. Chandrasekhar, Phys. Rev. Lett. **97**, 237003 (2006).

[127] I. Asulin, O. Yuli, G. Koren, and O. Millo, Phys. Rev. B **74**, 092501 (2006).

[128] C. B. Whan and T. P. Orlando, Phys. Rev. B, **54**, 5255 (1996).

[129] A. Levy Yeyati, J. C. Cuevas, A. López-Dávalos, and A. Martín-Rodero, Phys. Rev. B **55**, 6137 (1997).

[130] K. Kang, Phys. Rev. B **57**, 11891 (1998).

[131] Y. Avishai, A. Golub, and A. D. Zaikin, Phys. Rev. B **67**, 041301 (2003).

[132] L. Dell'Anna, A. Zazunov, and R. Egger, Phys. Rev. B **77**, 104525 (2008).

[133] Yu. V. Nazarov, Phys. Rev. Lett. **73**, 1420 (1994).

[134] R. Fazio and R. Raimondi, Phys. Rev. Lett. **80**, 2913 (1998).

[135] R. Fazio and R. Raimondi, Phys. Rev. Lett. **82**, 4950 (1999).

[136] A. A. Clerk, V. Ambegaokar, and S. Hershfield, Phys. Rev. B **61**, 3555 (2000).

[137] J. C. Cuevas, A. Levy Yeyati, and A. Martín-Rodero, Phys. Rev. B **63**, 094515 (2001).

[138] M. G. Pala, M. Governale, and J. König, New J. Phys. **9**, 278 (2007).

[139] M. Governale, M. G. Pala, and J. König, Phys. Rev. B **77**, 134513 (2008).

[140] V. Koerting, B. M. Andersen, K. Flensberg, and J. Paaske, Phys. Rev. B **82**, 245108 (2010).

[141] D. Futterer, M. Governale, and J. König, Europhys. Lett. **91**, 47004 (2010).

[142] J.-F. Feng, S.-J. Xiong, Phys. Rev. B **67**, 045316 (2003).

[143] Y. Zhu, T.-H. Lin, and Q.-F. Sun, Phys. Rev. B **69**, 121302(R) (2004).

[144] B. Sothmann, D. Futterer, M. Governale, and J. König, Phys. Rev. B **82**, 094514 (2010).

[145] D. Futterer, M. Governale, M. G. Pala, and J. König, Phys. Rev. B **79**, 054505 (2009).

[146] R. Mélin, H. Jirari, and S. Peysson, J. Phys.: Condens. Matter **15**, 5591 (2003).

[147] O. Sauret, T. Martin, and D. Feinberg, Phys. Rev. B **72**, 024544 (2005).

[148] D. S. Golubev and A. D. Zaikin, Phys. Rev. B **76**, 184510 (2007).

[149] D. Chevallier, J. Rech, T. Jonckheere, and T Martin, Phys. Rev. B **83**, 125421 (2011).

[150] J. Eldridge, M. G. Pala, M. Governale, and J. König, Phys. Rev. B **82**, 184507 (2010).

[151] B. D. Josephson, Phys. Lett. **1**, 251 (1962).

[152] M. Tinkham, *Introduction to superconductivity*, 2nd edition, McGraw-Hill (1996).

[153] L. I. Glazman and K. A. Mateev, JETP Lett. **49**, 659 (1989).

[154] A. V. Rozhkov, D. P. Arovas, and F. Guinea, Phys. Rev. B **64**, 233301 (2001).

[155] J. Bardeen, Phys. Rev. Lett. **9**, 147 (1962).

[156] J. König, H. Schoeller, and G. Schön, Phys. Rev. Lett. **76**, 1715 (1996).

[157] J. König, J. Schmid, H. Schoeller, and G. Schön, Phys. Rev. B **54**, 16820 (1996).

[158] A. L. Fetter and J. D. Walecka, *Quantum Theory of Many-Particle Systems*, McGraw-Hill (1971).

[159] L. V. Keldysh Sov. Phys. JETP **20**, 1018 (1965).

[160] N. E. Fletcher, J. Ebbecke, T. J. B. M. Janssen, F. J. Ahlers, M. Pepper, H. E. Beere, and D. A. Ritchie, Phys. Rev. B **68**, 245310 (2003).

[161] J. Ebbecke, N. E. Fletcher, T. J. B. M. Janssen, F. J. Ahlers, M. Pepper, H. E. Beere, and D. A. Ritchie, Appl. Phys. Lett. **84**, 4319 (2004).

[162] A. Fuhrer, C. Fasth, and L. Samuelson, Appl. Phys. Lett. **91**, 052109 (2007).

[163] B. Kaestner, V. Vashcheyevs, G. Hein, K. Pierz, U. Siegner, and H. W. Schumacher , Appl. Phys. Lett. **92**, 192106 (2008).

[164] B. Hiltscher, *Adiabatisches Pumpen in einem Quantenpunkt-Aharonov-Interferometer*, diploma thesis (Ruhr-Universität Bochum, 2008)

[165] L. DiCarlo, C. M. Marcus, and J. S. Harris, Jr., Phys. Rev. Lett. **91**, 246804 (2003).

[166] R. Leturcq, D. Sánchez, G. Götz, T. Ihn, K. Ensslin, D.C. Driscoll, and A. C. Gossard, Phys. Rev. Lett. **96**, 126801 (2006).

[167] L. Angers, E. Zakka-Bajjani, R. Deblock, S. Guéron, H. Bouchiat, A. Cavanna, U. Gennser, and M. Polianski, Phys. Rev. B **75**, 115309 (2007).

[168] M. Moskalets and M. Büttiker, Phys. Rev. B **72**, 035324 (2005).

[169] M. L. Polianski and M. Büttiker, Phys. Rev. B **76**, 205308 (2007).

[170] S. Lindebaum, D. Urban, and J. König, Phys. Rev. B **79**, 245303 (2009).

[171] M. Braun, J. König, and J. Martinek, Phys. Rev. B **70**, 195345 (2004).

[172] J. Barnas and I. Weymann, J. Phys.: Condens. Matter **20**, 423202 (2008).

[173] F. M. Souza, J. C. Egues, and A. P. Jauho, Phys. Rev. B **75**, 165303 (2007).

[174] P. Stefanski, Phys. Rev. B **79**, 085312 (2009).

[175] K. Hamaya, S. Masubuchi, M. Kawamura, T. Machida, M. Jung, K. Shibata, K. Hirakawa, T. Taniyami, S. Ishida, and Y. Arakawa, Appl. Phys. Lett. **90**, 053108 (2007).

[176] B. R. Bułka, Phys. Rev. B **62**, 1186 (2000).

[177] W. Rudziński, J. Barnaś, R. Świrkowicz, and M. Wilczyński, Phys. Rev. B **71**, 205307 (2005).

[178] S. Braig and P. W. Brouwer, Phys. Rev. B **71**, 195324 (2005).

[179] D. C. Langreth, Phys. Rev. **150**, 516 (1966).

[180] I. Weymann, J. König, J. Martinek, J. Barnaś, and G. Schön, Phys. Rev. B **72**, 115334 (2005).

[181] D. V. Averin and A. A. Odintsov, Phys. Lett. A **140**, 251 (1989).

[182] D. V. Averin and Y. V. Nazarov, Phys. Rev. Lett. **65**, 2446 (1990).

[183] I. Weymann, J. Barnaś, J. König, J. Martinek, and G. Schön, Phys. Rev. B **72**, 113301 (2005).

[184] J. Wang, Y. Wei, B. Wang, and H. Guo, Appl. Phys. Lett. **79**, 3977 (2001)

[185] M. Blaauboer, Phys. Rev. B **65**, 235318 (2002)

[186] F. Taddei, M. Governale, and R. Fazio, Phys. Rev. B **70**, 052510 (2004).

[187] J. Splettstoesser, M. Governale, J. König, F. Taddei, and R. Fazio, Phys. Rev. B **75**, 235302 (2007).

[188] L. Hofstetter, A. Geresdi, M. Aagesen, J. Nygård, C. Schönenberger, and S. Csonka, Phys. Rev. Lett. **104**, 246804 (2010).

[189] A. V. Rozhkov and D. P. Arovas, Phys. Rev. B **62**, 6687 (2000).

[190] Y. Tanaka, A. Oguri, and A. C. Hewson, New J. Phys. **9**, 115 (2007).

[191] C. Karrasch, A. Oguri, and V. Meden, Phys. Rev. B, **77**, 024517 (2008).

[192] T. Meng, S. Florens, and P. Simon, Phys. Rev. B **79**, 224521 (2009).

[193] M. Leijnse and M. R. Wegewijs, Phys. Rev. B **78**, 235424 (2008).

[194] R.-P. Riwar and J. Splettstoesser, Phys. Rev. B **82**, 205308 (2010).

[195] B. Wunsch, M. Braun, J. König, and D. Pfannkuche, Phys. Rev. B **72**, 205319 (2005).

[196] C. W. J. Beenakker and H. van Houten, *Single-Electron Tunneling and Mesoscopic Devices*, edited by H. Koch and H. Lübbig (Springer, Berlin), pp. 175-179 (1992).

[197] D. Matsumoto, J. Phys. Soc. Jpn. **70**, 492 (2001).

[198] E. Vecino, A. Martín-Rodero and A. Levy Yeyati, Phys. Rev. B **68**, 035105 (2003).

[199] A. V. Rozhkov and D. P. Arovas, Phys. Rev. Lett. **82**, 2788 (1999).

[200] F. Siano and R. Egger, Phys. Rev. B, **93**, 047002 (2004).

[201] G. Sellier, T. Kopp, J. Kroha, and Y. S. Barash, Phys. Rev. B **72**, 174502 (2005).

[202] E. N. Bratus, V. S. Shumeiko, and G. Wendin, Phys. Rev. Lett. **74**, 2110 (1995).

[203] D. Averin and A. Bardas, Phys. Rev. Lett. **75**, 1831 (1995).

[204] Q.-F. Sun, H. Guo, and J. Wang, Phys. Rev. B **65**, 075315 (2002).

[205] T. Jonckheere, A. Zazunov, K. V. Bayandin, V. Shumeiko, and T. Martin, Phys. Rev. B **80**, 184510 (2009).

[206] E. Perfetto, G. Stefanucci, and M. Cini, Phys. Rev. B **80**, 205408 (2009).

[207] G. Stefanucci, E. Perfetto, and M. Cini, Phys. Rev. B **81**, 115446 (2010).

List of Publications

(A) *Interference and interaction effects in adiabatic pumping through quantum dots*, B. Hiltscher, M. Governale, and J. König, Phys. Rev. B **81**, 085302 (2010).

(B) *Spin-dependent transport through quantum-dot Aharonov-Bohm interferometers*, B. Hiltscher, M. Governale, and J. König, Phys. Rev. B **82**, 165452 (2010).

(C) *Adiabatic pumping in a double-dot Cooper-pair beam splitter*, B. Hiltscher, M. Governale, J, Splettstoesser, and J. König, Phys. Rev. B **84**, 155403 (2011).

(D) *AC Josephson transport through interacting quantum dots*, B. Hiltscher, M. Governale, and J. König, in preparation.

Major parts of this thesis have already been published. In Ref. **(A)** a single-dot and a double-dot Aharonov-Bohm interferometer have been investigated. Chapter 4 is a reproduction of the results for the double-dot setup. The chapters 5 and 6, are mainly reproductions of Ref. **(B)** and **(C)**, respectively. Chapter 7 is going to be published soon in Ref. **(D)**.

Acknowledgements

Finally, I would like to thank all people, who have been important for this thesis:

Prof. Dr. Jürgen König for having given me the possibility to do my PhD in his group. He has been a real good supervisor and found a convenient balance between being included in my work and giving me the opportunity to work independently. I have had a lot of fruitful scientific discussions with him but also learned a lot about presenting contents.

Prof. Dr. Michele Governale and **Prof. Dr. Janine Splettstoesser** for good collaborations. I have had several interesting discussions with them.

David Futterer and **Stephan Lindebaum** for having made my working days so much better. I have had a lot of fun with them in discussions about physics and especially in doing many other things. But I am even more grateful that they have stood by me whenever I was frustrated for any reason. I am very glad to have these guys as friends.

Dr. Björn Sothmann for all the support he has given me by answering so many questions.

Stephan Rojek for taking over my tutoring obligations during the last weeks and making the lunch breaks much funnier.

All members of the AG König and AG Entel for the nice atmosphere.

Meiner Frau Birte Hiltscher möchte ich ganz besonders danken. Sie hat mir immer den Rücken freigehalten und all meine Launen ertragen. Dabei hat sie mir so viel Liebe geschenkt. Ich bin unglaublich glücklich, eine so tolle Frau zu haben.

Lebenslauf

Der Lebenslauf ist in der Online-Version aus Gründen des Datenschutzes nicht enthalten

Duisburg, 26.06.2012

Erklärung

Ich bestätige mit meiner Unterschrift, dass ich die vorliegende Dissertation ,,Coherent Transport through Interacting Quantum Dots" selbständig verfasst habe und dabei nur die angegebenen Hilfsmittel verwendet habe. Wörtlich oder inhaltlich übernommene Stellen sind als solche gekennzeichnet.

Darüber hinaus bestätige ich, dass die vorliegende Dissertation ,,Coherent Transport through Interacting Quantum Dots" nur in diesem Promotionsverfahren an der Fakultät für Physik an der Universität Duisburg-Essen eingereicht wurde.

Bastian Hiltscher